SENSING OF PATHOLOGICAL TREMOR USING SURFACE ELECTROMYOGRAPHY AND ACCELEROMETER FOR REAL-TIME ATTENUATION

FERDINAN WIDJAJA

School of Mechanical and Aerospace Engineering

A thesis submitted to the Nanyang Technological University
in partial fulfillment of the requirement for the degree of
Doctor of Philosophy

2011

Acknowledgements

In this limited space I would like to give my gratitude to:

- My supervisor, Dr. Ang Wei Tech, for his commitment in advising me, both in engineering matters and other things. I really appreciate the time given to me in the middle of his hectic schedule.
- Fellow students, especially Tan U-Xuan and Adrian Tan, and staffs in our research lab, Win Tun Latt, and Shee Cheng Yap. Indeed, a threefold cord is not quickly broken.
- Laboratory technicians, Mr. Lim Eng Cheng, Ms. Toh-Tan Siok Kuan, and Mr You Kim San, for maintaining the laboratory in a good shape and helping out in all the delicate administrative works.
- Our collaborators at National Neuroscience Institute, Singapore, Drs. Au Wing Lok, Emmanuel Pica, Paulito Palmes, and Ms. Irene Seah, for their generous assistance, especially in arranging the experiments and working with the patients and healthy subjects.
- Dr. Domenico Campolo, for providing me the opportunity to do the necessary revision for my thesis, while working with him in the same school in NTU.
- The external reviewers, Drs. Lan Ning (University of Southern Carolina, USA), and Maria Chiara Carrozza (Scuola Superiore Sant'Anna, Italy), and the internal examiners, Drs. Gerard Seet, Sunita Chauhan, and Jaspreet Singh, for giving a lot of inputs which in the end have significantly improved my thesis.
- My family back in Indonesia, for supporting me through their loving care since I was born.
- Last but not least, to Yosetine, who has helped me get through the tough times especially after I submitted my thesis.

Table of Contents

Abstract

Tremor is one of the most common movement disorders. Based on Elble and Koller' s definition, it is defined as, "the involuntary rhythmic or semi rhythmic oscillation of a body part resulting from alternating of simultaneous contractions of antagonistic muscle groups". Tremor caused by injuries or diseases such as Parkinsons disease, stroke, etc., can be problematic both physically and emotionally. If the tremor is affecting the upper limb, the patient will have difficulties even to do activities of daily living such as buttoning, inserting key to keyhole, writing, etc, thus degrading his quality of daily life. Furthermore it may lead to social embarrassment and isolation. The cost of the treatment and the cost borne by the family and community are also significant. This thesis shows the feasibility of real-time tremor attenuation by proposing novel algorithms in an assistive technology solution.

The contribution of the proposed system is using surface Electromyography (SEMG) as the sensor to detect the upper limb movement. SEMG is used because it precedes the kinematics data (accelerometer–ACC in this case) by 20-100 ms. This time lead provides the necessary time to process the information and to do real-time compensation of tremor.

To estimate tremor parameters necessary for the compensation from both the SEMG and ACC, an Extended Kalman Filter (EKF) is proposed. Other than parameter estimation, the EKF is also able to separate tremor and voluntary motion. This is important so that only tremor is suppressed without hindering the intended motion by the subject. Simulations with real tremor data have shown that the estimation RMS error from the SEMG signal can be as small as 28% and the algorithm is able to provide the necessary information for the tremor compensation.

Functional Electrical Stimulation (FES) is proposed to counteract the tremor movement. If tremor is detected at the agonist, the algorithms will set the FES to stimulate the antagonist in the correct moment

such that tremor is diminished (anti phase cancellation). Two issues associated with FES are also tackled, namely the FES artifacts and how the anti phase cancellation is achieved (when to start/stop the FES).

Experiment with one Essential Tremor patient has achieved 57% tremor compensation. This compensation is confirmed to be caused by the anti phase cancellation method. During the electrical stimulation, tremor activity is still detected in the muscle, while there is reduction in movement. This result may further be improved given a more sophisticated control algorithm.

List of Figures

List of Tables

List of Symbols and Abbreviations

Abbreviations

AC	Alternating Current
ACC	Accelerometer
A/D	Analog to Digital
ANF	Adaptive Notch Filter
APB	Abductor pollicis brevis
AR	Auto Regressive
ASUR	Autonomous Sensing Unit Recorder
AT	Assistive Technology
CEDO	Controlled Energy Dissipation Orthosis
CMOS	Complementary Metal Oxide Semiconductor
CMRR	Common Mode Rejection Ratio
CMIV	Common Mode Input Voltage
CNS	Central Nervous System
DAQ	Data Acquisition
DBS	Deep Brain Stimulation
DC	Direct Current
DoF	Degree of Freedom
DPDT	Double Pole Double Throw
DRIFTS	Dynamically Responsive Intervention for Tremor Suppression
EEG	Electroencephalography
EKF	Extended Kalman Filter
EMD	Electromechanical Delay
EMG	Electromyography
ET	Essential Tremor
FDI	First Dorsal Interossei
FES	Functional Electrical Stimulation
FFT	Fast Fourier Transform

FLC	Fourier Linear Combiner
FP	False Positive
FPGA	Field Programmable Gate Array
FN	False Negative
IED	Inter Electrode Distance
ISEK	International Society of Electrophysiology and Kinesiology
KF	Kalman Filter
LLL	Lead Line Length
LMS	Least Mean Square
MecFES	Myoelectrically controlled Functional Electrical Stimulation
MLP	Multi Layer Perceptron
MS	Multiple Sclerosis
MU	Motor Unit
MUAP	Motor Unit Action Potential
MUAPT	Motor Unit Action Potential Train
PC	Personal Computer
PCA	Principal Component Analysis
PD	Parkinson's Disease
PiG	Plug in Gain
RMSE	Root Mean Square Error
SA	Stimulation Artifact
SEMG	Surface Electromyography
STFT	Short Time Fourier Transform
SVM	Support Vector Machine
TEMPO	Technology Enabled Medical Precision Observation
TP	True Positive
TN	True Negative
TTL	Transistor Transistor Logic
UPDRS	Unified Parkinson's Disease Rating Scale
UTRA	Unified Tremor Rating Assessment
WOTAS	Wearable Orthosis for Tremor Assessment and Suppression

Symbols

Mathematical Conventions

x	a scalar
$\mathbf{x}$	a vector
$\mathbf{X}$	a matrix

$\mathbf{X}^T$	transpose of matrix $\mathbf{X}$
$\mathbf{X}^{-1}$	inverse of matrix $\mathbf{X}$
$\dot{x}$	first derivative of x

Accelerometer

$a(k)$	Acceleration at time k
$a_C(k)$	Centripetal acceleration at time k
$a_{CG}(k)$	Inertial acceleration of the link at time k
$a_{CR}(k)$	Coriolis acceleration at time k
$a_T(k)$	Tangential acceleration at time k
g	gravitational acceleration at time k
k	time index
$R_{\theta k}$	Rotation matrix at time k

Adaptive Notch Filter (ANF)

Γ	diagonal matrix of $[\gamma_0\gamma_1\gamma_2]$
α,λ,γ_1,γ_2	arbitrary positive number
ξ	state vector, $[1, \xi_1, \xi_2]^T$
A	amplitude
A_0	bias
ω	frequency

Gradient-descent

A	amplitude
ω	frequency
ϕ	phase
x	measured signal
y	estimated signal
T	sampling period
μ_1,μ_2,μ_3	convergence factor

Weighted-frequency Fourier Linear Combiner (WFLC)

$\mathbf{x}_k = [x_{1_k}, \ldots, x_{2M_k}]^T$	state vector (sinusoidal terms)

$\mathbf{w}_k = [w_{1_k}, \ldots, w_{2M_k}]^T$	adaptive weight vector of the amplitudes
M	number of harmonics
s_k	input signal at time k
μ_0,μ_1	adaptive gain parameter
w_{0_k}	frequency weight
$\hat{\mathbf{w}}_k$	amplitude weight
μ_b	adaptive gain for bias

AR model for tremor simulation

f	frequency
f_s	sampling frequency
a_1,a_2	AR coefficients
τ	relaxation time
ϵ	Gaussian noise

Kalman Filter (KF)

$\theta(k)$	joint angle of the tremulous limb
r	tremor amplitude
ω	tremor frequency
T	sampling time
$\mathbf{w}(k)$	process noise (zero mean Gaussian)
$\mathbf{Q}(k)$	covariance matrix of $\mathbf{w}(k)$
$\mathbf{v}(k)$	measurement noise (zero mean Gaussian)
$\mathbf{R}(k)$	covariance matrix of $\mathbf{v}(k)$
c_{ACC},c_{EMG}	coefficients estimated by least square method

Extended Kalman Filter (EKF)

$y(k)$	tremor signal to be estimated at time k
m	number of sinusoidal terms to model the tremor
$r(k)$	amplitude estimate
$\omega(k)$	frequency estimate
$\theta(k)$	total phase estimate $(0 \leq \theta(k) \geq 2\pi)$¡
$\phi(k)$	relative phase estimate
$\mathbf{x}(k)$	state vector
$\mathbf{F}$	state update matrix

$\mathbf{w}(k)$	process noise (zero mean Gaussian)
$\mathbf{Q}(k)$	covariance matrix of $\mathbf{w}(k)$
$v(k)$	measurement noise (zero mean Gaussian)
$R(k)$	covariance of $v(k)$
$h(\mathbf{x}(k))$	expected measurement of $\mathbf{x}(k)$
$\mathbf{P}$	error covariance matrix
$\mathbf{K}$	Kalman gain
$\Omega(k)$	covariance of the innovation term
λ	weight factor for AR model

Comb filter

$x(k)$	SEMG signal
$y(k)$	result of comb filter on $x(k)$
T_s	sampling period

Anti phase tremor compensation

f_k	tremor frequency estimate from EKF at time k
$\phi_d(k)$	phase delay estimate from low pass filter
T_s	sampling period
θ_{EMG}	total phase estimate from EKF on SEMG signal
ϕ_{EMG}	relative phase estimate from EKF on SEMG signal
ω_{EMG}	frequency estimate from EKF on SEMG signal
θ_{ACC}	total phase estimate from EKF on ACC signal
ϕ_{ACC}	relative phase estimate from EKF on ACC signal
ω_{ACC}	frequency estimate from EKF on ACC signal
θ_{EMD}	EMD estimate of voluntary motion
$\theta_{EMD-FES}$	EMD estimate of electrically stimulated motion
θ_{FES}	phase of control signal output to the FES

Miscellaneous

R_{xy}	Cross correlation between two signals, x and y
f	frequency
N	number of data points
$Y(f)$	Fourier transform of signal y
P_y	Tremor power

Chapter 1

Introduction

1.1 Background

Tremor is defined as, "the involuntary rhythmic or semi rhythmic oscillation of a body part resulting from alternating or simultaneous contractions of antagonistic muscle groups" [Elble and Koller, 1990]. All human beings have inherent tremor, called physiological tremor. Due to its small amplitude (< 0.5 mm peak to peak [Elble and Koller, 1990]), physiological tremor does not hinder us in performing our daily activities, thus it is not included as movement disorders. Nevertheless, in some cases physiological tremor can be more apparent due to medical conditions. This is clinically categorized as enhanced physiological tremor and it is usually reversible [Smaga, 2003].

More problematic, physically and emotionally, is the tremor caused by injuries or diseases, such as Parkinson's disease (PD), multiple sclerosis (MS), stroke, etc. This type of tremor is called pathological tremor, usually of larger amplitude and smaller frequency than physiological tremor. Pathological tremor is further classified broadly into rest (e.g. Parkinson's disease/PD), postural (essential tremor/ET), and kinetic tremor (multiple sclerosis/MS). Table 1.1 shows a more detailed classification and characteristics of various tremors [Smaga, 2003].

Table 1.1: Classification and characteristics of tremor [Smaga, 2003]

Type of tremor	Frequency	Amplitude	Occurrence	Examples
Rest tremor	Low to medium (3 to 6 Hz)	High, decreases with target-oriented movement	Limb supported against gravity; muscles are not activated	Parkinson's disease; drug-induced parkinsonism (neuroleptics; metoclopramide)
Action tremor	—	—	Any voluntary motion contraction	
Postural tremor	Medium to high (4 to 12 Hz)	Low, increases with target-oriented movement	Limb maintains position against gravity	Physiologic tremor; essential tremor; metabolic disturbance; drug or alcohol withdrawal
Kinetic tremor				
Simple kinetic	Variable (3 to 10 Hz)	Does not change with target-oriented movement	Simple movements of the limb	—
Intention	Low (<5 Hz)	Increases with target-oriented movement	Target-directed movement	Cerebellar lesion (stroke, multiple sclerosis, tumor); drug-induced (lithium, alcohol)
Isometric tremor	Medium	Variable	Muscle contraction against static objects	Holding a heavy subject in one hand
Task-specific tremor	Variable (4 to 10 Hz)	Variable	Occurs with specific action	Handwriting tremor; musician's tremor

Tremor (hereafter only pathological tremor is considered) in upper limb can cause difficulties for the patients even to do simple things like buttoning, inserting key to keyhole, writing, etc. Thus, it may lead to social embarrassment and sometimes isolation [Louis and Rios, 2009]. Overall, the patient's quality of life is reduced. The economic impact of tremor cannot be neglected. People with diseases involving tremor will need to spend a lot of money for their treatment, e.g. €12.5 billion in year 2005 for MS in Europe [Sobocki et al., 2007] and $23

billion in 2002 for PD in US [Findley, 2007]. Furthermore, it has also been reported that a large proportion of the economic burden is not incurred within the health care system, but borne by social systems, communities or families [Miltenburger and Kobelt, 2002].

Both economic and social impacts of tremor are going to increase as the proportion of aging people will increase significantly in the future especially in Europe and US. It is projected that in 2050, the elderly population will increase more than threefold [Bureau, 2004].

Even now, tremor is mentioned as one of the most common movement disorders [Milanov, 2001]. The prevalence of pathological tremor is reported to be quite significant, though slightly varying among the sources (see Table 1.2 and Table 1.3). Essential tremor is reported to be the most common tremor-related movement disorder, the prevalence being about 1 in 20-25 people (more than 4%) aged over 40 [Louis, 2005]. Another common disease involving tremor is Parkinson's disease. In Europe, it affects about 1.28-1.5% of the population older than 60 years [von Campenhausen et al., 2005], compared to 0.8-1.0% of the US population older than 50 years [Manto et al., 2003]. These statistics mean there must be more than 6% of the population aged over 60 years with either Parkinson's disease or essential tremor. Then, extrapolating from the finding that these two diseases represent 50% of all the tremor cases in neurophysiology [Pradalier et al., 2002], we have at least 12% of the population over 60 years affected by pathological tremor.

Unfortunately many aspects underlying the tremor are still unknown [Deuschl et al., 2001] and there is no blood test or other laboratory tests which can give conclusive diagnosis of the diseases [Bishop, 2006]. Furthermore, there is a lack of the objective automatic methods for the recognition and classification of different types of tremor [Jakubowski et al., 2002]. Diagnosis of pathological tremor

Table 1.2: Prevalence of pathological tremor in US respectively (from various sources)

Parkinson's disease	200 out of 100,000 of US population aged over 70 years, 10 times higher in Iceland, India, Scotland, and Australia [Miller, 2002]
Essential tremor	0.4 - 3.9% (in essence, it is about 1 in 20-25 people aged over 40 years) [Louis, 2005]
Multiple Sclerosis	400,000 in USA (The most common disease of central nervous system in UK, Northern Europe, and USA for people aged from 20 to 40 years [Whitmarsh, 2003].)
Orthostatic tremor	4% of tremors in neurophysiology (http://orthostatictremor.org/)
Primary writing tremor	One third in the case of writer's cramp (69/100,000) in USA. This is thought to be an underestimation because a high percentage of patients never seek medical assistance. (http://www.emedicine.com/NEURO/ topic614.htm)

Table 1.3: Prevalence of pathological tremor in Europe (from various sources)

Parkinson's disease	22% of tremors in neurophysiology (http://orthostatictremor.org/). Crude prevalence rate estimates ranged from 65.6 per 100,000 to 12,500 per 100,000 For age groups > 60 years, rates of prevalence were much higher: 1280 to 1500/100,000 [von Campenhausen et al., 2005]
Essential tremor	28% of tremors in neurophysiology (http://orthostatictremor.org/). 0.4 - 3.9% (in essence, it is about 1 in 20-25 people aged over 40 years). The most common movement disorder [Louis, 2005]
Multiple Sclerosis	Per 100,000: Scotland = 145-193, England &Wales = 74-112, Republic of Ireland = 66, North Ireland = 168, Danish, Norwegian, and Swedes worldwide = 112, Faroe Islands = 66, Germany = 85-108, Switzerland = 110, Austria = 22-44, Netherlands and Belgium = 76 and 74, France = 28-58, Iceland = 98, Czech Republic = 89, Hungary = 32-79, Spain = 32-65, Portugal = 47, Italy = 40-70, Sardinia = 144-152, Malta = 4, Slovenia = 83, Croatia = 40, Yugoslavia = 20, Romania = 27-42, Bulgaria = 30-43, Macedonia = 16, Greece = 29, Baltic Republics, Belarus, Ukraine and European Russia = 25-55 [Pugliatti et al., 2002]
Orthostatic tremor	4% of tremors in neurophysiology (http://orthostatictremor.org/, [Pradalier et al., 2002])
Primary writing tremor	Internationally because of the small percentage of affected patients seeking medical attention, accurate prevalence estimates are not available. (http://www.emedicine.com/NEURO/topic614.htm)

usually depends on rather subjective clinical assessments such as the medical history of the patient and standard qualitative physical examinations, e.g. Unified Parkinson's Disease Rating Scale (UPDRS) and Unified Tremor Rating Assessment (UTRA). Although they are easy to use, these scales are not able to differentiate slight change in the tremor characteristics and their validity has been questioned [Lundervold et al., 2003]. These difficulties in obtaining objective and precise diagnosis of tremor hinders correct treatments of tremor.

1.2 Tremor suppression methods

Two common options for tremor treatment are medications and surgery. Medications must be individualized for each patient thus conducted in a trial and error method [Reich, 1995]. Side effects, addiction, and withdrawal symptoms are also the risks in having those medications [Chou, 2008; Pahwa and Lyons, 2003]. It has also been found that about 50% of the pathological tremor cannot be adequately controlled by pharmacological therapy [Weiner and Lang, 1989]. When medications have failed, brain surgery (Deep Brain Stimulation, DBS) may be undertaken. Recent research has shown that DBS is among the best medical therapies, though still with serious adverse effects [Hariz, 2009; Weaver et al., 2009]. They include brain haemorrhage, seizures, death [Samii et al., 2004], and also marked cognitive problems [Pahwa and Lyons, 2003].

The rise of assistive technology gives another alternative solution for tremor suppression. Assistive Technology (AT) is defined as any device that assists a person with an impairment in performing a task [Cooper, 1998]. Coupled with the rise of wearable technology in biomedical engineering [Bonato, 2003], AT can provide another alternative which is more affordable, compared to DBS, for example. Assistive technology in tremor suppression exists in two forms: (i) to suppress tremor at the man-machine interface, and (ii) to attenuate the tremor directly.

Most types of tremor are characterized by having a higher frequency band than voluntary motion (about 1 Hz in [Mann et al., 1989]). Many implementations of the first category have taken advantage of this frequency separation. Riley and Rosen [Riley and Rosen, 1987] have investigated low-pass filtering, while Riviere and Thakor [Riviere and Thakor, 1995] use an adaptive notch filter to suppress pathological tremor at computer pen input. Taking a slightly different approach, Gonzalez et al. [Gonzalez et al., 2000] have proposed a digital signal equalizer technique using FIR linear filters to equilibrate tremor at human-computer interface. Pledgie et al. [Pledgie et al., 2000] have presented methods that suppress the power of pathological tremors by adjusting the impedance at the control interface. Although tremor can be suppressed at the human machine interface, once the subject is not using the interface, the tremor will show up again. This will not give the subjects flexibility to do their other daily activities.

Solutions that fall into the second category attenuate the tremor at the limbs instead of at the human-machine interface. Recent examples include Bionic Glove [Gillard et al., 1999; Popović et al., 1999; Prochazka et al., 1992] and WOTAS (Wearable Orthosis for Tremor Assessment and Suppression) [Rocon et al., 2007].

Using the framework of DRIFTS [Manto et al., 2003], Rocon et. al. developed WOTAS (Wearable Orthosis for Tremor Assessment and Suppression) [Rocon et al., 2007]. This orthosis provides a way of testing non-grounded tremor reduction strategies in three joints of the upper limb. DC motor is used for the actuation. Despite the good result (highest compensation is about 80%), the patients considered that the use of the exoskeleton "should cause social exclusion". Furthermore, although adding weight to the tremulous limb may reduce tremor [Héroux et al., 2009], the effect of the exoskeleton mass (reported to be around 850 g) on the attenuation of tremor is not discussed.

Prochazka et al. [Prochazka et al., 1992] have shown that it is possible to use feedback-controlled functional electrical stimulation (FES) to attenuate pathological tremor. Gillard et. al., [Gillard et al., 1999] later report improvements of the

Prochazka's implementation, i.e. 84% compensation compared to 65% compensation previously. It is achieved by using digital feedback system controlled by a microprocessor and making it in the form of an armlet called the 'Bionic Glove' to attenuate wrist tremor. The wearable orthosis developed is less obtrusive than WOTAS but it only suppresses tremor at finger or hand flexion-extension. The digital filter designed for the compensation is not adaptive. Based on experiments to approximate the wrist transfer function, a filter is designed such that the system will attenuate only 2-5 Hz motion (tremor). In summary, the approaches surveyed in this section is given in Table. 1.4.

Table 1.4: Comparison of tremor suppression methods

	Positive	Negative
Conventional:		
1. Medicine	Ease of application	Must be individualized
2. Surgery	Effective attenuation	Adverse effects, high cost
Assistive Technology:	Maybe cheaper	No rehabilitative function
1. Through man-machine interface	Effective attenuation	Only at the interface
2. Direct attenuation:		
a. Exoskeleton [Rocon et al., 2007]	Effective attenuation	Probable social exclusion
b. FES [Prochazka et al., 1992]	Less obtrusive than exoskeleton	Non-adaptive solution

1.3 The proposed tremor suppression approach

The two approaches, discussed in the previous section, do not consider surface electromyography (SEMG) for sensing the motion, although SEMG has been used to analyze tremor, e.g. [Strambi et al., 2004]. One important advantage of using SEMG signal is that it precedes kinematics signal by 20-100 ms [Corcos et al., 1992]. This delay is called electromechanical delay (EMD). By utilizing EMD, tremor can be detected before the limb oscillates and then compensated by the

FES at the moment the tremor occurs. The compensation may not be in time if the time taken for FES to actuate a muscle is the same as the EMD. However it has been shown that the EMD caused by FES is shorter than that caused by voluntary motion [Hopkins et al., 2007]. Therefore, if the tremor is detected at the flexor, FES can compensate the tremor by stimulating the extensor and vice versa.

To determine the EMD, another sensor is required which measures the kinematics signal. The use of accelerometer (ACC) for analyzing human movement has been well documented, e.g. [Godfrey et al., 2008]. Therefore we combine both information from SEMG and ACC to measure the tremor. To extract all the information needed for the tremor compensation, an algorithm based on Extended Kalman Filter (EKF) is proposed in Chapter 4 and 5.

Other methods, compared to EKF, sacrifice one thing, e.g. convergence speed, to gain other things, e.g. compensation error [Ziarani and Konrad, 2004] and initial condition [Trapero et al., 2007]. Furthermore, convergence speed is essential for time-varying signals such as tremor. Estimation capability of a method proposed in [Riviere et al., 1998] is comparable to EKF, but it requires a bandpass filter which distorts the crucial phase information of the original signal. Thus it will be shown in detail that EKF can find the necessary balance to achieve our objectives.

The EKF is able to track the fluctuation of tremor characteristics in real-time while keeping a low computation cost. The proposed EKF-based algorithm is also able to separate the tremor from the intended motion. This is important so that the FES does not suppress the intended motion which in the end does not help the subject to do his tasks.

All these algorithms are implemented in the framework of sensing-filtering-actuation shown in Fig. 1.1. The upper limb motion is recorded using SEMG and ACC. Then an EKF-based algorithm obtains the tremor parameters and separates the tremor from the intended motion. The tremor information is processed to activate the FES to counteract the tremor in anti phase. Anti phase cancellation

means that when tremor is detected at the agonist, the counter tremor provided by FES is applied to the antagonist, or vice versa. Everything is done within one sampling time to ensure the real-time requirement of the tremor compensation system.

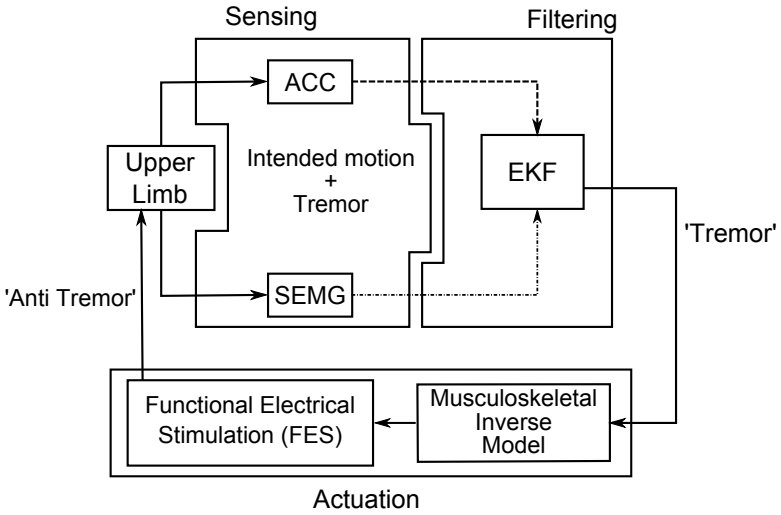

Figure 1.1: Proposed tremor compensation system.

1.4 Scope

This thesis delineates the feasibility of using SEMG, with its advantages and the aid of ACC, to attenuate pathological tremor in real-time framework. It elaborates on how to obtain the necessary information from both sensors and manipulate it to counteract the tremor using Functional Electrical Stimulation (FES). Thus the main focuses of this thesis are sensing and filtering (tremor estimation and separation from intended motion), as shown in Fig. 1.1. For the actuation part, no complex musculoskeletal inverse modeling for control is proposed. Instead a proportional controller is used as it is enough to show the effectiveness of the proposed sensing and filtering algorithm.

However, it should be noted that the proposed sensing chain is adequate to control the musculoskeletal model. Recent work by our collaborator has proposed

a simplified musculoskeletal model to estimate angular acceleration of tremor based on SEMG signal [Rank et al., 2008]. The main advantage of this model, compared to classical model, is the direct measurability of the angular acceleration. In classical Hill model, the output is torque and we cannot measure this directly. Thus a model-based predictive controller is developed for tremor suppression. This work therefore has shown the adequacy of the sensing chain for tuning the musculoskeletal model. However this model has only been tested in simulation.

At the current stage, all algorithms are implemented in a desktop computer. Nevertheless, in the long run it is expected that the whole system can be implemented in a wearable device. With that purpose in mind, all the sensing and actuation proposed in this work are non-invasive and non-obtrusive. Therefore in the end, the subject wearing it will still be able to do his activities of daily living without much hindrance, both physically and emotionally.

In proposing this alternative solution for tremor compensation, only one degree of freedom (DoF) is considered in one upper limb joint. This is to show the feasibility of our solution. The proposed method can be extended to multiple joints, and compensation at multiple DoF per joint may even be possible under some constraints, e.g. the muscles activity can be recorded by surface electrodes and stimulated at the same time, etc.

Consequently 1 DoF tremor compensation experiments are conducted with one healthy subject and one Essential Tremor patient. These are enough to show the possibility of tremor compensation with the proposed solution. Further trials requiring a large number of tremor patients will be part of the future works.

The sensing system proposed here can also provide useful information about tremor to the clinicians. It is expected that a lot of tremor data from various types of tremor will be collected through the collaboration with some hospital and rehabilitation centers in Singapore. Data collection with some patients is carried out and some preliminary results are presented here. This preliminary result

shows that the tremor analysis can be done in a more objective and quantitative manner, hence improving the overall diagnosis and treatment for the patients.

1.5 Technical challenges

Within the scope of this thesis, there are some technical challenges associated with the proposed approach of implementing real-time tremor compensation system:

1. Real-time issues

   The overall system must be implemented in real-time, in the sense that when tremor is detected at a particular time, it must be compensated at that particular sampling period. Phase delay due to the algorithms involved must be avoided, because at worst the actuation can even make the limb to have larger tremor.

2. Estimation issues

   When the recorded signal from the sensors contains the tremor, we should extract useful information from the raw data for real-time compensation. This also includes separation of tremor from the voluntary motion as the recorded upper limb data may contain both components.

3. Actuation issues

   The issues are not about actuation *per se* because the musculoskeletal inverse modeling is not within the scope of this thesis, although it deserves further study.

   Nevertheless, by using FES for the actuation, there are two arising issues which are related to the estimation part. The first is the fact that FES corrupts SEMG signal in significant manner. This FES artifact must be removed as much as possible so that a good tremor signal can be obtained. Another important issue in using FES to compensate tremor is the timing to start and stop the stimulation. This problem is not straightforward due

to the EMD and its different value for voluntary and involuntary motion as discussed in Section 1.3. Thus using the tremor information and the EMDs, a method is proposed so that tremor can be compensated in anti phase.

1.6 Objectives

Based on the technical challenges, the objectives of this dissertation research are as follow:

1. To provide a hardware platform for real-time tremor compensation. For the study undertaken in this thesis, the algorithms are implemented in a desktop computer, but it can be extended into a wearable orthosis.

2. To develop an algorithm to extract various tremor parameters from both SEMG and ACC signal.

3. To develop an algorithm which is able to separate tremor and intended motion.

4. To implement an artifact suppression algorithm. Signal from FES will contaminate SEMG reading. Therefore these artifacts have to be minimized so that useful information can be extracted from the SEMG.

5. To propose a method to determine when to start and stop the stimulation based on the estimated tremor parameters.

6. To test the feasibility of the proposed algorithm in healthy subjects and tremor patients.

1.7 Organization

The remaining chapters of this report are organized as follow:

- Chapter 2 presents a literature survey for tremor sensing and compensation. It also gives justification for the choice of sensor (SEMG and ACC) and actuator (FES) used in this work.

- Chapter 3 presents some useful results from the tremor data collection. It shows that the sensing system is able to detect tremor and it gives possibility for compensation. The results are also useful to provide the clinicians with more objective assessment of tremor.

- Chapter 4 proposes an EKF-based algorithm to obtain the tremor parameters and to remove the intended motion. The separation of tremor and intended motion is also discussed here.

- Chapter 5 proposes an FES artifact suppression algorithm. This algorithm is necessary so that the SEMG signal contains lesser noise and artifacts. This chapter also presents a way to utilize the advantage of using SEMG signal, especially in the timing consideration (start/stop) for real-time tremor compensation. Lastly, experimental results from healthy subject and tremor patients are shown.

- Chapter 6 summarizes the contributions of this thesis and lays out some future directions for the work.

Chapter 2

Tremor Sensing System

This chapter gives a survey of the available options in the literature for tremor sensing and compensation system. It also provides justification for the selection of our sensor and actuator for the proposed tremor suppression system, i.e. surface electromyography (SEMG), accelerometer (ACC), and Functional Electrical Stimulation (FES).

2.1 Survey of sensing systems for hand tremor

Sensors can be classified into two major groups, externally referenced sensors and internally referenced sensors (inertial sensors). In externally referenced sensors, a sensor is attached to the object, but there is another receiver or source to obtain the measurement. In tremor sensing literature such examples are laser system, electromagnetic system, and optical motion capture system.

2.1.1 External sensors

When using a laser system and optical motion capture system, a 'line of sight' is required between the sensor and the receiver. If this line of sight is blocked, information is lost. The velocity transducer developed in [Norman et al., 1999]

is used to measure finger tremor and requires the measured limb to remain approximately perpendicular to the laser beam for accurate measurement, which may restrict the clinical utility of this system. An index based on tremor amplitude, frequency, and harmonicity is proposed from a laser system to differentiate Parkinson's Disease (PD) tremor from control subjects [Edwards and Beuter, 1999].

Examples of optical motion capture for tremor analysis is given in [Cappello et al., 1997; Pellegrini et al., 2004]. In [Cappello et al., 1997], the camera is used to analyze tremor quantitatively using auto regressive (AR) method, while in [Pellegrini et al., 2004] the system is used to analyze hand tremor when performing goal-oriented postural pointing.

Electromagnetic system such as one proposed in [Rajaraman et al., 2000] does not need a line of sight, but metallic items nearby can cause interference to the system. In their work, the system is used to observe the effect of Pramipexole intake by measuring finger tremor at rest and while performing various tasks. Operating range is also a challenge, e.g. in [Yu et al., 2003]. The electromagnetic data glove they developed to analyze hand tremor has an operating range of 0.4 m. For classification purpose, a commercial electromagnetic system is used to differentiate between PD, ET, and normal subject [Spyers-Ashby et al., 1999]. Applying AR modeling and k-nearest algorithm to the data, a maximum of 80% classification is obtained.

This category of sensors is then useful for recording tremor data in constrained environment and for further offline tremor analysis. Nevertheless it cannot be possibly implemented as a wearable system in daily life. On the other side, internally-referenced sensor is "self-contained" and therefore suitable for wearable system.

2.1.2 Internally-referenced sensors

2.1.2.1 Accelerometer (ACC)

Accelerometer has been proposed for long term continuous tremor monitoring [Yang et al., 2003]. The ACC chip is wrist-worn, thus enabling the long recording outside clinical environment. The recorded signal is a complete ACC data compared to the similar system proposed in [Van Someren et al., 1998].

From the accelerometer data, some features can be extracted and some differentiation of different type of tremor can be obtained, as described in the following examples. Discriminant analysis is applied to tremor amplitude, frequency, and shape and k-means clustering is able to separate between essential and physiological tremor (94.74% correct) [Wharrad and Jefferson, 2000]. As tremor is considered as a stochastic signal, higher order statistics is used to characterize tremor. Thirty features are extracted and multi layer perceptron (MLP) is able to get less than 3% error between PD, ET, and physiological tremor [Jakubowski et al., 2002]. Another neural network approach to differentiate the same types of tremors is proposed in [Engin, 2007]. The learning algorithm used is Broyden-Fletcher-Goldfarb-Shanno (BFGS) algorithm, and the feature vector consists of wavelet based entropy and variance for six scales, linear prediction coefficients for third order model, and the power ratio for 28 Hz band. The classification accuracy obtained is 91.02% [Engin, 2007].

Latest development in sensor technology has enabled a production of low power, wireless, noninvasive, low cost, and real time wearable system based on triaxial ACC [Powell Jr. et al., 2009]. Signal processing methods based on cross correlation and filter banks give a further useful information for clinical assessment of tremor. Their proposed system is called Technology Enabled Medical Precision Observation (TEMPO) and it has the following features [Powell Jr. et al., 2009]:

- It can support 4 triaxial ACC (12 inputs).

- The battery is capable of supporting more than 8 hours of recording.
- It costs less than US$ 1000.

It should be noted that in all these methods, no position and orientation of the limb is estimated from the ACC data. This is another separate issue and it has been tackled by many. In [Giansanti et al., 2003], the ACC placement scheme proposed by [Padgaonkar et al., 1975] and [Morris, 1973] is analyzed and it is argued that those schemes are in fact not suitable for clinical setting. This is because the errors in the ACC axes and the offset error are not negligible even when we consider short time recording (4s). Tan and Park [Tan and Park, 2005] examine the feasibility of designing an inertial navigation system which uses only ACCs to compute the linear and angular motions of a rigid body. A sufficient condition is proposed to determine whether a configuration of ACCs is feasible to compute linear and angular motions. Then a simple algorithm is developed based on the corresponding dynamical system equations for a special cube configuration.

2.1.2.2 Accelerometer and gyroscope

Another commonly used inertial sensor is gyroscope, which measures angular velocity. However in the literature it has not been used frequently in tremor measurement. A noted example is the work by [Salarian et al., 2007]. They attach 2 uniaxial gyroscopes on the wrist to detect and measure the tremor of PD patients during daily activities such as sitting, standing, eating, writing, walking, etc. The gyroscopes are integrated with a data logger, memory card, and battery in a small package, so that the system can record continuously for 14 hours with 200 Hz sampling rate. The system is called ASUR (Autonomous Sensing Unit Recorder). The data processing is able to obtain 95% sensitivity and 94.2 % specificity in tremor identification.

Combination of accelerometer and gyroscope is proposed in [Luinge et al., 2007] and [Hyde et al., 2008]. In [Luinge et al., 2007], Kalman filtering is used to

fuse the information from both sensors and anatomical restriction in the elbow are found to be not sufficient for practical applications. This is because the error can reach up to 20°. A better estimation is achieved by a composite filter and it is applied to upper limb tremor quantification for multiple sclerosis patients [Hyde et al., 2008].

There are other efforts to estimate upper limb position and orientation using inertial sensors, such as in [Giansanti et al., 2005], Kalman filter based algorithm [Zhu and Zhou, 2004], and quaternion based algorithm [Yun and Bachmann, 2006]. Nevertheless these algorithms have never been tested for tremor quantification which requires higher system bandwidth. Their proposed system is constructed using $2g$ accelerometer and 90°/s angular rate sensors. The angular velocity of a 5 Hz rest tremor with 10°amplitude is 100°/s, which is higher than the proposed system in [Yun and Bachmann, 2006].

2.1.2.3 Surface Electromyography (SEMG)

Surface electromyography provides another possible alternative for tremor recording outside clinical setting, albeit at a higher cost. Some works have been done to analyze tremor with SEMG system. Milanov [Milanov, 2001] examines the possibility of using electromyographic inspection to differentiate tremors. Data from 525 patients with various types of tremor is observed (repeated at least 3 times in a 1-year period). Evaluating the common parameters of tremor such as frequency, amplitude, this work also uses burst duration and pattern for the classification. Statistical analysis is performed and an algorithm for differentiation is developed. He concludes that SEMG may serve as a tool for differentiation of tremors. A simpler classification work is also proposed previously by [Spieker et al., 1995].

Using the same tremor parameters, he also employs SEMG to re-evaluate the clinical and electromyographic pattern of different PD tremors [Milanov, 2000], study the effect of beta-blocker and primidone on essential tremor [Milanov, 2002],

and investigate the SEMG pattern of tremor in patients with depression [Milanov et al., 2000].

2.1.2.4 Combination of ACC and SEMG

Both ACC and SEMG have also been used to extract information from tremor for further analysis or classification. Time and frequency information from ACC and SEMG is analyzed to gain more understanding in assessing individuals with PD [Vaillancourt and Newell, 2000]. Cross spectra method is used to study whether bilateral tremor can be explained by a common source or not, though ACC is only used to quantify tremor severity and as a mechanical reference [Lauk et al., 1999].

The usual tremor parameters such as amplitude and frequency have been extracted from ACC and SEMG to distinguish physiological tremor from early stage and low amplitude pathologic tremor [Raethjen et al., 2004]. However, quantitative measures like frequency and amplitude are very sensitive to the details of the recording condition or technique and therefore need to be normalized for each individual lab. Together with the bursting pattern, 86% correctness in classifying PD and 95% in ET is achieved [Burne et al., 2002]. More complex features are extracted, such as kurtosis variable, coherence, and sample entropy in [Rissanen et al., 2008]. The total 12 features are then reduced by PCA and k-means clustering algorithm is employed as the classifier. One cluster contains 90% of the normal subject, while two other clusters contain 76% of the patients. ACC and SEMG signals have also been used to differentiate pathological tremors using data mining techniques [Bonato et al., 2004] and to identify functional activity [Nawab et al., 2004].

A summary of tremor sensing system surveyed above is given in Table 2.1.

Table 2.1: Survey of tremor sensing system

External
Laser [Norman et al., 1999], Optical [Pellegrini et al., 2004], Electromagnetic [Yu et al., 2003] (+) Accurate (–) Expensive, requiring line of sight, not applicable in activities of daily living
Internally-referenced *Accelerometer only* [Yang et al., 2003]: Wrist -worn ACC chip for long term tremor monitoring. [Wharrad and Jefferson, 2000]: Discriminant analysis to tremor parameters. [Jakubowski et al., 2002]: Higher order statistics to characterize tremor. [Engin, 2007]: Neural network approach to classify tremor. No position and orientation (P&O) But, there is extraction of parameters, such as amplitude, frequency, etc. P&O estimation: [Giansanti et al., 2003]: ACC only is not suitable for clinical use. [Tan and Park, 2005]: feasibility of ACC only system. *Accelerometer and gyroscope* Gyroscope only, e.g. [Salarian et al., 2007]. Combination with ACC, e.g.: [Hyde et al., 2008]: quantification of multiple sclerosis. [Yun and Bachmann, 2006]: quaternion-based algorithm to estimate P&O. *Surface electromyography* Usually for tremor classification, e.g. [Milanov, 2001] *Accelerometer and surface electromyography* Parameter extraction and classification from both sensors [Lauk et al., 1999; Raethjen et al., 2004; Vaillancourt and Newell, 2000]

2.1.3 Tremor compensation system

So far, the sensing considered in the literature review above is focused more on tremor analysis and not for suppression purpose. As mentioned in the introduction chapter, there are two categories of assistive technology in tremor suppression: (i) to suppress tremor at the man-machine interface, and (ii) to attenuate the tremor directly.

In the first category, if the interface is computer based, then the sensor is basically the input of the computer, such as joystick [Gonzalez et al., 2000; Riley and Rosen, 1987], pen input [Riviere and Thakor, 1995], or haptic interface [Pledgie et al., 2000]. The input to the computer is actually the command added with

tremor. The computer can then apply various algorithms to remove the tremor. The supposedly clean signal is then used for moving the cursor in the computer screen.

If the interface is mechanical, usually it will provide some kind of damping. A spring-mass-damper system is proposed as vibration absorber to attenuate rest tremor in PD [Hashemi et al., 2004]. Previously, a controlled energy dissipation orthosis (CEDO) has also been developed using the concept of velocity-dependent resistive load [Arnold et al., 1993]. Another viscous damper system, also available commercially, is called Neater Eater (Neater Solutions Ltd, Derbyshire, UK). The concern about all these solutions is that they are very specific to a certain task and once the patient is not attached to the system, tremor cannot be attenuated.

Rocon et. al. have developed a robotic exoskeleton called Wearable Orthosis for Tremor Assessment and Suppression (WOTAS) [Rocon et al., 2007]. This exoskeleton uses gyroscope and strain gauge to sense 3 Degree-of-Freedom (DoF) motion of upper arm (wrist and elbow flexion-extension and forearm pronation-supination). DC motor is used for the actuation. Despite good compensation result, the patients considered that the use of the exoskeleton "should cause social exclusion". Furthermore, although adding weight to the tremulous limb may reduce tremor [Héroux et al., 2009], the effect of the exoskeleton mass (reported to be around 850 g) on the attenuation of tremor is not discussed.

Prochazka et al. have shown that it is possible to use feedback-controlled Functional Electrical Stimulation (FES) to attenuate pathological tremor [Prochazka et al., 1992]. Later on, its implementation was improved by using a digital controller and accelerometer as the sensor. Better attenuation result is achieved (84% for digital controller compared to 65% for the analog version) [Gillard et al., 1999]. The wearable orthosis developed is less obtrusive than WOTAS but it only suppresses tremor at finger or hand flexion-extension. However the digital filter designed for the compensation is not adaptive.

2.2 Proposed real-time tremor compensation system

The approaches in [Rocon et al., 2007] and [Prochazka et al., 1992] do not consider surface electromyography (SEMG) for sensing the motion, although SEMG has been used to analyze tremor, e.g. [Strambi et al., 2004]. One important advantage of using SEMG signal is that it precedes kinematics signal by 20-100 ms [Corcos et al., 1992]. This delay is called electromechanical delay (EMD). By utilizing EMD, tremor can be detected before the limb oscillates and then compensated by the FES at the moment the tremor occurs. The compensation may not be in time if the time taken for FES to actuate a muscle is the same as the EMD. But it has been shown that the EMD caused by FES is shorter than that caused by voluntary motion [Hopkins et al., 2007]. The shorter EMD is caused by reverse recruitment order, in which larger muscle fibers are recruited first during electrical stimulation, thus enhancing the rate of force development [Hopkins et al., 2007]. Therefore, if the tremor is detected at the flexor, FES can compensate the tremor by stimulating the extensor and vice versa.

To determine the EMD, another sensor is required which measures the kinematics signal. The use of accelerometer (ACC) for analyzing human movement has been well documented, e.g. in [Godfrey et al., 2008]. Therefore we combine both information from SEMG and ACC to measure the tremor. This thesis delineates the feasibility of using SEMG, with its advantages and the aid of ACC, to attenuate pathological tremor in real-time. To extract all the information needed for the tremor compensation, an algorithm based on Extended Kalman Filter (EKF) is proposed. The EKF is able to track the fluctuation of tremor characteristics in real-time while keeping a low computation cost.

This section will describe each of the sensors and actuator proposed for our real-time tremor compensation system, followed by the overview of the complete implemented system for tremor attenuation.

2.2.1 Surface EMG

With the advancement in technology, electromyography has been used in many applications in different fields related with muscle activity. Neurologists use EMG recordings to determine the integrity of neural pathways, neurophysiologists use EMGs to test control and reflex mechanism and identify synergistic patterns, clinicians use EMGs in a wide range of pathologies to identify atypical motor patterns, biomechanists and bioengineers use EMGs in a wide variety of muscle models and to actuate myoelectric prostheses, and ergonomists use EMGs as indicators of stress and fatigue [Kumar and Mital, 1996]. This section will give a brief overview on SEMG.

In order to understand EMG signal some basic physiological concepts of it need to be understood. The most fundamental unit of a muscle is called motor unit (MU). It consists of a single α motor neuron, its neuromuscular junction, and the muscle fibers it innervates. The cell body of α motor neuron is located in anterior horn of the spinal cord and the axon connects the body with the muscle fibers. Hereafter, in referring to either cell body or axon of the motor neuron, the term 'motor neuron' will simply be used. The net membrane current induced in this motor neuron by various synaptic innervation sites determines the discharge (firing) pattern of the motor unit. Each muscle may have 100-1000 MU [Merletti and Parker, 2004].

The electrical signal that emanates from the activation of the muscle fibers of a motor unit is called the motor unit action potential (MUAP). The activation from the central nervous system (CNS) is repeated continuously as long as the muscle is required to generate force. This continued activation generates motor unit action potential trains (MUAPT). These trains from the concurrently active motor units superimpose to form the EMG signal and finally with this electrical activity, the muscle will contract. These processes are depicted in Fig. 2.1 and Fig. 2.2. More detailed explanation on physiology and biophysics of EMG signal

generation can be found in chapter 1 and 4 of Merletti and Parker [Merletti and Parker, 2004].

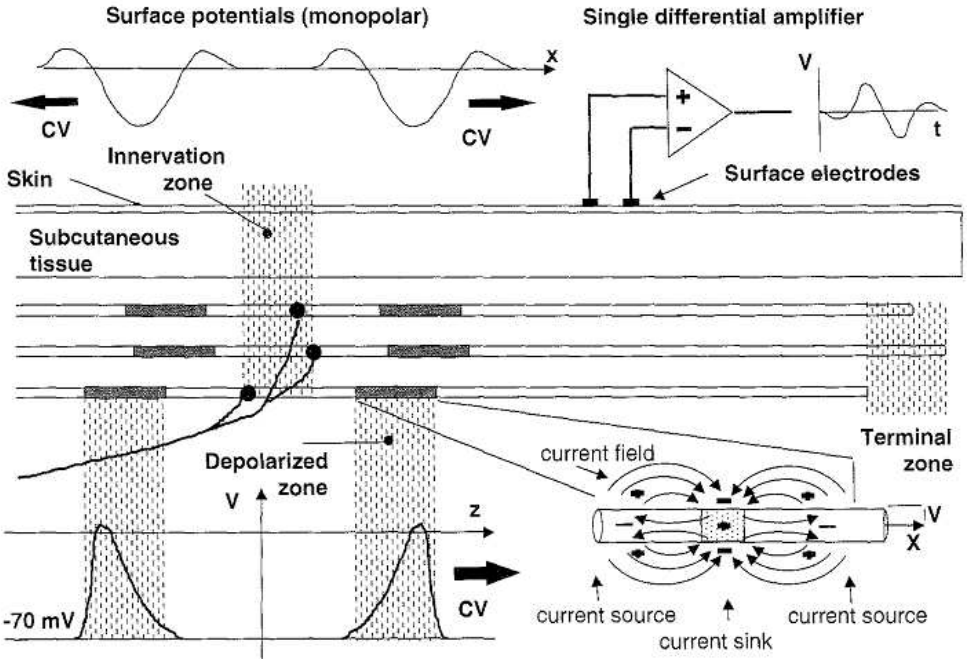

Figure 2.1: Representation of a motor unit (MU) and of a motor unit action potential (MUAP) [Merletti and Parker, 2004]

There are two types of electrodes used to detect EMG signal. The first is surface electrode (attached to the surface of skin) and the other is indwelling electrode (wire or needle). The electrodes are usually used singularly (monopolar) or in pairs (bipolar).

Indwelling needle and wire electrodes are inserted into the muscle tissue. This indwelling type is usually employed in studies of physiology and pathology of the MU, e.g. diseases affecting the muscle fiber (e.g. muscular dystrophies) or neuromuscular junction (e.g. myasthenia gravis), firing rate of MU, and recruitment pattern of MU. This is because needle and wire electrodes are small and fine in size such that they have a high selectivity with minimal interference signals from adjacent cells. Using indwelling electrodes will also benefit the study of deep muscles. But the method is poorly repeatable in some applications such as recording

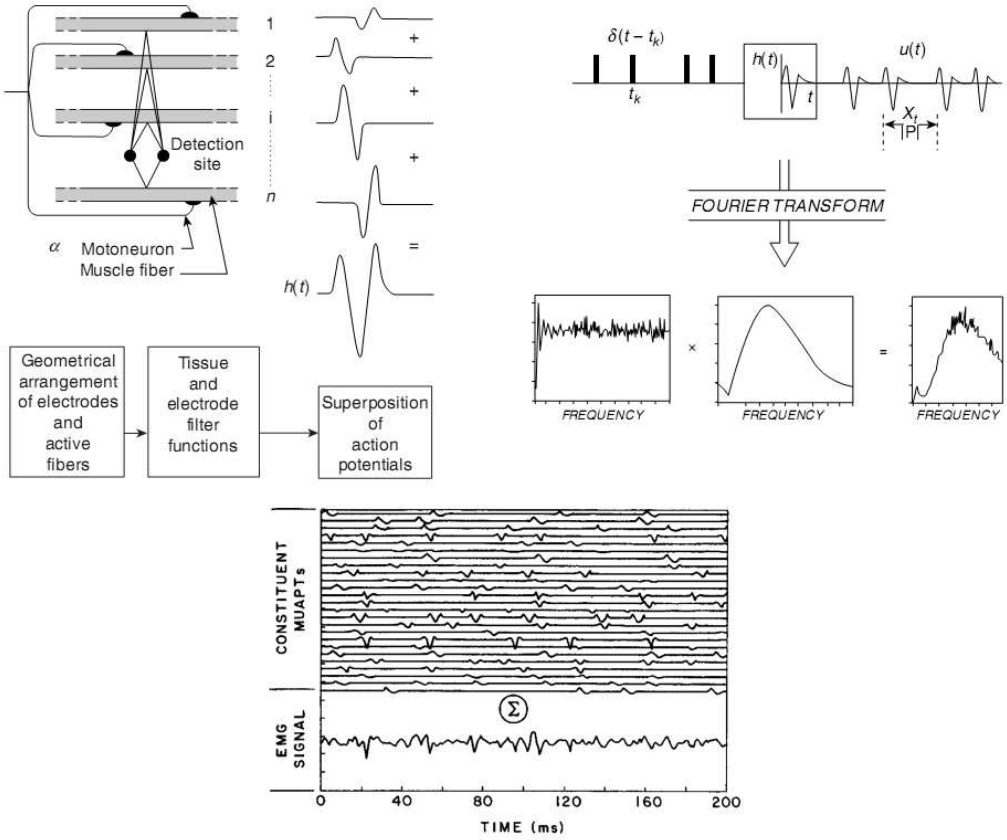

Figure 2.2: Schematic representation of the generation of the EMG signal [Luca, 2006]

distinguishable MUAPT because it is not certain whether the electrode has been inserted in the same place or not. Also, there is a tendency for the electrode to move with respect to the tissue during contraction/movement. This implies a number of restrictions for the interpretation of the signal.

On the other hand, surface electrodes are usually better suited for studies in which information is sought on the various aspects of behavior, temporal pattern of activity, or fatigue of the muscle as a whole or of muscle groups [Merletti and Parker, 2004]. The noninvasive nature of surface electrode also finds its way in many applications such as sport and rehabilitation where needle techniques are not acceptable or, when assessments have to be repeated frequently. Additionally, surface electrode becomes increasingly important in the diagnosis of neuromuscular disorders [Rau et al., 2004].

It is well established that surface electromyogram (SEMG) recorded from bipolar electrodes during constant force, constant-angle, nonfatiguing contractions can be well modeled as a zero-mean, correlation-ergodic, random process which is Gaussian distributed [Clancy and Hogan, 1999]. Because of the nature of motor unit activation in muscle, the measured signal resembles a zero-mean random (stochastic) process whose standard deviation is proportional to the number of active motor units and the rate at which motor units is activated [Clancy et al., 2002].

The amplitude of the signal can range from 0 to 10 mV (peak-to-peak) or 0 to 1.5 mV (RMS). The usable energy of the signal is in the frequency range of 10-400 Hz. The mean frequency (centroid or center of gravity, indicated as MNF) of the spectrum is in the range of 70-130 Hz, and the median frequency (frequency value that splits the spectrum into two parts containing equal power, indicated as MDF) is in the range of 50-110 Hz [Merletti et al., 2001].

There are two groups of factors which affect SEMG signal: (1) geometrical and anatomical factors and (2) physiological factors. The geometrical and anatomical factors are those related with the electrode structure and its placement on the muscle thus can usually be controlled. On the other side physiological factors

cannot be controlled because they are associated with the muscle characteristics of the subject. There are some papers which discuss the factors affecting SEMG signal in more exhaustive manner [Farina et al., 2002; Luca, 1997; Merletti et al., 2001].

Another consideration to bear in mind is that the factors mentioned above may change over time. It means that the parameters extracted from SEMG recording from different time (of the same patient) may change [Rainoldi et al., 1999]. Nevertheless, by proposing adaptive algorithm for SEMG parameter estimation (Chapter 4), it is expected that the effect of SEMG recording variability is minimized.

SEMG is chosen as it can provide motion information ahead of time compared to ACC (electromechanical delay, as explained in the following section). Moreover, the neuromuscular information which cannot be provided by ACC will be useful later on for modeling purpose.

2.2.1.1 Electromechanical Delay (EMD)

Electromechanical delay is the time delay between the onset of muscle activation and the onset of force or motion as detected by the sensing system [Corcos et al., 1992]. The delay is caused by the propagation of the action potential along the excitable muscle membranes, Ca^{++} release into the sarcoplasma and subsequent binding to active sites, the formation of cross bridges, and tension to the series elastic component (SEC) [Hopkins et al., 2007]. Nevertheless, it has been argued that this delay is also sensitive to the way data is collected and processed [Corcos et al., 1992]. One of the reasons is that estimation of this value depends on a certain thresholding. This thresholding certainly depends on the noise level of the equipment, resolution of analog to digital converter, etc, which are actually not related to the generation of movement itself. Thus as long as the recording setup is consistent, this fact should pose no problem. We are only interested in the overall time delay, not the physiological meaning of the EMD.

Joint angle (of knee flexion-extension) has been found to have significant effect on the EMD measured in the knee extension [Sinclair et al., 2004]. In that work, the stimulation is used to evoke isometric knee extension. It is found that at 15°, the EMD is twice compared to an angle of 90°. We have not investigated this effect on upper limb, however we propose an algorithm to estimate this fluctuating EMD discussed in later chapters.

2.2.2 Accelerometer

A sensor detecting acceleration is preferred to one measuring displacement or velocity because of the motion characteristics. Tremor usually has higher frequency and lower amplitude than voluntary movement. Hence, in acceleration domain, the tremor signal is enhanced and captured better by the sensor.

Accelerometer is an inertial sensor detecting static (gravity) and dynamic (motion) acceleration. The measured acceleration defined in 2.1 comprises of 5 components: the inertial acceleration of the link, a_{CG}, centripetal acceleration, a_C, tangential acceleration, a_T, Coriolis acceleration, a_{CR} (0 if there is no translational motion), and gravitational acceleration, g.

$$\begin{aligned} a(k) &= a_{CG}(k) + a_C(k) + a_T(k) + a_{CR} + R_{\theta(k)}g \\ &= a_{CG}(k) + \omega(k) \times (\omega(k) \times P_a) + \alpha(k) \times P_a + R_{\theta(k)}g \end{aligned} \tag{2.1}$$

where $k = 1, 2, 3, \ldots$, P_a, is the position of the accelerometer with respect to the world coordinate, and assuming sampling period is 1 without losing generalization.

In this thesis, we use an analog accelerometer solution (DE-ACCM3D, 21 x 10 x 8 mm - incorporating the ADXL330) produced by Dimension Engineering (Ohio, US). The ADXL330 is a 3-axis MEMS acceleration measurement system on a single monolithic integrated circuit produced by Analog Devices Inc. and has a minimum measurement range of ± 3 g.

There are two main reasons why this board is chosen. Firstly, DE-ACCM3D provides integrated operational amplifier buffers for direct connection to a microcontroller's analog inputs, or for driving heavier loads. The output impedance of ADXL330 is considered high (32 kΩ) and previous experience has shown impedance matching problem (the impedance of the data acquisition input channel is not significantly larger than 32K). A buffer significantly reduces this problem. Secondly, DE-ACCM3D has an onboard 3.3 V regulator and decoupling capacitor to give great flexibility when powering the device. The accelerometer output depends on many factors, one of which is the power supply. A noisy power supply produces a noisy output. Therefore, a voltage regulator is useful.

In DE-ACCM3D, the bandwidth of the ADXL330 is set to be 500 Hz. Default operating voltage is 3.33 V and the current consumption is 0.9 mA. It is designed to fit the DIP-16 form factor, making it suitable for breadboarding, perfboarding, and insertion into standard chip sockets. The board layout is given in Fig. 2.3. Each of the accelerometer board, DE-ACC3MD, glued into Perspex (acrylic) casing, is then attached to the limb using velcro strap.

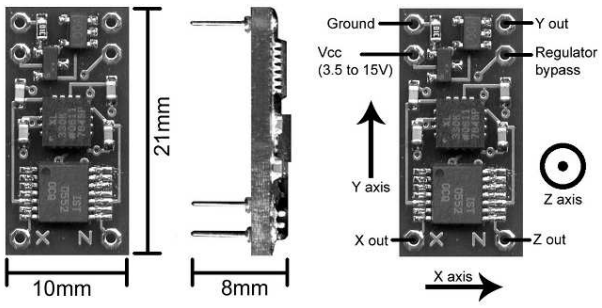

Figure 2.3: Board layout of accelerometer used in this thesis

2.2.3 Functional Electrical Stimulation (FES)

For the actuator, we are using Functional Electrical Stimulation (FES). Short pulses of electrical stimulation cause muscle to contract. Thus if a tremor burst is detected in a muscle in an antagonistic pair, then electrical stimulation can be

used to stimulate the other muscle in the pair so that the tremor is attenuated. Strictly speaking, what is stimulated is actually the motor neurons, therefore the motor neurons in the subject must be intact to enable the usage of FES [Popovic et al., 2001]. Clinically, electrical stimulation is divided into therapeutic and functional stimulation. Functional stimulation aims to provide movements which in turn restores the function they serve [Rushton, 1997]. Thus electrical stimulation for tremor attenuation which enables the person to do their activities of daily living is categorized as functional.

As with EMG, the electrodes for FES can be transcutaneous (surface) or implanted. Another option is percutaneous electrode which uses wire electrodes inserted to the muscles close to the motor neurons with an epidermal needle [Peckham and Knutson, 2005]. Implanted electrode gives a better selectivity in stimulation but it is invasive. The approach taken in this work is non-invasive sensing and actuation.

There are four important factors to consider in generating electrical stimulation: pulse amplitude, pulse width, frequency, and pulse shape. An asymmetric biphasic pulse is employed. Biphasic signal is chosen to remove the induced electric charge from FES. If such sharp edge negative monophasic current pulse is applied over a long period of time, the unidirectional ion current flow has the potential for ion accumulation and skin irritation. Asymmetric stimulation pulses are produced such that the action potential is only generated under one of the two stimulation electrodes [Keller, 2001]. The typical pulse used in this thesis is shown in Fig. 2.4.

The stimulation pulse width is generally be set to 100 - 300 μs because longer pulses will only recruit a few more nerve fibers [Keller, 2001]. On the other hand, less than 50 μs will require a high stimulus intensity. Thus the average, which is 200 μs will be used in this thesis. Pulse frequency is set to 25 Hz so that it will not cause more fatigue by extreme tetanization [Keller, 2001] and it is the submultiple of 50 Hz (the power line frequency in Singapore). This is necessary so that the comb filter can remove the power line interference and the residual

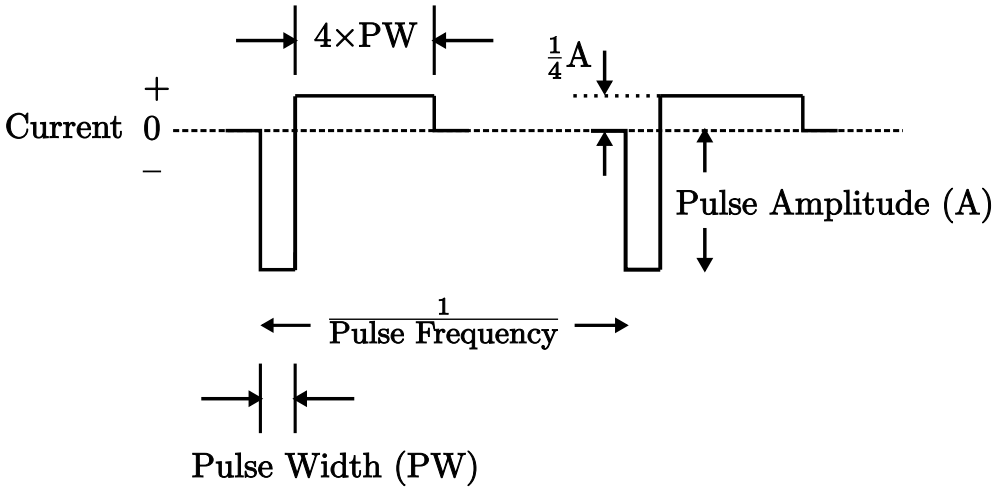

Figure 2.4: Stimulation pulse generated by the FES system in this thesis. Pulse width = 100-300 μs and pulse frequency is 25 Hz. Pulse amplitude is about 20 mA for upper limb. Note that each pulse is charge balanced.

artifacts from the FES [Frigo et al., 2000]. If it is set lower than 25 Hz, but still a submultiple of 50 Hz, e.g. 16.67 Hz, more noise/artifact is introduced since it will require higher current to produce a given amount of force.

It should be noted that there are few fundamental differences between voluntary motion and electrically stimulated motion. Firstly, in electrical stimulation, many motor neurons are stimulated at the same time. To maintain a tetanic contraction (sustained, constant tension) in voluntary motor tasks, the pulses are sent asynchronously from many motor neurons to ensure that at a particular time there is always contraction in any muscle fibers. Electrical stimulation cannot do this. It can only stimulate the motor neurons at the same time. The consequence is that the pulse frequency for electrical stimulation is higher (20-40 Hz) than that in voluntary motion (6-8 Hz) [Lynch and Popovic, 2008]. This higher frequency causes fatigue to come in faster as there are more contractions that occur during FES stimulation.

Another debatable difference between movement caused by electrical stimulation and CNS is the muscle fiber recruitment. In physiological muscle contraction, the slow, low-force, fatigue-resistant motor units are recruited first [Rushton,

1997]. On the contrary, the fast and fatigable motor units are recruited first in electrical stimulation. This type of fibers is innervated by axons with a larger diameter than that of the slow type fibers. Larger diameter axons cause the fast fibers to respond at lower stimulation level [Lynch and Popovic, 2008]. This fact results in more fatigue. But recently this reverse recruitment order has been contented in [Gregory and Bickel, 2005].

2.2.4 System overview of the proposed system

The hardware setup for this system is shown in Fig. 2.5. To show the feasibility of using both SEMG and ACC in tremor compensation, only one DoF at one joint is considered in this thesis, i.e. wrist flexion-extension. Both SEMG readings from wrist flexor and extensor are obtained and a 3-axis accelerometer is attached to the dorsum of the hand. All the signals are acquired by a data acquisition (DAQ) card installed in a PC, where all the algorithms are implemented. The output command to attenuate the tremor is sent to the FES system via the DAQ analog output ports.

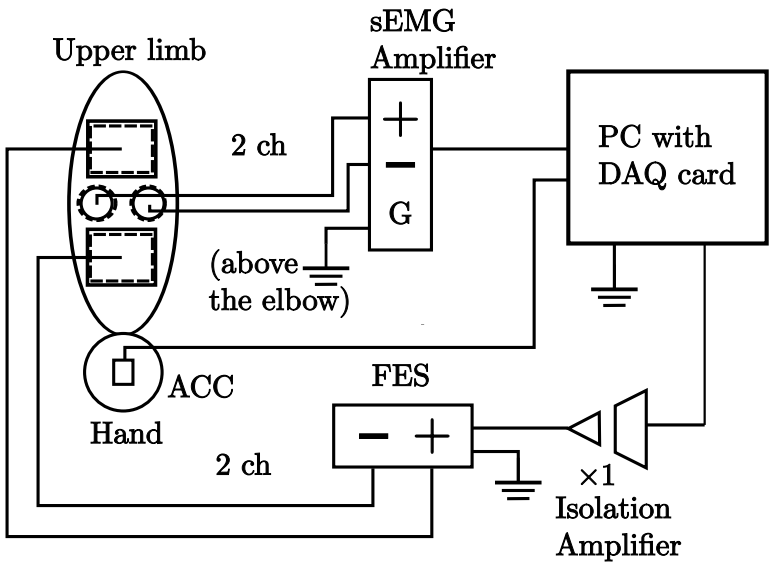

Figure 2.5: Hardware setup of real time tremor compensation.

The EMG amplifier is used in differential mode (EMG100C from Biopac, USA). The gain is set at 500 and the internal filters to let through 10-500 Hz signal. The electrodes used are Skintact F-301: Ag/AgCl, disc, 10 mm diameter (contact area), 30 mm diameter adhesive foam backing, disposable, pre-gelled. Alcohol is applied to clean the skin before placing the electrodes. Inter electrode distance is about 25-30 mm. The bipolar electrodes are placed with the orientation perpendicular to the muscle fibers. This orientation is chosen because it can reduce the stimulation artifacts by increasing the common mode components [Frigo et al., 2000]. For wrist flexion, the muscle used is flexor carpi ulnaris and for extension, extensor carpi radialis. The reference electrode is placed just above the elbow. Details about the SEMG electrode and amplifier specifications are laid out in the next chapter.

We use an analog accelerometer solution (DE-ACCM3D, 21x10x8 mm) produced by Dimension Engineering. The ADXL330 chip (Analog Devices Inc., USA) on the DE-ACCM3D is a 3-axis MEMS accelerometer and it has a typical measurement range of $\pm 3.6g$. DE-ACCM3D provides integrated operational amplifier buffers and voltage regulator. The bandwidth of the ADXL330 is set to be 500 Hz and this accelerometer board is enclosed in a Perspex casing.

The data acquisition card that is used to digitize the SEMG signal is the PD2-MF-16-150/16H Multifunction board (United Electronic Industries, USA). It has 16 channels of analog inputs with 150 KHz total sampling rate (16 bit resolution). For the output, the PD2-AO Analog-Output board (United Electronic Industries, USA) is used. It has 32 analog output channels with 100 KHz total output rate (16 bit resolution). These analog outputs are connected to the analog input port of the FES system. Both cards are installed in a P4-3GHz, 1GB RAM PC via the PCI slots.

The programming of the algorithms is done using C language in a real time operating system, QNX (QNX Software System International Corporation, Canada). Using QNX ver. 6.3.B4 in this PC, an output rate of 1 KHz is guaranteed for

controlling 2 output channels for FES while acquiring data from 2 channels of SEMG and 3 channels of accelerometer input.

The FES system used is Compex 2 from Compex SA, Switzerland. It has four stimulation channels and two analog inputs. The analog inputs of Compex 2 (0-5 V) can be programmed to control the FES current amplitude. Compex 2 has an amplitude resolution 1 mA and it can produce current up to 125 mA. For safety purpose, the connection between the DAQ system and FES is isolated with analog isolation amplifier, ISO124 (Texas Instruments Inc., USA).

Chapter 3

Tremor Sensing Experiments

This chapter will show that the proposed sensing modalities can obtain useful information about tremor. Data collection has been carried out in 20 tremor patients (age: 22-71 years, with average 53.75 years). Among the subjects with tremor, 7 of them are PD patients, 6 were diagnosed with ET, and other types of tremor. For the baseline, eighteen normal subjects (mean age 44.9 years, range 17-70 years) were also recruited. Before doing the data collection, a neurologist is there to explain the experiment to the subjects and the subjects sign a consent form which has already been approved by the ethical board.

The inclusion and exclusion criteria is given below. Then the sensing system setup is discussed. The system consists of SEMG, ACC, and an optical tracking system. Following that, some results are shown. Further analysis done by our collaborator from National Neuroscience Institute of Singapore has also shown that a classifier can be designed to differentiate types of tremor.

3.1 System setup for data collection

3.1.1 Patient selection

Inclusion criteria: If the subject has tremor and the tremor affects at least one of the upper limbs, the subject is categorized as patient. If the subject does not

have tremor and past medical history of a tremor disorder, he/she is categorized as normal.

Exclusion criteria:

- Subject has difficulty giving informed consent
- Subject has a cardiac pacemaker or similar device
- Subject has a deep brain stimulator or similar device
- Subject has a sensitive skin condition
- Subject requires support/assistance to sit
- Subject has difficulty following verbal instructions
- Subject has severe comorbidities or any other conditions that may hinder their ability to participate in the study (e.g. chronic obstructive lung disease, angina, congestive cardiac failure, severe renal or liver failure, malignancy).

3.1.2 SEMG amplifier specifications

The amplifier and A/D system used in this thesis is from Biopac EMG100C. The detection mode used in this thesis is differential mode. The cutoff frequencies used are 10 Hz for high pass filter and 500 Hz for low pass filter. Gain is set to be 500. The specifications of the SEMG amplifier is given below for completeness.

- Gain: 500, 1000, 2000, 5000
- Output range: $\pm$10V (analog)
- Low pass filter: 500 and 5000 Hz
- High pass filter: 1, 10, and 100 Hz
- Notch filter: 50dB rejection 50/60Hz

- Noise voltage: 0.2μV rms (10-500Hz)
- Z input: 2MΩ (differential) or 1000MΩ (common mode)
- CMRR: 110dB minimum
- CMIV: $\pm$10V (referenced to amplifier ground)
- Input voltage range: $\pm$10V peak to peak

3.1.3 SEMG electrode specifications

Although there is a rapid growth of EMG applications, most centres or laboratories develop their own acquisition methodology. Thus, there is a need in standardization to make the results more comparable and to create a large common body of knowledge on the use of EMG in the various fields of applications [Hermens et al., 2000]. The International Society of Electrophysiology and Kinesiology (ISEK) has published a standard in reporting EMG data [Merletti, 1999]. This standard will be used in this report. The first part will describe the specifications regarding the electrodes and the amplifier in the second part.

- Muscles observed by the EMG system. They are shown from left to right in Fig. 3.1.
    1. *Biceps brachii* for elbow flexion
    2. *Triceps brachii* (medial head) for elbow extension
    3. *Flexor carpi ulnaris* for wrist flexion
    4. *Extensor carpi radialis brevis* for wrist extension
    5. *Extensor indicis* for index finger extension
    6. *Dorsal interossei I* (FDI) for index finger abduction
    7. *Abductor pollicis brevis* (APB) for thumb abduction

The main consideration for the muscles selection is that the muscles must be superficial muscles, not deep muscles. If the SEMG electrodes are placed on the skin overlying the deep muscles, it can pick up unwanted SEMG signals and may not pick up the signal from the muscle we want.

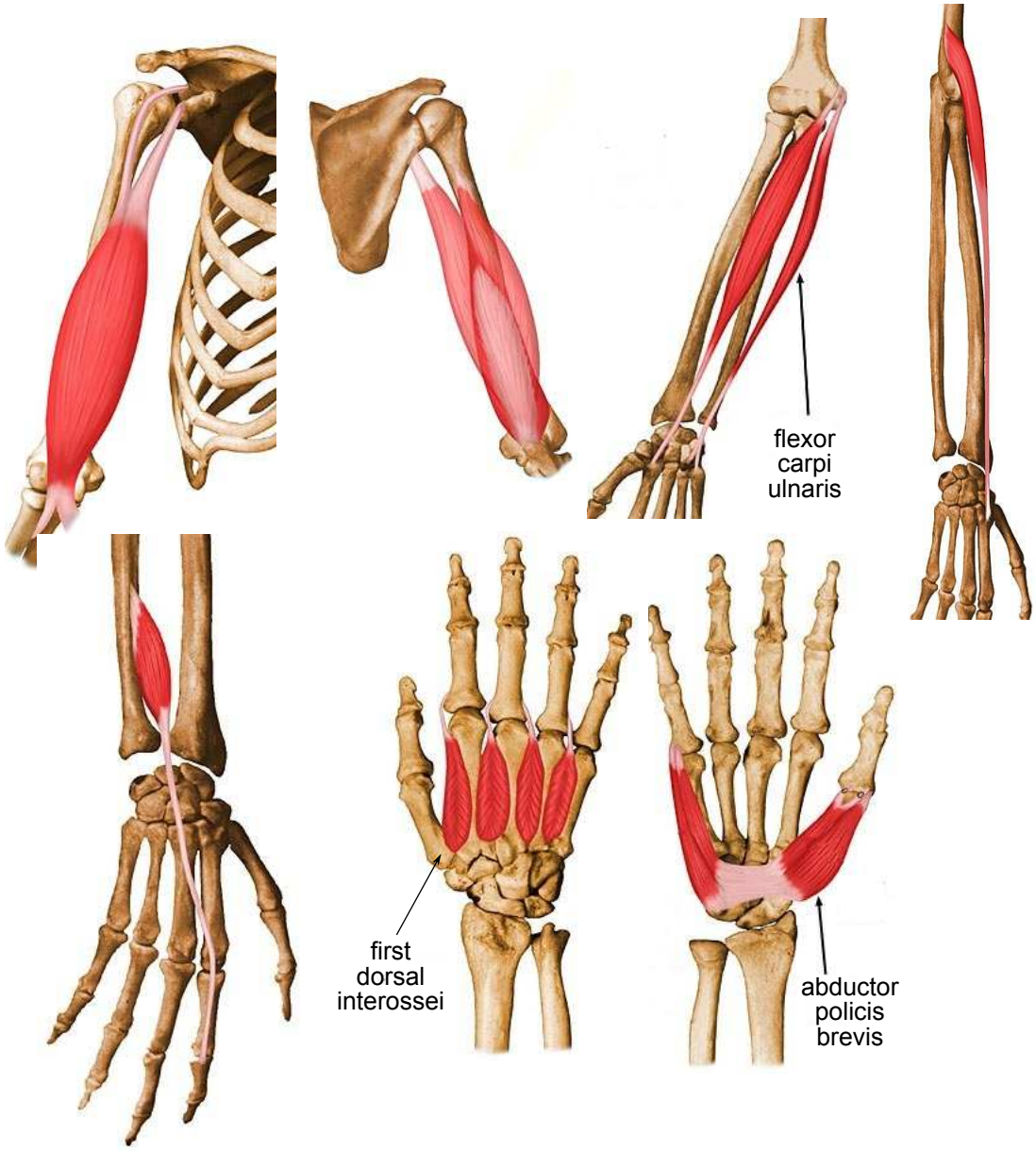

Figure 3.1: Upper limb muscles (right side) observed in this thesis (taken from http://www.rad.washington.edu/atlas/)

- Electrode material: Silver/silver chloride (Ag/AgCl).
  Silver/silver chloride are the most commonly used materials for SEMG electrodes (43% of the scanned publications by Merletti and Parker [Merletti and Parker, 2004]). The skin-Ag contact or skin-AgCl contact has an almost resistive impedance in the EMG frequency range, while other metals present capacitive components that introduce additional filtering [Merletti and Parker, 2004].

- Electrode shape: Disc/circular (most often used [Merletti and Parker, 2004])

- Electrode size: 10 mm diameter (contact area)
  The electrodes used are disposable and pre-gelled with adhesive backing (Skintact F-301 → 30 mm diameter circular foam backing, for the first four muscles, and Biopac EL504 → 1" square cloth base, for the rest).
  With a layer of gel between the electrode and skin, any mechanical disturbances caused by relative motion between the electrode and the skin are damped and their effect on the signal is limited (this will prevent electrode motion artifact).

- Skin preparation: Alcohol is applied to cleanse skin.
  Skin preparation is done to get good electrode-skin contact which can result in better recordings (lower impedance of the skin contact), fewer and smaller artifacts, and less noise [Hermens et al., 2000].

- Inter electrode distance (IED): For the first 4 muscles, IED is about 35-40 mm, while for the last 3, it is about 25-30 mm [Hermens et al., 2000]. This may not be ideal case as explained below due to the large backing area.
  It is recommended that the bipolar SEMG electrodes are applied between the innervation zone and a tendon, with an inter electrode distance of no more than 20 mm. When a bipolar sensor is applied on relatively small muscles, the inter electrode distance should not exceed $\frac{1}{4}$of the muscle-fiber length, and both electrodes should be on one side of the innervation zone.

This way tendon and motor end plate effects can be reduced or avoided. In dynamic contractions the conditions above should be met for the full movement range [Merletti and Parker, 2004].

- Electrode location: In determining the location, the guidelines developed by Zipp and Hermens et al. are used [Hermens et al., 2000; Zipp, 1982]. The goal of placement is to obtain a high-quality and stable SEMG. According to Zipp, electrode placement should consider individual body dimensions and is given with reference to anthropometrical landmarks. First, we should draw a 'lead line' connecting two anatomical landmarks. Then, decide a 'central lead point' about which the two electrodes of a bipolar lead are placed symmetrically on the lead line. An example for placing bipolar electrodes on biceps brachii is shown in Fig. 3.2 and Table 3.1.

- Orientation of muscle: Bipolar electrodes are placed at the recommended sensor location with the orientation parallel to the muscle fibers.

- Reference electrode: Spinous process of C7 (seventh cervical vertebrae). The reference electrode needs to be placed at a location in which the risk for a large common mode disturbance signal is minimal, so preferably on electrically inactive tissue [Hermens et al., 2000]. Other common locations for reference electrode are wrist and ankle.

- Clinical test: After placing the electrodes, a clinical test can be done to ensure the muscle activity is indeed captured by the system. It should be noted that this test does not mean that only the desired muscle is active and the others are not. These tests are simply generally accepted tests. The complete tests for all muscles are presented in Table 3.2. These clinical tests are taken from [Zipp, 1982] and www.seniam.org. However, in actual data collection, the subject will be asked to perform movements which will activate the corresponding muscles (no external resistance).

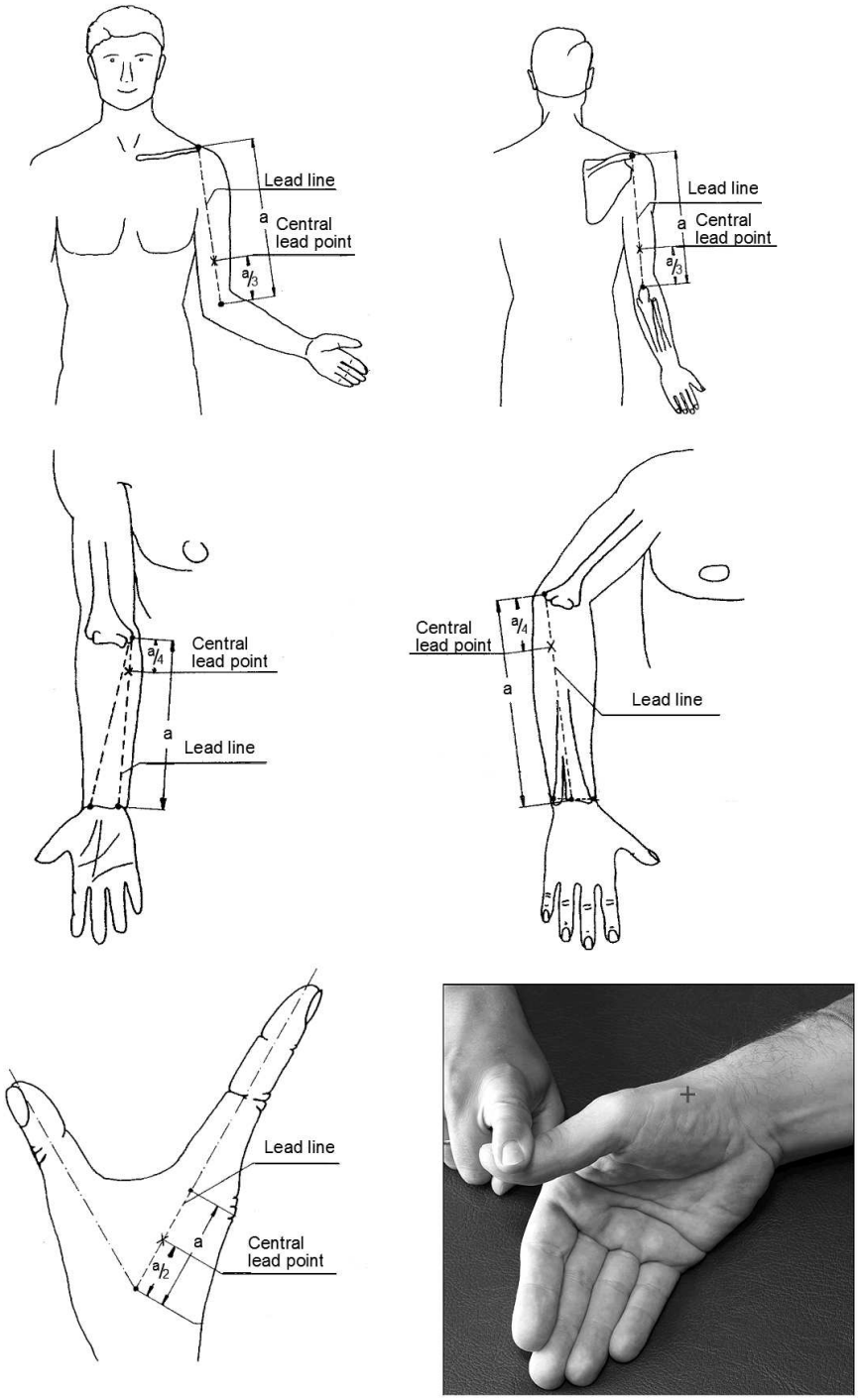

Figure 3.2: Electrode placement on biceps and triceps brachii (top), wrist flexor and extensor (middle), and FDI and APB (bottom) [Zipp, 1982]

Table 3.1: Lead placement for arm muscle

Muscle	**Posture**	**Lead line**	**Central lead point**
Biceps brachii	Sitting, upper arm is vertical, forearm is horizontal, palm upward	Acromion Tendon of the biceps muscle in the cubital fossa	1/3 LLL (lead line length) from the cubittal fossa
Triceps brachii	Sitting, arm limp	Acromion Olecranon	1/3 LLL from the olecranon
Flexor carpi ulnaris	Sitting, fore arm on a table, elbow slightly turned inward, palm upward	Medial epicondyle of the humerus Styloid process of radius	$\frac{1}{4}$LLL from the epicondyle
Extensor carpi radialis brevis	Sitting, upper arm is abducted laterally, forearm on a table, palm downward	Midpoint between the lateral epicondyle of the humerus and the olecranon Styloid process of the ulna	$\frac{1}{4}$LLL from the epicondyle
Extensor indicis	Sitting, upper arm is abducted laterally, forearm on a table, palm downward	About four/five fingers from Styloid process of the ulna	
Dorsal interossei I	Sitting, forearm on a table, thumb and index finger are extended forming a V	Vertex of the V Basal joint of the index finger	$\frac{1}{2}$LLL
Abductor pollicis brevis	Sitting or supine with the back of the hand stabilised on a table	Parallel to the 1st ossa metacarpalia.	Slightly medial of the distal $\frac{1}{4}$of the 1^{st} ossa metacarpalia.

Table 3.2: Function check for arm muscles

Biceps brachii	Place one hand under the elbow to cushion it from table pressure and flex the elbow slightly below or at a right angle, with the forearm in supination. Press against the forearm in the direction of extension.
Triceps brachii	Extend the elbow while applying pressure to the forearm in the direction of flexion.
Flexor carpi ulnaris	Flexing the wrist against an external resistance
Extensor carpi radialis brevis	Abducting the hand sideward toward the ulna
Extensor indicis	Extending the index finger against an external resistance
Dorsal interossei I	Squeezing the thumb and index finger together
Abductor pollicis brevis	Abduct the thumb central ward from the palm while applying pressure against the proximal phalanx in the direction of adduction toward the palm

- Electrode fixation: When necessary, electrode cables can be taped to the skin using surgical tape to prevent motion artifacts. When the electrodes are pulled during movement, the reading will give some unwanted values. Thus, we have to ensure that during movement, electrodes do not collide to each other.

3.1.4 Accelerometers placement

Each of the accelerometer board, DE-ACC3MD, glued into Perspex (acrylic) casing, are attached on the upper arm, forearm, dorsal of hand, index finger, and thumb. Index finger and thumb are also chosen to observe finger affecting tremor, such as finger rolling tremor in Parkinson's disease. For the purpose of kinematics calculation, the position of accelerometers with respect to the link observed must be known. As optical motion system is used in this thesis, reflective markers are put on the anatomical landmarks of the upper limb, such as, shoulder, elbow, wrist, etc. These markers will be used to calculate the joint angles of the upper limb and certainly the position of the markers will be known. As a result, by also placing the reflective markers on top of the accelerometer's casing, we are

able to obtain the position of the accelerometers with respect to arm joints. The configuration is shown in Fig. 3.3.

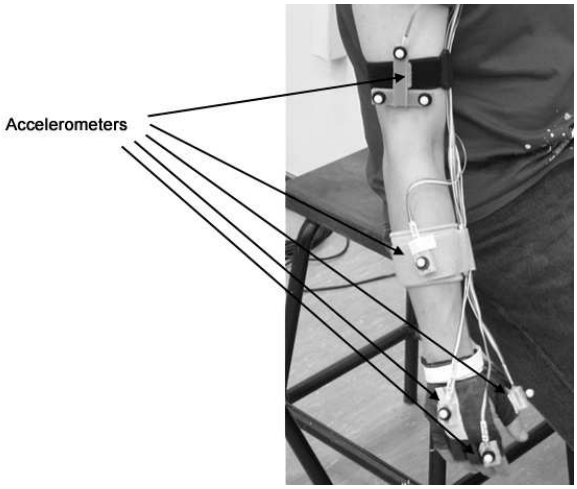

Figure 3.3: Accelerometer placement

The voltage output from the accelerometers will be fed into the 16 bit 64 channel A/D card provided by Vicon MX Control (optical tracking system). The sampling rate used is 150 Hz considering that maximum frequency of pathological tremor is around 12 Hz.

3.1.5 Optical tracking system

In this thesis, 4 Vicon MX3+ cameras, each fitted with a 6 mm C-mount lens are used. At full resolution (659H x 494V), the angle of view is 57.06°(H) x 44.35°(V). The upper limb Plug-in-Gait (PiG) model is furnished by Vicon to provide the user with useful kinematics information (joint angle) of the upper limb. The model is available for one arm only and for both arms. Here we will concentrate on the model for one arm only. Sampling rate is 100 Hz for each camera.

The upper limb model presented consists of four rigid segments: thorax, right (left) upper arm, right (left) forearm, right (left) hand; and seven degrees of freedoms (DOF): 3 DOF at shoulder, 2 DOF at the elbow, and 2 DOF at the wrist.

The shoulder is modeled as a ball and socket joint (3 DOF), the elbow and wrist as a universal joint with 2 DOF respectively. The markers used to define the model (right arm) are shown in Fig. 3.4 and the whole setup is shown in Fig. 3.5.

3.1.6 Experimental design

This section outlines the experimental protocol for the clinical trials using the whole sensor system described previously.

1. **Performing standard clinical tests (done by the neurologist)**
   - Consent taking, 1 copy for patient, 1 copy for filing
   - Tremor Rating Scale (except spiral and line diagrams)
   - Unified Parkinson's Disease Rating Scale part III
   - Basic Element of Performance I (Central Processing and Upper Extremity Motor Control
2. **Triggering**
   Data from the three different types of sensors has to be captured at the same time (synchronize) for analysis purpose. Because the accelerometer output is fed into the A/D card of the Vicon MX optical tracking system, we only need to synchronize the data from Biopac (SEMG) and Vicon MX (optical data and accelerometer). Both systems provide respective triggering input, so a simple double pole double throw (DPDT) switch is enough to do the synchronization. A DPDT switch is A pair of on-off switches which operate together.
3. **Running the trials**
   - The trials are first done on the right hand. After the whole set (except frequency entrainment test) is done, the trials are repeated for the left hand. Finally, frequency entrainment is carried out.

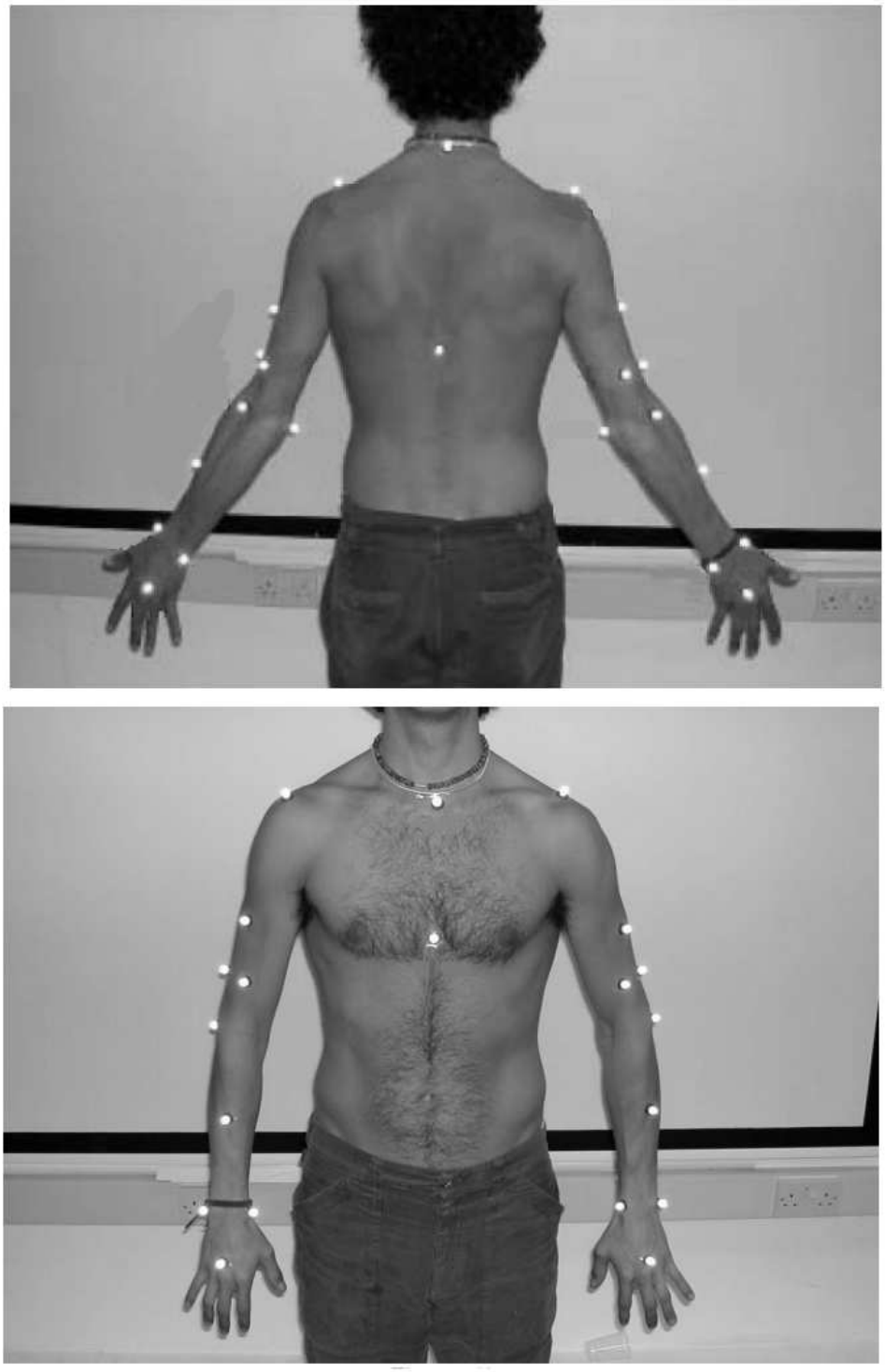

Figure 3.4: Marker setup for optical tracking system

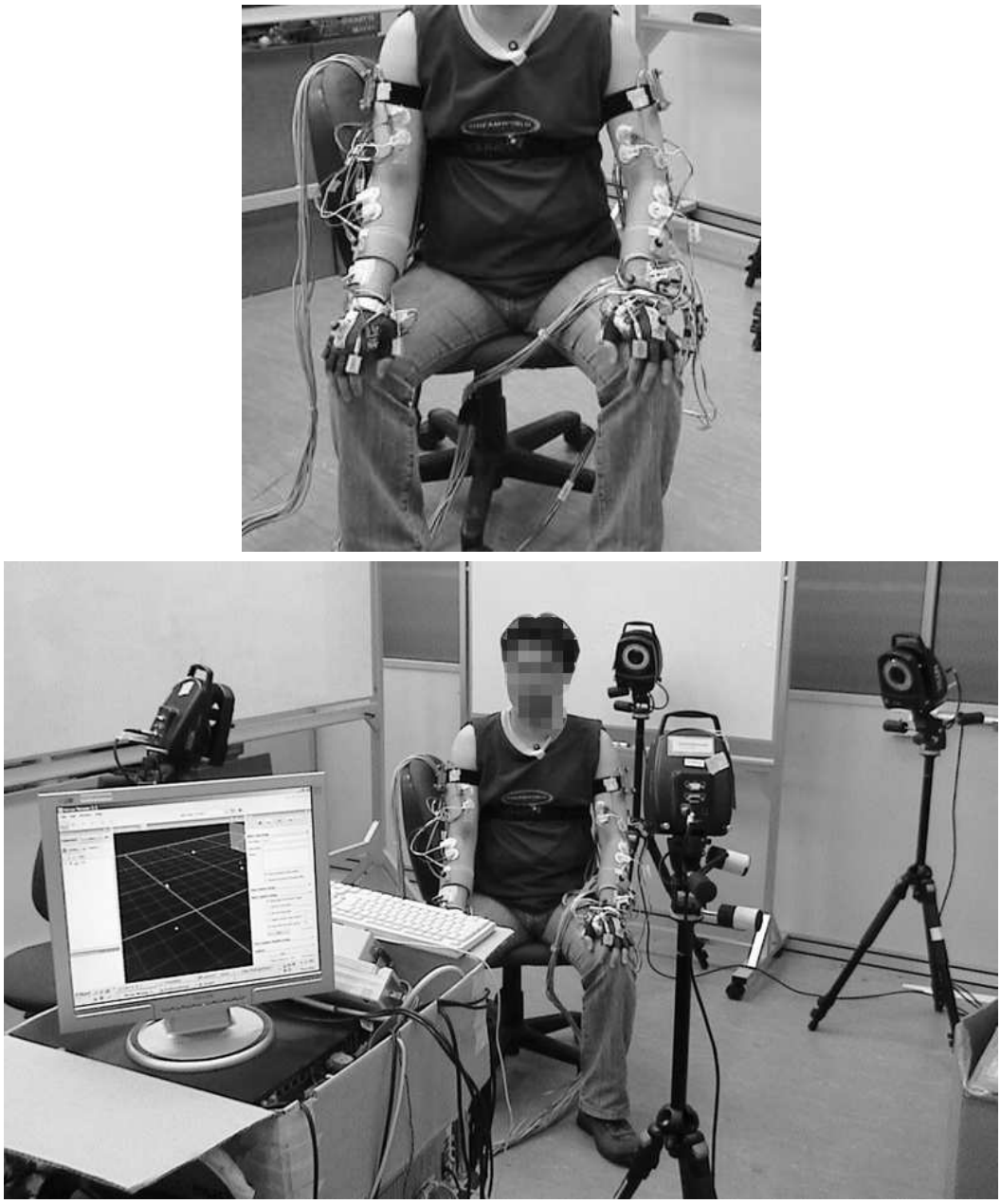

Figure 3.5: The whole setup for tremor data collection

- Rest, upper limb resting on right thigh, with fingers fully relax, distract subject by asking them to keep subtracting 7 from 100 (24 s)
- Outstretched posture, with fingers extended and wrist neutral (24 s) (90 degrees)
- Flexed posture, with fingers extended and wrist neutral (24 s)
- Finger to nose (24 s) (right, left) (fully stretched)
- Index finger tapping with thumb, as fast and wide as possible, rest of fingers flexed, forearm perpendicular to ground (12 s)
- Fist open-and-close, as fast and wide as possible, forearm perpendicular to ground (12 s)
- Alternating hand movement, as fast and wide as possible, forearm perpendicular to the ground - screwing a light bulb in the air (12 s)
- Alternating hand movement, as fast and wide as possible, tapping on the thigh (12 s)
- Archimedes spiral drawing (from Tremor Rating Scale), forearm unsupported (as needed)
- Drawing line (1, 2, and 3), forearm unsupported (as needed)
- Forearm supported, finger extended and wrist neutral (20 s)
- Forearm supported, finger extended and wrist neutral, with 1 lb load over hand (24 s)
- Final test (for both arms) is frequency entrainment:
  Both hand outstretched, fingers extended, wrists neutral
  - While keeping in position (a), right fist open-and-close from slow to fast to slow;
  - While keeping in position (a), left fist open-and-close from slow to fast to slow.

- While keeping in position (a), pronate-supinate at right elbow from slow to fast to slow;
- While keeping in position (a), pronate-supinate at left elbow from slow to fast to slow;
- Usually around 90 seconds or longer.

3.2 Results from tremor data collection

3.2.1 Parkinson's Disease patient - postural position

The cardinal feature in PD patients is resting tremor (resembling pill-rolling) with a frequency of 3-6 Hz [Samii et al., 2004]. Therefore it is expected to see this feature from the recordings at resting posture. The tremor in PD patient is also usually asymmetric. However, this does not mean that aside from the resting position, the patient's performance is as good as normal subjects as tremor is not the only symptoms of PD. The other two prominent features are rigidity and bradykinesia, the effects of which can be seen from tests such as finger tapping, alternating movement, and fist closing and opening [Connor et al., 2001]. The signals recorded for resting position by the PD patient are shown in Fig. 3.6.

It has been reported that postural tremor is also present in PD patients, although the characteristics of the postural tremor differ [Milanov, 2000]. Comparing the power from the ACC and joint angle power spectra, the resting tremor has more power than the postural tremor for this subject. The frequency is also considered high (around 8-9 Hz). This phenomena is not unique because similar cases have been reported [Milanov, 2000].

The power of the EMG signals for postural is higher than for resting because during postural position the corresponding muscle must contract to maintain the hand position, while during rest position the muscle is relaxed. Thus the EMG signals recorded here is actually tremor EMG added with the force needed to maintain the hand position.

It should be noted that mild postural tremor can be captured by ACC and EMG system, but not by Vicon. This is probably due to the hardware limitation of the camera. The camera has 659x494 resolution with angle of view of 57°x44°. Combined with about 1m distance between the camera and the subject (see Fig. 3.5), a few millimeter of tremor will be almost impossible to detect.

By using the cross correlation function, it can be observed also that during the postural position, there is a window of time when the flexor and extensor EMG are actually in phase. The delay calculated from the cross correlation function is zero and using visual inspection the zero delay can also be observed as depicted in Fig. 3.6. In the figure, the voltage reading is the result of 500 times magnification, thus '(V×500)'. The joint angle plots are also given in the figure. It should be noted that the joint angle during postural position is very small compared to that during resting position. In the figure, the joint angle during resting position has been scaled down by 20 times. Therefore, Vicon does not capture any tremor during postural position, while there is tremor recorded in the SEMG. The accelerometer does not pick up any tremor also during the postural position (no distinct peak in the power spectrum).

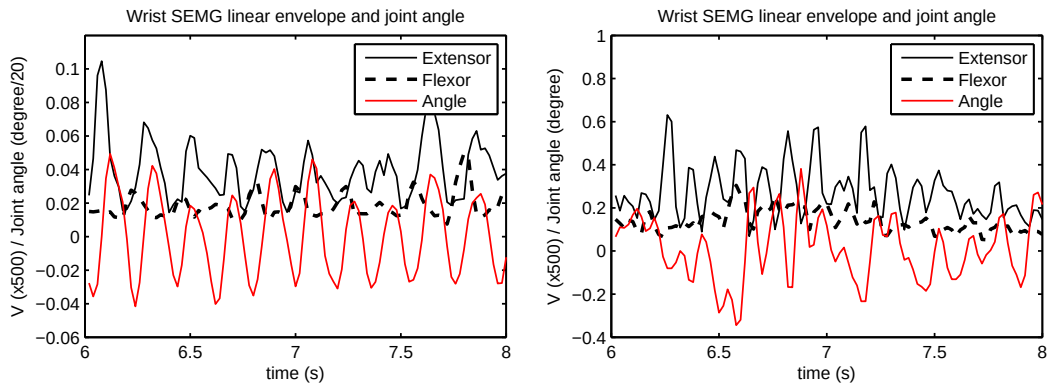

Figure 3.6: Wrist flexor extensor EMG and joint angle of a PD patient during rest position (left) and postural position (right).

Clinically this can explain the rigidity suffered by the patient. Thus using the system, the tremor can be appreciated better compared to observation by naked

eye only. The cross correlation function between two signals $x(k)$ and $y(k)$ with N elements is defined by

$$R_{xy}(m) = \begin{cases} \frac{1}{N}\sum_{n=0}^{N-m-1} x_{n+m}y_n & m \geq 0 \\ \frac{1}{N}R_{yx}(-m) & m < 0 \end{cases} . \tag{3.1}$$

3.2.2 Holmes' tremor patient - postural position

Holmes' tremor is a combination of rest, postural, and intention tremor. It is caused by lesions in rubral or midbrain area [Deuschl et al., 2001]. This tremor is often not as rhythmic as other tremors. Its frequency is mostly below 4.5 Hz and usually there is a variable delay (4 weeks to 2 years) between lesion onset and first occurrence of tremor. One subject has been diagnosed with Holmes' tremor and we had the opportunity to take his data. From the patient's medical history, it is shown that he had a stroke around 2 years ago and currently has tremor at all position (rest, postural, and kinetic). The frequency of the tremor observed is about 2.8 Hz.

Holmes' tremor is a rare case and this tremor occurs at resting, postural, and kinetic position. As it can be seen in Fig. 3.7, the patient shows a postural tremor at around 2.8 Hz, which is almost the same to the frequency at the resting position. This observation conforms to the clinical diagnosis of Holmes' tremor.

The amplitude of the wrist flexor EMG is irregular as shown in Fig. 3.8, whereas for the extensor, it is more regular. One of the possible clinical explanations is that there is tremor at the wrist extensor and the brain is compensating the tremor by sending a counter signal to the wrist flexor. The jerky behavior of the wrist flexor can be explained by one of Holmes' tremor characteristics which is irregularity in amplitude. The corresponding joint angle and accelerometer data, shown in Fig. 3.9, also supports the hypothesis. For example, from $t = 10$s to $t = 13$s, there is significant activity in both flexor and extensor although the amplitude of both accelerometer and joint angle data is relatively smaller than in the other period.

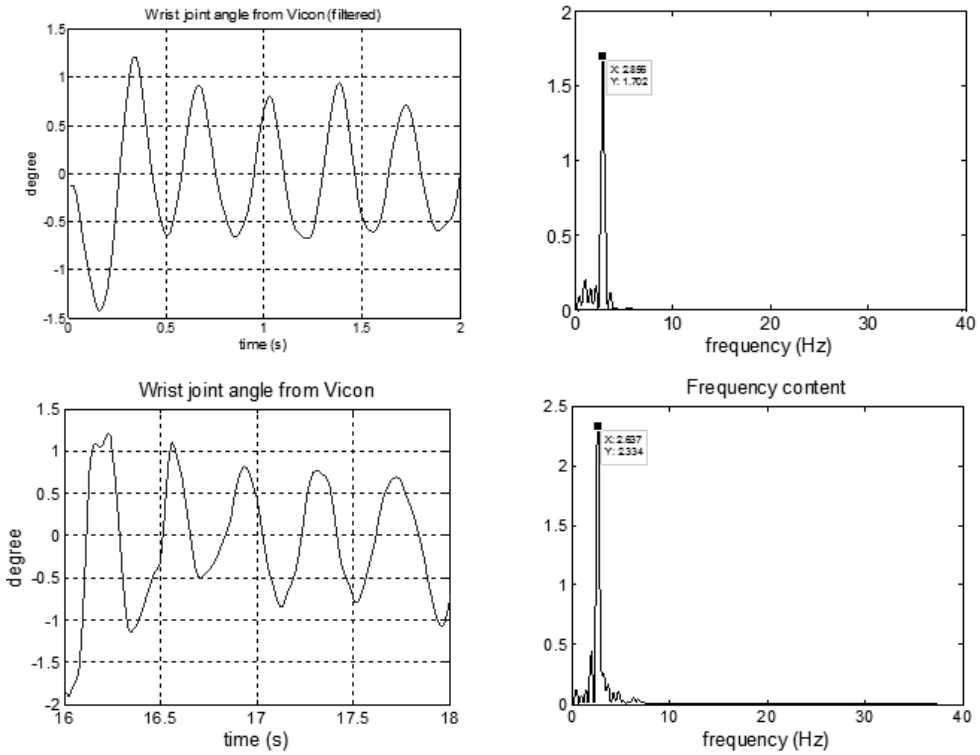

Figure 3.7: Wrist flexor and extensor EMG of a Holmes' tremor patient during resting (top) and during postural position (bottom). The figure on the right are the power spectrum of the plot in the left.

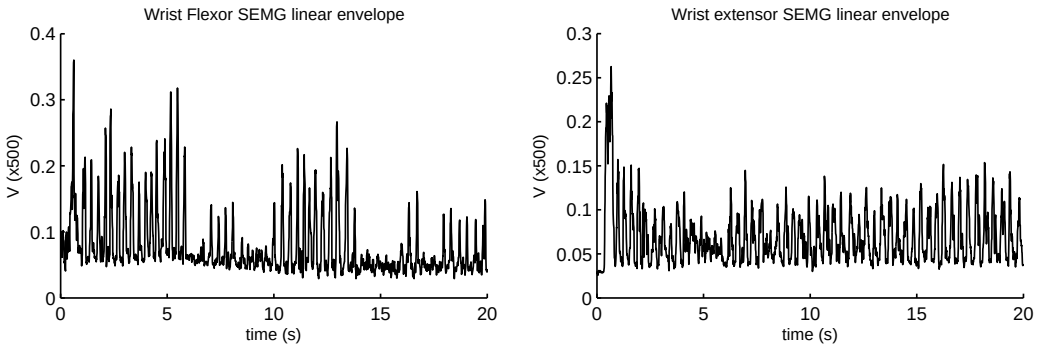

Figure 3.8: Wrist flexor (left) and extensor (right) EMG of a Holmes' tremor patient during postural position.

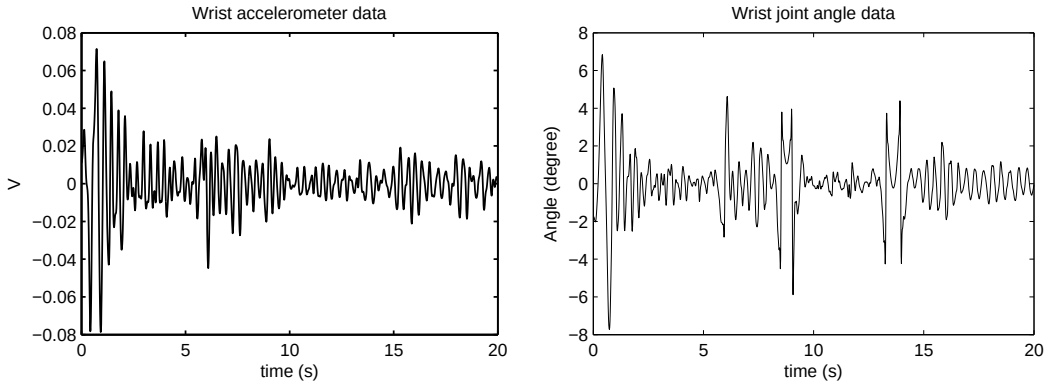

Figure 3.9: Wrist accelerometer (left) and joint angle (right) data of a Holmes' tremor patient during postural position.

This explanation may not be a correct one and further investigation can be done whether this phenomena (together with that observed at resting position) can reveal some characteristics of the tremor or other information. This case also serves as a good example where a clinician may not be able to pick up the irregularity. Consequently the system can give better information to the clinicians in doing their diagnosis.

3.3 Tremor classification result

Apart from the above findings, our collaborators have done further analysis of the collected tremor data. The goal of their work is to develop a classifier for automatic recognition of different tremor types using Support Vector Machine (SVM) modeling and ensemble learning of the extracted electromyographic (SEMG) features from subjects performing motor tasks. The result has been accepted for publication and is now in press [Palmes et al., 2010]. This section will briefly report the method and result presented in that paper. It should be noted also that this work is done by the author's collaborator, although the full experiments for the data collection are conducted by the author. Thus this section is added to show the potential of the work that has been done.

3. TREMOR SENSING EXPERIMENTS

The detection and quantification of tremor are of clinical interest for diagnosis of neurological disorders and objective evaluation of their treatment. To prescribe correct therapy for pathological tremor, clinicians have to be able to classify different types of pathological tremor correctly and distinguish tremor from other movement disorders.

However, the diagnosis is not that straightforward, especially in the early stage of the disease where one symptom may be common in few types of diseases and may lead to misdiagnosis. Furthermore current assessment methods are based on subjective evaluation of the neurologists which do not give consistent diagnosis. Thus the motivation to develop algorithm to diagnose various types of tremor, and if possible, with different degree of severity.

The method reported in [Palmes et al., 2010] is briefly laid out below. Some ambiguities are excused in this description because all the details can be found in the cited work.

1. *Pre-processing.* There is no further software pre-processing apart from the hardware filter from Biopac (10-500 Hz, 6^{th} order Butterworth).

2. *Feature extraction.* The candidates for the feature set are those usually used in SEMG signal analysis. After some preliminary tests on the performance of some combination of the features and several Support Vector Machine (SVM) models, the feature set chosen in their work consists of 4 terms: **Zero Crossing**, **Mean Absolute Value**,**Variance**, and **Mean Spectral Density using periodogram method**.

3. *Modeling and Feature selection.* There are 12 tasks and 7 upper limb SEMG channels which make up for 84 possible feature combinations as inputs to classify 4 different classes of subjects. We have chosen the SVM model in the implementation because of its robustness and simplicity of implementation in terms of the number of parameters to optimize. A series of

statistical comparisons are conducted to identify the most effective feature transformation and its optimal number of components or features.

4. *Parameter Optimization.* After identifying the optimal set of extracted features, the classifier model is optimized further our by searching the best values of its parameters. In this proposed algorithm, three important parameters are in focus: feature transformation, SVM kernel, and classifier architecture.

5. *Evaluation.* The proposed algorithm is tested for two problems, i.e. differentiating: a) tremor patient with healthy subject and b) PD patient with ET patient. The classification accuracy of the proposed method is also compared with some methods available in the literature.

For the first problem, data from 14 healthy subjects and 11 tremor patients (PD and ET) is used, while for the second problem, the data is from 6 PD patients and 7 ET patients. Classification accuracy for each method is calculated by the number of correct classification divided by the total number of subjects. The representative result from the proposed algorithm is shown in Fig. 3.10. It can be seen that the proposed method (SVM ensemble) consistently performs better than other algorithms. For differentiating tremor patients from normal, the accuracy is 98.4±3.3%, while for differentiating PD from ET, the accuracy is 99.2±2.4%.

In conclusion, initial analysis of the EMG data has shown promising result to improve the objectivity of tremor diagnosis.

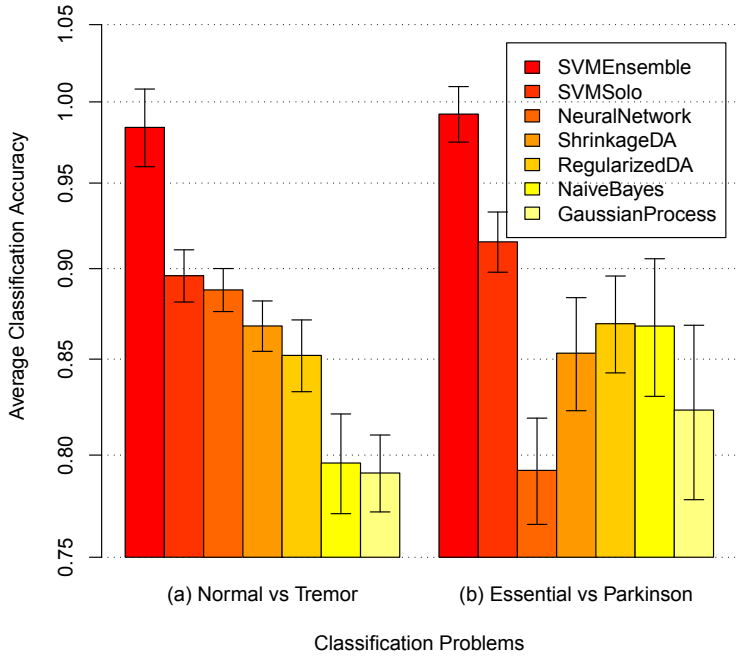

Figure 3.10: Comparison of the proposed classification algorithm (SVM ensemble) and other methods. The left chart shows the classification accuracy in differentiating between healthy subjects and tremor patients (either PD or ET). The right chart shows the classification accuracy in differentiating between PD and ET patients.

Chapter 4

Extended Kalman Filtering for Estimation of Tremor Parameters

Since tremor can be detected by the proposed system, we can now move on to estimate the parameters necessary for the compensation. As discussed in Chapter 2.2.3, FES has a few parameters to be determined to generate the desired pulses: pulse amplitude, frequency, width, and shape. Usually pulse frequency and shape are fixed throughout the experiment, while the amplitude or width is modulated to vary the strength of the stimulation. The strength of stimulation depends on the tremor magnitude, therefore an estimate of tremor amplitude must be obtained. Tremor amplitude will then reflect how much compensation should be applied to the muscles.

Another important factor is the FES timing, i.e. when to start and stop the stimulation. This information can be obtained by estimating the tremor phase assuming tremor is roughly sinusoidal [Elble and Koller, 1990]. Suppose the angle of tremor in a certain arm joint is recorded and it has sinusoidal profile as shown in Fig. 4.1. The peaks of the sine wave are actually the turning point from flexion to extension or vice versa.

The last factor to be considered in this chapter is the separation of intended motion and tremor. The obvious difference between these two terms is the frequency. It has been reported that the average predominant frequency of activities

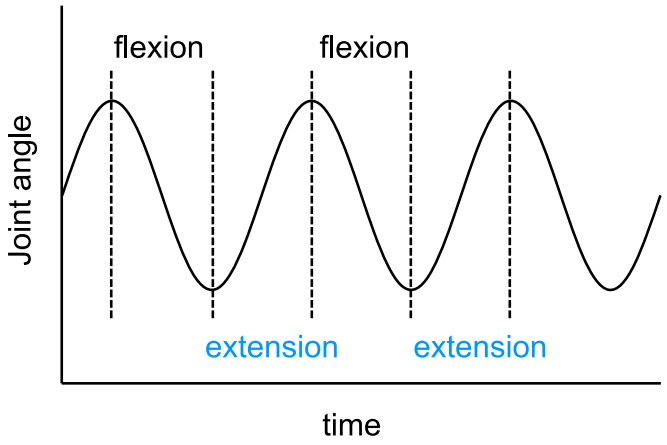

Figure 4.1: Tremor phase information is useful to determine FES timing.

in daily life is about 1 Hz [Mann et al., 1989]. On the other hand the tremor frequency is generally larger than about 3 Hz [Smaga, 2003]. Therefore tremor frequency estimate is also needed.

The following section gives a brief review of the current literature in the estimation of signal parameters, especially of sinusoidal. Then an attempt in tremor estimation with KF algorithm is proposed. Its limitations are discussed and an EKF model is laid out to overcome the limitations. Further refinements are introduced regarding the separation of tremor and voluntary motion. Finally the efficacy of the complete algorithm is shown using real data from patients with tremor.

4.1 Literature review

Estimation of signal parameters, especially sinusoids, has been well researched for decades [Kay and Marple Jr., 1981; Stoica, 1993]. Among the many methods, we are interested in the methods which can be implemented in real-time application such as in the proposed tremor compensation system. Thus the algorithm should ideally be computationally efficient and have fast convergence.

The first adaptive online frequency estimator of a sinusoid is probably the adaptive line enhancer set forth by Bernard Widrow et al. in 1975 [Hsu et al., 1999]. This method can be viewed as adaptive notch filter (ANF). Since then the method has been improved and a major breakthrough is proposed in [Regalia, 1991]. In that work, a novel lattice based adaptive IIR notch filter is shown to have a better performance than the previous methods. Some modifications have also been put forward in that line of approach.

Hsu et al. modified the scaling of the ANF forcing term in [Regalia, 1991] to cater large frequency adaptation [Hsu et al., 1999]. With further nonlinear time scaling, a globally convergent scheme is obtained for frequency estimator. For multiple harmonics and sinusoids which are not pure, the ANF in [Hsu et al., 1999] is modified in [Mojiri and Bakhshai, 2004, 2007]. Another modification that does not impose any upper bound for the signal amplitude is given in [Marino and Tomei, 2002]. Finally, this ANF is extended to estimate both amplitude and frequency in [Hou, 2005]. The algorithm is a seventh order system:

$$\dot{\xi}_1 = -\lambda\xi_1 + 3\lambda y \tag{4.1a}$$

$$\dot{\xi}_2 = -\lambda\xi_2 - 2\lambda y^2 \tag{4.1b}$$

$$\dot{\hat{z}}_1 = \hat{z}_2 + \xi'\hat{\theta} + (1+\alpha\lambda)(\lambda y^2/2 - \hat{z}_1) \tag{4.1c}$$

$$\dot{\hat{z}}_2 = \lambda\xi'\hat{\theta} + \alpha(\lambda y^2/2 - \hat{z}_1) \tag{4.1d}$$

$$\dot{\hat{\theta}} = \Gamma\xi(\lambda y^2/2 - \hat{z}_1) \tag{4.1e}$$

where the scalars α, λ, and the components of the diagonal matrix $\Gamma = \texttt{diag}\,[\gamma_0\ \gamma_1\ \gamma_2]$ are arbitrary positive real numbers. These numbers influence the frequency estimator behavior regarding the tracking features and the obtained precision [Trapero et al., 2007]. The states of adaptive observers in 4.1a and 4.1b, conform to an augmented vector denoted by $\xi = [1, \xi_1, \xi_2]^T$. It can be verified that vector

$\hat{\theta}$ converges to θ [Hou, 2005]:

$$\begin{aligned} \theta_0 &= (A^2 - A_0^2)\omega^2 \\ \theta_1 &= A_0\omega^2 \\ \theta_2 &= \omega^2 \end{aligned}$$

where A, A_0, and ω are the amplitude, bias, and the frequency of the sinusoid respectively.

We will discuss two recent methods which claim to achieve better performance than the aforementioned ANF variants. Another method which has been used for physiological tremor compensation system will also be considered. Comparison with Kalman-filter based method is given to argue for its selection in tremor estimation.

4.1.1 Gradient-descent method

The solution in [Ziarani and Konrad, 2004] is based on nonlinear differential equations as proposed in [Hsu et al., 1999], although derived through fundamentally different approach. Their method is basically trying to minimize the distance between the parameter estimate and the actual estimate by using gradient-descent method. The differential equations, in discretized form, are as follow

$$A_{k+1} = A_k + 2T\mu_1 e_k \sin(\phi_k) \tag{4.2a}$$

$$\omega_{k+1} = \omega_k + 2T\mu_2 e_k A_k \cos(\phi_k) \tag{4.2b}$$

$$\phi_{k+1} = \phi_k + T\omega_k + 2T\mu_2\mu_3 e_k A_k \cos(\phi_k) \tag{4.2c}$$

$$y_k = A_k sin(\phi_k) \tag{4.2d}$$

$$e_k = x_k - y_k \tag{4.2e}$$

where A, ω, and ϕ are the amplitude, frequency, phase estimate of the sinusoid, and $k = 1, 2, 3, \ldots$. The measured signal is x and its estimate is y. The sampling

period is T. The values of the μ_1, μ_2, and μ_3 determine the convergence speed versus the error compromise. In general, the faster the convergence, the more steady-state error is introduced in the estimates [Ziarani and Konrad, 2004]. The required initial condition is only the frequency.

They have compared their proposed method with EKF and ANF from [Hsu et al., 1999]. From that comparison, their reservations with EKF are: 1) EKF is more prone to initial conditions and covariance matrices. Their proposed method only requires frequency as the initial condition. Further, in estimating a unit amplitude, 60 Hz sinusoid with 20 dB SNR, a 50% variation in μ_1, μ_2, and μ_3 does not affect the estimation. 2) EKF assumes Gaussian noise, while their proposed method does not, 3) Their proposed method is more immune to noise. The estimation error is 0.2% using the aforementioned signal. However in EKF, it results in 3% error, although they use a different signal (amplitude of 400 and frequency of 50 Hz, same SNR).

Comparing their method with that of [Hsu et al., 1999], they claim that their method is more immune to noise and able to estimate the amplitude and phase in direct manner besides the frequency. They also report that assuming the same signal (unit amplitude, 60 Hz frequency, 20 dB SNR) error of 1.5% is achieved using the method by [Hsu et al., 1999]. However, in their implementation of the method by [Hsu et al., 1999], a very large adaptation speed (10^8) is used, which causes the proneness to numerical error. Why such a large adaptation speed is used, as compared to examples given in [Hou, 2005; Hsu et al., 1999], is not clear.

4.1.2 Algebraic derivative method

Another method based on algebraic derivative method is proposed in [Trapero et al., 2007]. The advantage of this method is that it does not require any initial conditions as the parameters are obtained from multiple integrations of the input

signal, $y(t)$. For example, the frequency estimate is obtained by

$$n_1(t) = z_1 + t^3 y(t) \qquad d_1(t) = z_4 \tag{4.3a}$$

$$\dot{z_1} = z_2 - 9t^2 y(t) \qquad \dot{z_4} = z_5 \tag{4.3b}$$

$$\dot{z_2} = \dot{z_3} + 18ty(t) \qquad \dot{z_5} = z_6 - t^3 y(t) \tag{4.3c}$$

$$\dot{z_3} = -6y(t) \qquad \dot{z_6} = 3t^2 y(t) \tag{4.3d}$$

where n_1 and d_1 are further low-pass filtered independently, i.e. $n_{1f}(t)$ and $d_{1f}(t)$. The frequency ω^2 is then $n_{1f}(t)/d_{1f}(t)$.

They also compared their method with that of [Ziarani and Konrad, 2004] and [Hou, 2005]. The test signal is a sinusoid with 20 unit amplitude, about 0.8 Hz frequency, 10 unit offset, and more than 80 dB SNR. It has been reported that the computation of frequency estimate converges after 0.4 s. Implementing the method by [Ziarani and Konrad, 2004], the frequency does not converge to the correct value, while there is bias in the amplitude estimate. This is expected because the model by [Ziarani and Konrad, 2004] does not cater for offset estimation, while the signal contains a significant offset. The method by [Hou, 2005] does converge to the correct frequency and amplitude, but after 25 s.

4.1.3 Extended Kalman Filter (EKF)

One tested method in parameter estimation is EKF. Hence we will explore this option and compare it with the above two methods. The first proposal using EKF to estimate time varying non-sinusoidal periodic signal is given in [Parker and Anderson, 1990]. The EKF estimates the amplitude, frequency, and phase of the first m harmonic components. In [La Scala et al., 1996], the problem of using EKF such as in [Parker and Anderson, 1990] when applied to a signal with low SNR (0 to -30dB) is pointed out. Then a new EKF algorithm which is applied to the Fourier coefficients, instead of the raw signal, is developed. However, this algorithm only tracks the signal frequency.

The EKF is further extended to incorporate complex sinusoidal in [Nishiyama, 1997]. That model has weaker nonlinearity than that proposed in [Parker and Anderson, 1990] because it has finite Taylor series. In Parker's model, a sin(.) is used and it has infinite Taylor series expansion. However only single sinusoid case is considered and the case for time varying amplitude is not discussed. In case of non sinusoidal signal, an Extended Kalman Smoother is proposed in [Kim and McNames, 2006] to estimate the instantaneous tremor frequency exhibited in binary spike trains detected from neural recordings. However this algorithm does not estimate the signal amplitude because of the binary nature of the estimated signal. Another EKF based frequency estimator has also been proposed in [Routray et al., 2002]. Thus, to compare with the method from [Ziarani and Konrad, 2004] and [Trapero et al., 2007], we implement the EKF model by [Parker and Anderson, 1990], since it can estimate all the sinusoid parameters (amplitude, frequency, and phase).

Simulations with the EKF model in [Parker and Anderson, 1990] in fact show that it is comparable with the method by [Ziarani and Konrad, 2004] and [Trapero et al., 2007]. The same test signal is used here as in Trapero's model (20 unit amplitude, 0.8 Hz frequency, 1 radian phase shift, and uniform distribution noise [-0.1,0.1]). However, the offset is not be included as the EKF model does not cater for that. The result in Fig. 4.2 shows that both amplitude and frequency converge faster using the EKF compared to Trapero's method (0.4 s). The error is also considerably small.

Compared with Ziarani's method (test signal: one unit amplitude, 60 Hz, 20dB SNR), the EKF is shown to give a similar result (Fig. 4.3). The amplitude estimate converges much faster than in Ziarani's, but the frequency converges a little bit slower. In terms of estimation error, the EKF does worse than Ziarani's proposed method, as what they have claimed, although not much worse (3% estimation error compared to 0.2% in their simulation). However, 2% of error in frequency estimate is still acceptable. This is probably the tradeoff from a faster amplitude estimate.

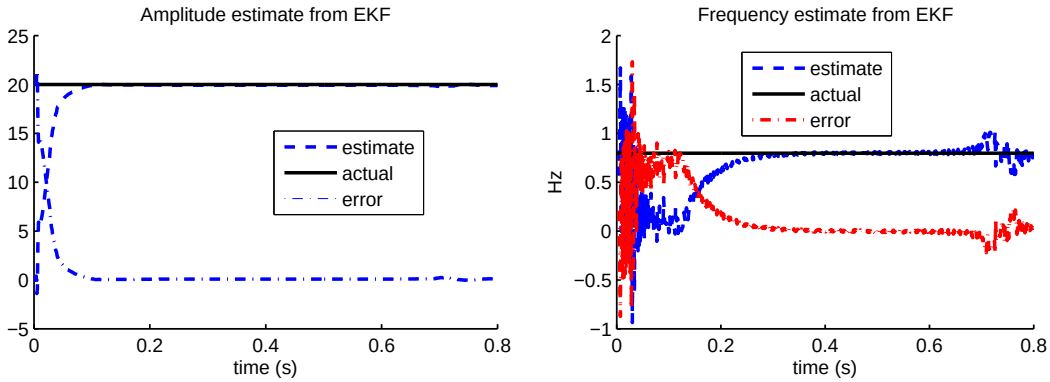

Figure 4.2: EKF estimate of amplitude (left) and frequency (right) using test signal from Trapero's case.

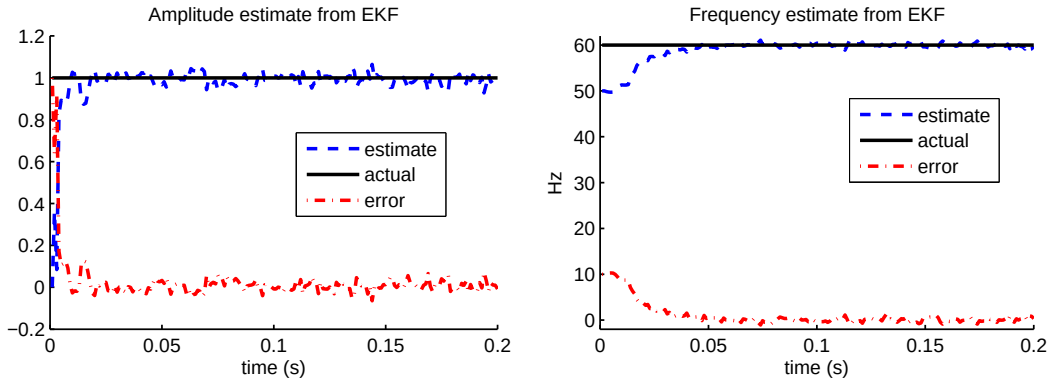

Figure 4.3: EKF estimate of amplitude (left) and frequency (right) using test signal from Ziarani's case.

4.1.4 Weighted-frequency Fourier Linear Combiner

In the application of physiological tremor, WFLC has been proposed as a modeling algorithm [Riviere et al., 1998]. WFLC is effectively a zero-phase adaptive notch or band-stop filter with the stop band centered at the dominant incoming frequency. This zero-phase characteristic of the filter and its iterative nature are crucial for developing a real-time tremor compensation system. This algorithm can track tremor amplitude and frequency.

WFLC is a modification from the previous FLC. In FLC, the frequency is assumed to be known, thus FLC only estimates the signal amplitude. WFLC is

then an extension of FLC in which the frequency is allowed to be unknown. The WFLC recursion is given below.

$$\begin{aligned} x_{r_k} &= \begin{cases} \sin\left(r\sum_{t=0}^{k} w_{0_t}\right) & 1 \le r \le M \\ \cos\left((r-M)\sum_{t=0}^{k} w_{0_t}\right) & M+1 \le r \le 2M \end{cases} \\ \epsilon_k &= s_k - \mathbf{w}_k^T \mathbf{x}_k \\ w_{0_{k+1}} &= w_{0_k} + 2\mu_0 \epsilon_k \sum_{r=1}^{M} r(w_{r_k} x_{M+r_k} - w_{M+r_k} x_{r_k}) \\ \mathbf{w}_{k+1} &= \mathbf{w}_k + 2\mu_1 \mathbf{x}_k \epsilon_k \end{aligned} \tag{4.4}$$

where $\mathbf{x}_k = [x_{1_k} \ \ldots \ x_{2M_k}]^T$ is the state vector (sinusoidal terms), $\mathbf{w}_k = [w_{1_k} \ \ldots \ w_{2M_k}]^T$ is the adaptive weight vector of the amplitudes of the sinusoidal components, M is the number of harmonics used, s_k is the input signal, and μ_0 and μ_1 are adaptive gain parameters for the frequency and amplitude estimation. Based on experience in tremor related application, the higher harmonics can be neglected. Thus when $M = 1$, the system essentially operates as an adaptive notch filter, in which the notch frequency is equal to the value of the frequency weight w_{0_k}. The system learns the unknown tremor frequency, tracking its modulation in order to maintain the proper notch frequency. The running sum of w_{0_k} values used to define s_k is necessary so that the crucial phase information is not lost.

The above equations are applied to the signal which has been bandpass filtered to the tremor frequency. This is to minimize the effect of voluntary motion to the w_{0_k}. The bandpass filter will indeed incur phase delay to the tremor signal. But the delay only affects the frequency estimate. In the amplitude estimation, it is the raw signal which is used. Thus, another set of amplitude weights $\hat{\mathbf{w}}_k$ operates on the raw signal to obtain zero-phase tremor estimation. Since tremor frequency fluctuates more slowly than amplitude, the effect of the delay is negligible [Riviere et al., 1998].

$$\begin{aligned} \hat{\epsilon}_k &= s_k - \hat{\mathbf{w}}_k^T \mathbf{x}_k \\ \hat{\mathbf{w}}_{k+1} &= \hat{\mathbf{w}}_k + 2\hat{\mu}\mathbf{x}_k \hat{\epsilon}_k \end{aligned} \tag{4.5}$$

Hence the above equations basically act as an FLC with time varying frequency. To accommodate the voluntary motion, a bias term with a separate adaptive gain μ_b may be added with the above FLC. The overall WFLC-FLC algorithm for $M = 1$ is shown in Fig. 4.4. The left part of the figure (representing (4.4)) estimates the frequency then passes it to the right side of the figure for amplitude estimation (representing (4.5) and (4.6)).

$$w_{b_{k+1}} = w_{b_k} + 2\mu_b \hat{\epsilon}_k \tag{4.6}$$

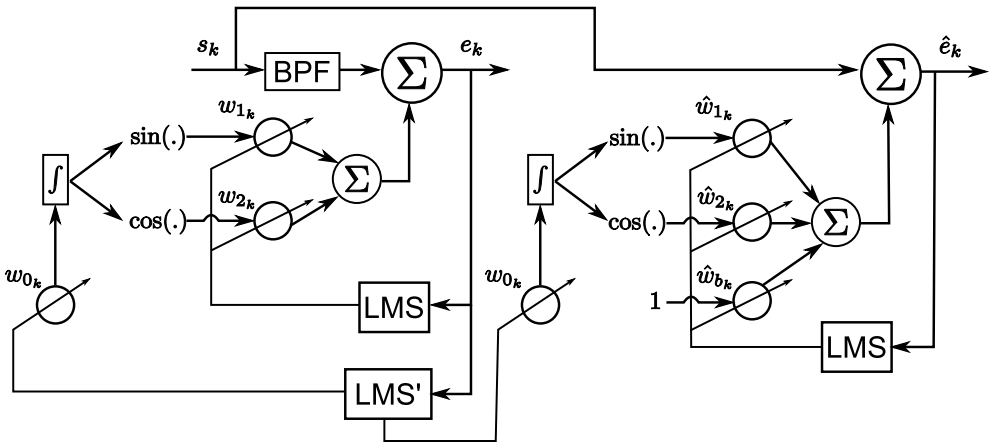

Figure 4.4: WFLC-FLC block diagram for one sinusoid term. LMS = Least Mean Square. LMS' = Modified LMS according to (4.4). BPF = Band Pass Filter.

Simulation result of WFLC-FLC in sinusoid estimation (including offset) is given in Fig. 4.5. The sinusoid signal is generated with the model proposed in [Timmer et al., 2000] to analyze physiological tremor. In that work, tremor is modeled as a second order AR model representing a stochastically driven damped linear oscillator.

$$\begin{aligned} y_k &= a_1 y_{k-1} + a_2 y_{k-2} + \epsilon_k \\ a_1 &= 2\cos(2\pi \frac{f}{f_s}) \exp(-\frac{1}{\tau}) \\ a_2 &= -\exp(-\frac{2}{\tau}) \end{aligned} \tag{4.7}$$

where ϵ_k is Gaussian noise, f is the sinusoid frequency, f_s is sampling frequency, and τ is the relaxation time. For the simulation shown in Fig. 4.5, f is 5 Hz and τ is 500 for the sinusoid component ('tremor'), while f is 0.3 Hz and τ is 2000 for the offset ('voluntary motion'). The parameters for WFLC-FLC algorithm are: $\mu_1 = 0.017, \mu_0 = 0.0012, \hat{\mu} = 0.017, \mu_b = 0.01$. The root mean square error of tremor estimate is 0.0751, which is 54.2% of the standard deviation of the actual tremor signal. This error level is comparable with the one obtained by implementing Parker's EKF (0.0794, which is 57.2% of the standard deviation of the actual tremor signal). However an advantage of this EKF is that the phase information is still the one from the original signal. In WFLC, the phase information is obtained from a filtered signal as mentioned before, thus delayed. The correct phase information is necessary for the real-time attenuation of tremor which will be discussed in the coming sections.

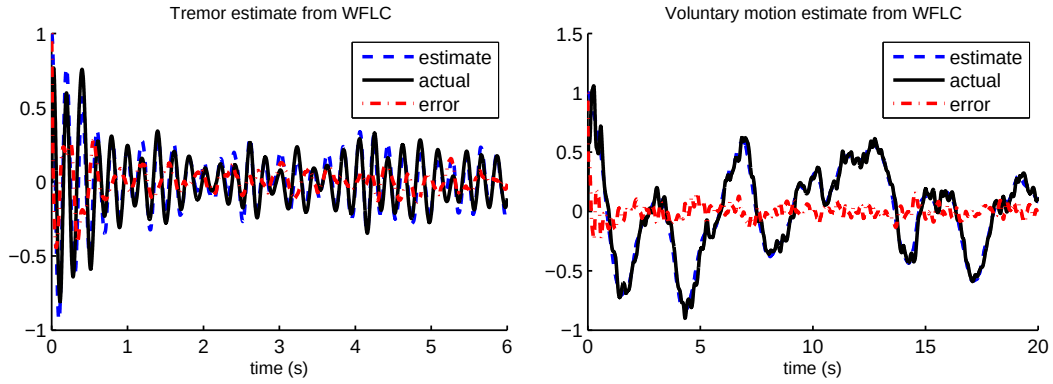

Figure 4.5: WFLC-FLC estimate of sinusoid and its offset. The sinusoid is generated by (4.7).

It seems that EKF is still a good method to implement as the simulations above have demonstrated. Indeed the performance of EKF depends on the initial conditions and the covariance matrices. However even in Ziarani's method, the adaptation parameters have to be set also. Compared to Trapero's method, EKF has been shown to converge faster. Furthermore, the factor t in (4.3) can result in unstable system due to the integration process. With these considerations,

EKF is chosen as the basic algorithm for tremor parameter estimation. It will also be shown subsequently that the EKF can meet the requirement in tremor application while the Kalman filter is not adequate. Finally the EKF proposed by [Parker and Anderson, 1990] will be extended so that it can filter off the voluntary motion.

A table summarizing the comparison between some of the methods surveyed above is given in Table 4.1.

Table 4.1: Comparison of signal parameter estimation methods. The numbers inside the bracket are those obtained from the methods which are being compared against EKF.

EKF & [Ziarani and Konrad, 2004]
error = 3% (0.2%) amplitude convergence = 0.01s (0.05s) frequency convergence = 0.06s (0.05s) Initial condition: frequency
EKF & [Trapero et al., 2007]
error = very small (very small) amplitude convergence = 0.05s (0.4s) frequency convergence = 0.3s (0.4s) Initial condition: none
EKF & [Riviere et al., 1998]
error = 57.2% (54.2%) convergence = not applicable, the estimated signal is stochastic. Initial condition: frequency, learning parameters

4.2 Kalman Filter (KF) for tremor estimation

Kalman filter is simply an optimal recursive data processing algorithm [Maybeck, 1979]. A system is driven by the control input and some variables from the system are monitored by measuring devices. The variables observed by the measuring devices may not be the same as the control input, though dependent

on it. Moreover, the measuring process is disturbed by some degree of various kinds of noise. We also may have more than one measuring device with its own distinct characteristics.

A Kalman filter combines all available measurement data, plus prior knowledge about the system and measuring devices, to produce an estimate of the desired variables in such a manner that the error is minimized statistically. The basic assumption of a Kalman filters is that the system is a linear model in which system and measurement noises are white and Gaussian. Under these conditions, there is in fact a unique "best" estimate of the value of the state. The state estimation cycle consists of two steps: 1) state and measurement prediction (or time update) and 2) state update (or measurement update). In each step, a model is necessary (process and measurement model respectively).

If tremor is approximated as a rhythmic and roughly sinusoidal signal [Elble and Koller, 1990], then linear process and measurement models can be developed to estimate the tremor signal. Furthermore, the KF can use both measurements from SEMG and ACC to make better estimate of the tremor.

Let $\theta(k)$ be the joint angle of the tremulous limb, then modeling the tremor as single sinusoidal signal we have

$$\theta(k) = r\sin(\omega kT), \qquad k = 1, 2, 3, \ldots \tag{4.8}$$

where r is the tremor amplitude, ω is the tremor frequency in rad/s, and T is the sampling time in s. Both r and ω are assumed to be constant. The state vector for the KF will be the joint angle and its angular velocity.

To get the dynamic plant equation, trigonometric addition formula is em-

ployed:

$$\begin{aligned}\theta(k+1) &= r\sin(\omega(k+1)T) \\ &= r\big(\sin(\omega kT)\cos(\omega T) \\ &\quad + \cos(\omega kT)\sin(\omega T)\big) \\ &= \theta(k)\cos(\omega T) + \frac{\dot{\theta}(k)}{\omega T}\sin(\omega T).\end{aligned} \tag{4.9}$$

Similarly

$$\dot{\theta}(k+1) = \dot{\theta}(k)\cos(\omega T) + \frac{\ddot{\theta}(k)}{\omega T}\sin(\omega T). \tag{4.10}$$

Notice that

$$\begin{aligned}\ddot{\theta}(k) &= -r(\omega T)^2\sin(\omega kT) \\ &= -(\omega T)^2\theta(k).\end{aligned} \tag{4.11}$$

Hence

$$\dot{\theta}(k+1) = \dot{\theta}(k)\cos(\omega T) - \omega T\theta(k)\sin(\omega T). \tag{4.12}$$

Therefore, the process model for the sinusoidal signal is

$$\begin{bmatrix}\theta(k+1)\\ \dot{\theta}(k+1)\end{bmatrix} = x(k+1) = \begin{bmatrix}\cos(\omega T) & \frac{\sin(\omega T)}{\omega T}\\ -\omega T\sin(\omega T) & \cos(T)\end{bmatrix} x(k) + \mathbf{w}(k) \tag{4.13}$$

where $\mathbf{w}(k)$ is zero mean white Gaussian noise with $\mathbf{Q}(k)$ as its covariance matrix:

$$E[\mathbf{w}(k)\mathbf{w}(k)'] = \mathbf{Q}(k) = \begin{bmatrix}\sigma_\theta^2 & 0\\ 0 & \sigma_{\dot{\theta}}^2\end{bmatrix} \tag{4.14}$$

This process is measured by two sensors, SEMG and ACC. The accelerometer reading is taken as it is (in voltage), but the raw SEMG is not used as the input to the KF. Its linear envelope is used instead to reflect tremor kinematics better. The linear envelope process consists of full rectification and 2$^{\text{nd}}$ order low-pass elliptic filter.

Information from both sensors can be fused together by the Kalman filter to give better estimate of the state rather than taking the estimate independently.

However, for the measurement model, a relationship between the joint angle and sensor readings from SEMG and ACC has to be defined. Existing literature that discusses the relationship between joint angle and EMG is rare. Most literature talks about EMG-force relationship and it is a complicated issue. Various models have been proposed. For example the work in [Hayashibe et al., 2009] focuses on parametric modeling using a modified Hill and Huxley model. On the other hand, non parametric approach is also done in [Mobasser et al., 2007], in which neural network is used as the modeling tool. The way of acquiring the input signal to the model also affects the result. For example, in [Clancy et al., 2006], a new method to acquire the SEMG amplitude is proposed, instead of the usual linear envelope. Indeed, with so much variability in the muscle, electrodes, within subject, and across subjects, it is stipulated that an adaptive EMG-force relationship is hardly feasible in the near future [Merletti and Parker, 2004].

By using neural network, it has been shown that EMG signals contain information about the arm kinematics, but the RMS error for joint angle estimation is between 8°and 20°[Au and Kirsch, 2000]. Different neural networks have been explored in the same line and the result is better in one plane only [Dipietro et al., 2003].

The relationship between joint angle and ACC reading is well defined, although it is nonlinear. The acceleration measured consists of 4 components, the inertial acceleration of the link, a_{CG}, centripetal acceleration, a_C, tangential acceleration, a_T, and gravitational acceleration, g. The accelerometer equation is given in (2.1).

For the 3-axis accelerometer implemented in the system, (2.1) contains 3 nonlinear equations (because of the 3-axis). By approximating the angular velocity and acceleration using backward difference method, there will be 3 unknowns in 3 equations. Thus, it is feasible to solve it theoretically using numerical method such as Levenberg-Marquardt algorithm. However, it is noted that the equations involve trigonometric function ($R_{\theta(k)}$) and will cause singularity problem.

Quaternion is another way to represent the direction cosine matrix without transcendental function, but the numerical method still cannot find the solution due to local minima problem. This may be caused by the minimal constraints we have in (2.1).

Even if the centripetal acceleration component is neglected (angular velocity is assumed to be comparably small than other components), the numerical method still cannot find a good approximation. The approximated equation is:

$$\begin{aligned} a_x(k) &= \ddot{\theta}_y(k)r_z - \ddot{\theta}_z(k)r_y - (\theta_x(k)\theta_y(k) + \theta_z(k))g \\ a_y(k) &= \ddot{\theta}_z(k)r_x - \ddot{\theta}_x(k)r_z - (\theta_y(k)\theta_z(k) - \theta_x(k))g \\ a_z(k) &= \ddot{\theta}_x(k)r_y - \ddot{\theta}_y(k)r_x - g \end{aligned} \tag{4.15}$$

Despite the difficulties to relate joint angle with EMG and ACC data, there is one way to overcome it by exploiting the periodic motion assumption. Since shape of all the signals from each sensor are quite similar (because of its periodicity), it is reasonable to try a simple first order polynomial for the relationship. Thus, linear regression will be applied to a slice of data to determine the coefficients of the polynomial. In linear regression, a first order relationship between the input and output can be modeled as in the equation below

$$y_i = a + bx_i + \epsilon_i, \qquad i = 1, 2, \ldots, n \tag{4.16}$$

where y is either the EMG or ACC data, x is the joint angle data, ϵ is the error. Coefficients a and b are estimated using least square method.

Therefore, the measurement for this system is

$$z(k) = \begin{bmatrix} EMG(k) \\ ACC(k) \end{bmatrix} = \begin{bmatrix} c_{EMG}(1) & 0 \\ c_{ACC}(1) & 0 \end{bmatrix} \begin{bmatrix} \theta(k) \\ \dot{\theta}(k) \end{bmatrix} + \begin{bmatrix} c_{EMG}(2) \\ c_{ACC}(2) \end{bmatrix} + \mathbf{v}(k) \tag{4.17}$$

where $\mathbf{v}(k)$ is also zero mean white Gaussian noise with $\mathbf{R}(k)$ as its covariance matrix. It is assumed that the noise from EMG and ACC are independent of

each other.

$$E[\mathbf{v}(k)\mathbf{v}(k)^T] = \mathbf{R}(k) = \begin{bmatrix} \sigma^2_{EMG} & 0 \\ 0 & \sigma^2_{ACC} \end{bmatrix} \tag{4.18}$$

The noise covariance matrix for measurement model is obtained by calculating the variance of the signal during stationary motion. It is assumed that the noise from EMG and ACC are Gaussian and they are independent of one another.

The result of applying the KF algorithm to data from a PD patient (labeled as PD1) is shown in Fig. 4.6. The tremor data are taken from the wrist flexion-extension during resting position (sitting down, arm on lap, and no voluntary motion). The KF algorithm estimates the wrist flexion-extension angle from the ACC (placed on dorsum of hand) and SEMG data (wrist flexor and extensor). Then the angle estimate is compared with the joint angle obtained from the optical tracking system. This angle information will act as the 'true' signal. The RMS error is 0.65°, compared with the standard deviation of the tremor signal, 2.72°. Thus the tremor is accounted for about 76.1%. Result from another PD patient (labeled as PD2) is shown in Fig. 4.8. Tremor is accounted for about 63.3%. Figure 4.7 and 4.9 show the power spectrums of the tremulous joint angle signal and the error signal (difference between measured and estimated signal). It should be noted that the power spectrum of the error signal is not Gaussian, which means that the KF cannot model the tremor completely. The next section will discuss the limitations of this KF model.

4.2.1 Limitation of KF modeling

Although the KF provides a way to do sensor fusion of both SEMG and ACC data, there are few problems with this implementation. The first is about the usefulness of the state vector to be estimated for actuation purpose (FES is used for this project). In the discussion above, the state to be estimated is the signal itself (and its derivative). This may not be directly useful for FES since the three main parameters for controlling the FES are the amplitude, pulse frequency, and pulse width. Usually the pulse frequency will be fixed, so we need to control the

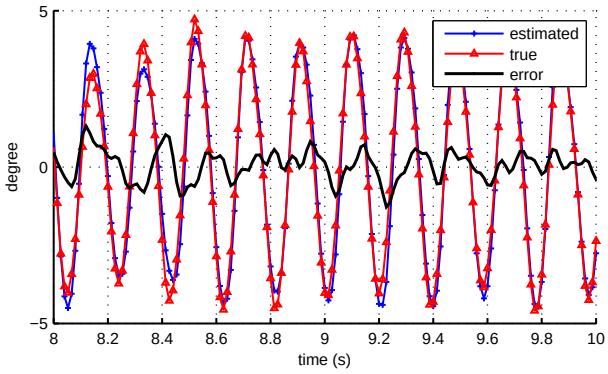

Figure 4.6: Result of joint angle estimation using Kalman filter from a Parkinson's Disease patient (PD1, rest).

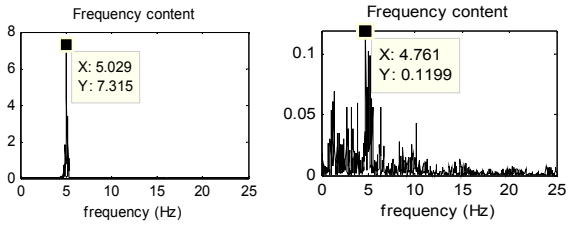

Figure 4.7: Power spectrum of the measured joint angle signal (left) and the error signal (right) using Kalman filter from a Parkinson's Disease patient (PD1, rest).

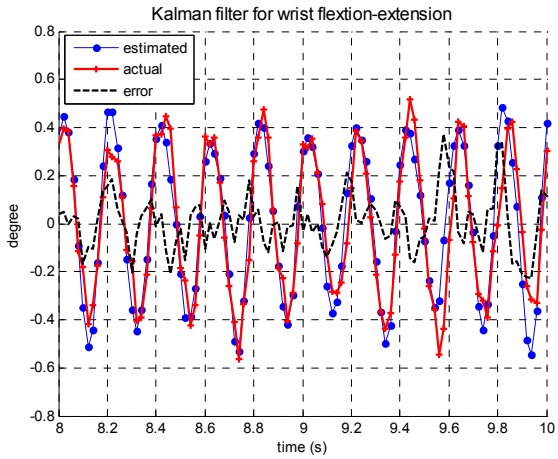

Figure 4.8: Result of joint angle estimation using Kalman filter from another Parkinson's Disease patient (PD2, rest).

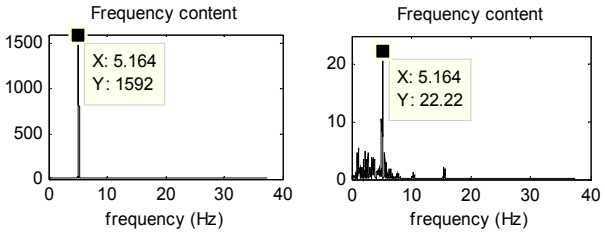

Figure 4.9: Power spectrum of the measured joint angle signal (left) and the error signal (right) using Kalman filter from another Parkinson's Disease patient (PD2, rest).

amplitude and the pulse width. To do this, the amplitude, frequency, and the phase of the tremor signal will be useful. It will be shown in the next section that using those parameters as the state will result in nonlinear measurement model. Thus in this work, an EKF based algorithm to estimate those three parameters from the tremor signal is proposed. The EKF approximates a nonlinear process by taking only the linear terms of its Taylor series expansion and substitutes the Jacobian for the linear transformation matrices in the KF equations. The remaining update equations remain the same.

The choice of using amplitude, frequency, and phase as the states of the EKF will also prevent us from assuming the linearity between SEMG and ACC information with joint angle (which is assumed in (4.13) and (4.17)). Although the linearity assumption seems to work quite well, probably due to the regular characteristics of rest tremor, the filter may not be robust enough for other types of tremor. The above algorithm was tested on data from PD patients and usually tremor from PD patient is quite regular. So it is preferable to have an algorithm to extract the information from the tremor which is not constrained by that assumption.

Another assumption used in the previous model in (4.13) is that the tremor has constant amplitude and frequency. Again this assumption, though it may work in some cases where the amplitude and frequency are relatively constant, seems a little naive. It has been found that the standard deviation of tremor frequency

in essential tremor and Parkinson's disease is about 10% of the mean, whereas the variation of amplitude is bigger, i.e. about 30% of the mean [Gao, 2004]. The EKF algorithm proposed here will be able to track the varying parameters.

In the KF implementation above, it has been assumed that the tremor signal recorded by the sensing system does not include voluntary motion. Clearly this is not the case in activities of daily living. Therefore another filtering process to differentiate between the tremor and the voluntary motion is needed. Although there is a clear frequency separation between tremor and intended motion, classical linear filter cannot be used here because of the phase shift incurred. Thus zero-phase characteristic of the filter is crucial. If the signals phase is changed due to classical filtering and the filtered signal is used for cancellation, then we are not canceling the actual tremor seen by the sensing process.

4.3 Formulation of the Extended Kalman Filter Algorithm

In this section, the EKF by [Parker and Anderson, 1990] is laid out before some modifications are proposed to cater for tremor parameter estimation. Afterwards, simulations and results of the modifications and the EKF are given.

It should be noticed that the input to the EKF model is the linear envelope of the raw SEMG (full rectification followed by a low pass filter). An example of a linear envelope of a tremor signal is given in Fig. 4.10. In the figure, the tremor amplitude unit is in Volt, but it is after 500 times magnification, thus '(V×500)'. This convention will be used throughout this thesis.

A slowly time-varying periodic signal with zero d.c. component, $y(k)$, is modeled as a summation of m sinusoidal terms. There is no offset estimation in

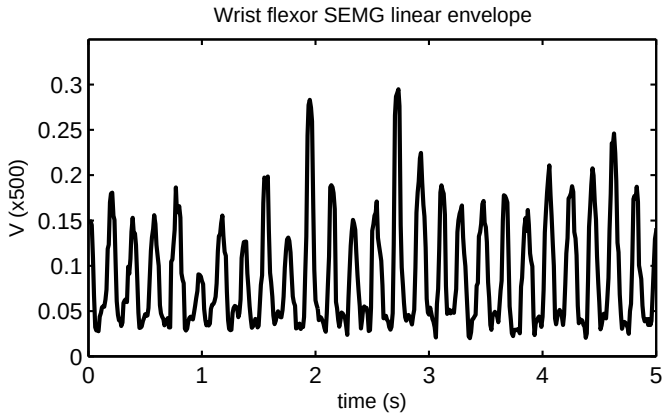

Figure 4.10: Linear envelope of tremor signal from a PD patient (wrist flexor). The amplitude unit is in Volt after 500 times magnification, thus '(V×500)'.

[Parker and Anderson, 1990].

$$\begin{aligned} \theta_i(k) &= \sum_{\rho=1}^{k} i\omega(\rho)T + \phi_i(k) \\ y(k) &= \sum_{i=1}^{m} r_i(k)\sin(\theta_i(k)). \end{aligned} \tag{4.19}$$

The state vector, $\mathbf{x}(k)$, includes the amplitude, $r_i(k)$, frequency, $\omega(k)$, phase, $\theta_i(k)$. Notice that the phase information in (4.19) is the total phase which includes the relative phase, $\phi_i(k)$. The process model is then defined as

$$\begin{aligned} \mathbf{x}(k) = \big[\, & r_1(k) \quad r_2(k) \quad \dots \quad r_m(k) \quad \omega(k)T \\ & \theta_1(k) \quad \theta_2(k) \quad \dots \quad \theta_m(k) \,\big]^T \end{aligned} \tag{4.20}$$

$$\mathbf{F} = \left[\begin{array}{c|ccccc} I_m & \multicolumn{5}{c}{0} \\ \hline & 1 & & & & \\ & 1 & 1 & & & \\ 0 & 2 & & 1 & & \\ & \vdots & & & \ddots & \\ & m & & & & 1 \end{array}\right] \tag{4.21}$$

$$\mathbf{x}(k+1) = \mathbf{F}\mathbf{x}(k) + \mathbf{w}(k), \tag{4.22}$$

where $\mathbf{F}_{2m+1\times 2m+1}$ is the state update matrix and $\mathbf{w}(k)$ is zero mean white Gaussian noise with $\mathbf{Q}$ as its covariance matrix.

It can be seen that from (4.21) and (4.22) that the states evolve as a random walk, with $\mathbf{Q}$ specifying the rate of the random change. In relation to the total and relative phase mentioned above, it is the relative phase which evolves as a random walk. This process model is linear.

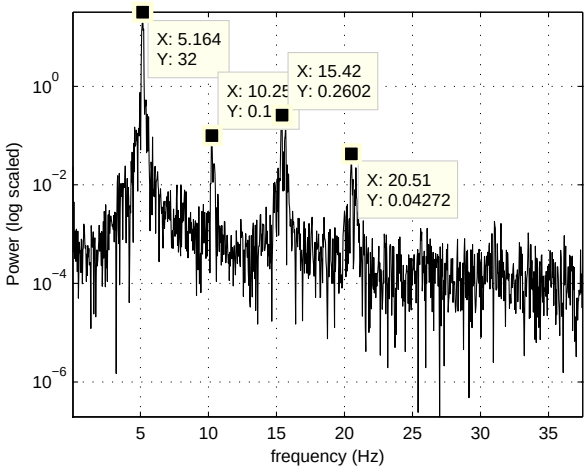

Figure 4.11: Power Spectral Density of the ACC data (mean subtracted)

For this experiment, only one sinusoid is used ($m = 1$) although the EKF can accommodate multiple harmonics. The power spectral density of the ACC data, already subtracted by its mean, is shown in Fig. 4.11 (in logarithmic scale). It can be seen that the tremor has multiple harmonics. However the amplitude of the next largest harmonics is only 0.6% from that of the fundamental frequency, thus not significant. Furthermore, using one sinusoid will also lessen the computational burden of the whole algorithm.

The measurement model is then given by

$$h(\mathbf{x}(k)) = \sum_{i=1}^{m} r_i(k) \sin\theta_i(k) \tag{4.23}$$

$$z(k) = h(\mathbf{x}(k)) + v(k). \tag{4.24}$$

where $v(k)$ is the measurement noise (zero mean white Gaussian) and R is the variance. The measurement process is nonlinear due to the $\sin(\centerdot)$ operation, thus the necessity to use EKF instead of Kalman Filter. In the EKF, the measurement process $\mathbf{h}(x(k))$ is approximated by expanding it in Taylor series and ignoring the higher order terms. This model does not separate tremor and intended motion. It assumes that the recorded signal only consists of tremulous movement.

With the model described in (4.20)-(4.24), we can apply the EKF equations [Anderson and Moore, 1979] to estimate the states, which consists of state and measurement prediction:

$$\mathbf{x}(k+1|k) = \mathbf{F}\mathbf{x}(k|k) + \mathbf{G}\omega(k) \tag{4.25a}$$

$$\mathbf{P}(k+1|k) = \mathbf{F}\mathbf{P}(k|k)\mathbf{F}^T + \mathbf{Q}, \tag{4.25b}$$

and state update or measurement update equation

$$\mathbf{x}(k|k) = \mathbf{x}(k|k-1) + \mathbf{K}(k)[z(k) - h(\mathbf{x}(k|k-1))] \tag{4.26a}$$

$$\mathbf{P}(k|k) = \mathbf{P}(k|k-1) - \mathbf{K}(k)\mathbf{H}(k)^T\mathbf{P}(k|k-1), \tag{4.26b}$$

where $\mathbf{P}$ is the error covariance matrix, $\mathbf{K}$ is the Kalman gain, and $\Omega(k)$ is the covariance of the innovation term $z(k) - h(\mathbf{x}(k|k-1))$, as defined below

$$\mathbf{K}(k) = \mathbf{P}(k|k-1)\mathbf{H}(k)\Omega(k)^{-1} \tag{4.27a}$$

$$\Omega(k) = \mathbf{H}(k)^T\mathbf{P}(k|k-1)\mathbf{H}(k) + \mathbf{R} \tag{4.27b}$$

$$\mathbf{H}(k) = \frac{\partial h(\mathbf{x}(k|k-1))}{\partial \mathbf{x}(k|k-1)} \begin{bmatrix} \sin\theta_1(k|k-1) \\ \sin\theta_2(k|k-1) \\ \vdots \\ \sin\theta_m(k|k-1) \\ 0 \\ r_1\cos\theta_1(k|k-1) \\ r_2\cos\theta_2(k|k-1) \\ \vdots \\ r_m\cos\theta_m(k|k-1) \end{bmatrix}^T. \tag{4.27c}$$

Finally, the filter is initialized by

$$\mathbf{x}(0|-1) = E\big[\mathbf{x}(0)\big] = \bar{\mathbf{x}}_0 \tag{4.28a}$$

$$\mathbf{P}(0|-1) = E\big[(\mathbf{x}(0) - \bar{\mathbf{x}}_0)(\mathbf{x}(0) - \bar{\mathbf{x}}_0)^T\big]. \tag{4.28b}$$

It should be noted that the only term inverted in the EKF, $\mathbf{H}^T(k)\mathbf{P}(k|k-1)\mathbf{H}(k)+\mathbf{R}$, is a scalar. The state transition matrix F is also sparse, causing a lower than expected computational load.

It has been shown by Parker and Anderson that the EKF estimator behaves like a generalized phase locked loop. When the phase estimation error is small, the update equations for the amplitude estimate are standard Kalman filter equations, identical with those when the phases are exactly known (and the decoupling is complete). It is also noticed that significant phase errors can presumably be tolerated before amplitude estimation becomes significantly different because of phase error.

The frequency-phase equation in effect defines two coupled phase locked loops. That there should be interconnection (through the integrator with output $\hat{\omega}$) is hardly any surprise, given the harmonic relationship between the different components in the signal.

From the implementation point of view, there are a few things to be considered [Parker and Anderson, 1990]:

1. Frequency estimate $\hat{\omega}$ can lock onto a fraction or multiple of the true frequency ω.

   This happens when there are multiple harmonics and the model also tries to estimate them. Suppose $\hat{\omega}$ locks onto $\frac{1}{2}\omega$. Then $\hat{r}_1$ is around zero; $\hat{r}_2$ tracks r_1, $\hat{r}_3$ is near zero, $\hat{r}_4$ tracks r_2, and so on. (The variable with $\hat{}$ on top symbolizes the estimate of the actual value.)

   It is well known that a phase locked loop may not capture a signal if its center frequency i.e. the initial frequency estimate is too distant from the signal's actual frequency. Therefore, good initialization is also important

in our more general problem. Nevertheless this issue only happens if the model includes estimation of the harmonics. As mentioned above, tremor is only modeled as a sinusoid without its harmonics.

2. Cycle slipping, i.e. $\theta(k)$ and $\hat{\theta}(k)$, for some k differ approximately by a multiple of 2π.
   It is acknowledged that it is not of much consequence because of the phase modeling. The phase information is modeled as cumulative sum of instantaneous frequency and a phase change, therefore both $\theta(k)$ and $\hat{\theta}(k)$ form a ramp function.
   However to prevent numerical overflow, the phase magnitude is limited to 2π by subtracting the phase estimate if it is larger than 2π.

3. A more subtle form of cycle slipping is that $\hat{r}(k)$ could become negative for some k, implying tracking of $-\hat{r}(k)$, and $\hat{\theta}(k)$ would then differ from $\theta(k)$ by π. Thus, if $\hat{r}(k)$ is negative, change its sign and add π to $\hat{\theta}(k)$.

Lastly, with respect to implementation issue, the data is obtained with 1000 Hz sampling rate, but the measurement update is run only at 100 Hz. In between both measurement updates only time update occurs and the innovation vector is set to zero. This is to save computational time as the measurement update loop is skipped 90% of the time.

We are now proposing two modifications for the EKF model above: 1) modeling of intended motion and related to it 2) restoring term for frequency estimate.

4.3.1 Filtering of intended motion

We have mentioned in the beginning of this chapter that the above EKF model does not take intended motion into consideration. This intended or voluntary motion has in general a lower frequency than that in tremor. Analysis of wrist

motion data has shown that the predominant average frequency of activities in daily living is around 1 Hz [Mann et al., 1989].

An example of tremor signal superimposed with voluntary motion is given in Fig. 4.12. The movement is from a Holmes' tremor patient doing a finger-to-nose movement. The top figure is taken from biceps and it shows that finger-to-nose movement. The middle and bottom figures show the wrist flexor activity including the tremor with its linear envelope. The frequency difference of tremor and voluntary motion frequency is shown in Fig. 4.13. This frequency difference is utilized to separate tremor and voluntary motion. Nevertheless, the profile of voluntary motion cannot be predicted and does not conform to a certain model (such as sinusoids in the case of tremor).

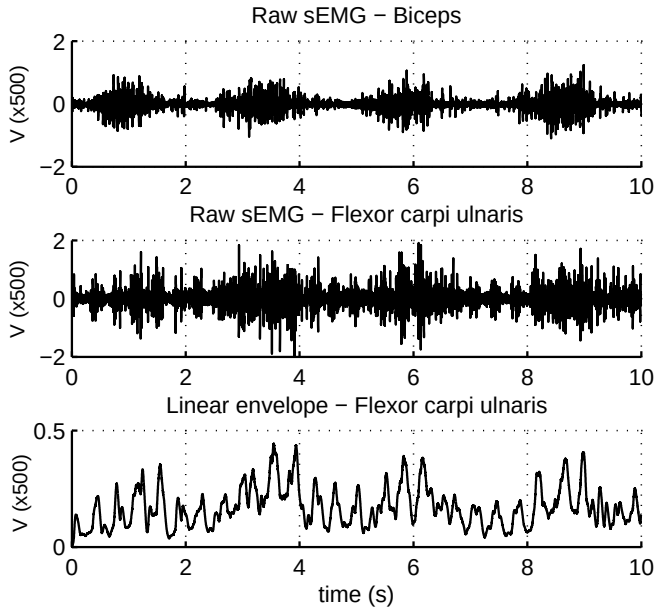

Figure 4.12: SEMG signal of Holmes' tremor patient. Top: biceps, middle: wrist flexor, bottom: linear envelope of wrist flexor.

One interesting approach is proposed to model the human upper limb motion [Yun and Bachmann, 2006] (Fig. 4.14). Considering the real time requirement for the motion tracking and based on extensive trial and error study, they have shown that a first order autoregressive (AR) model system is enough to represent

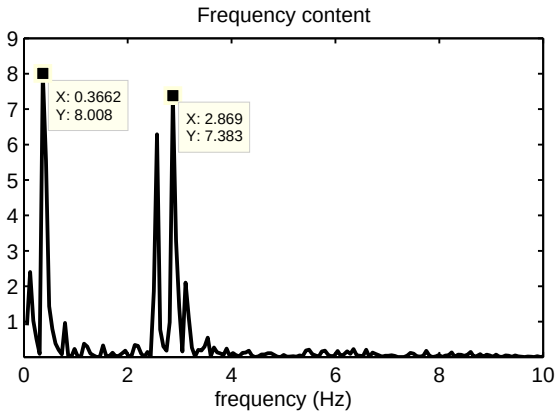

Figure 4.13: Power spectrum of SEMG signal from Holmes' tremor patient in Fig. 4.12

the angular velocity of a human upper limb segment. The input to the linear system is a white noise w, and the output is the angular velocity ω of the limb segment. The most important parameter in this model is the time constant τ, which determines how fast a limb segment (e.g., upper arm) can move in typical human motion conditions. The angular velocity is thus modeled as a colored noise generated by a linear system with a white noise input.

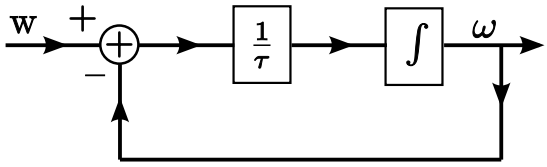

Figure 4.14: Human upper limb motion model in [Yun and Bachmann, 2006]

This model is basically a first order autoregressive (AR) model and it can be easily incorporated into the EKF developed above by adding one more state. In fact, the random walk model is actually a specific case of a first order AR model.

$$y(n+1) = \lambda y(n) + w(n) \tag{4.29}$$

When $\lambda = 1$, the AR model becomes a random walk.

Hence, using only one sinusoid to represent tremor and adding the intended motion term to (4.22), we have

$$\begin{bmatrix} r(k+1) \\ \omega(k+1) \\ \theta(k+1) \\ b(k+1) \end{bmatrix} = \begin{bmatrix} 1 & 0 & 0 & 0 \\ 0 & 1 & 0 & 0 \\ 0 & 1 & 1 & 0 \\ 0 & 0 & 0 & 1 \end{bmatrix} \begin{bmatrix} r(k) \\ \omega(k) \\ \theta(k) \\ b(k) \end{bmatrix} + \mathbf{w}(k). \tag{4.30}$$

where $b(k)$ is the term for the intended motion. Its noise variance determines the bandwidth of the motion and it will be set to a relatively small value to emulate low frequency movement.

It should be noted also that the inclusion of this term is also useful for removing the offset of the sinusoid (as shown in Fig. 4.10), despite the absence of any intended motion from the subject.

4.3.2 Restricting term for tremor frequency

Another modification may be necessary because of the inclusion of the intended motion in (4.30). The intended motion term does not restrict the other sinusoid parameters and vice versa. With no restriction, it is possible that the EKF will track the frequency of intended motion instead of tremor. While tremor frequency is higher, the amplitude is probably smaller than voluntary motion.

To tackle this problem, a restriction is imposed to the tremor frequency estimate, i.e. it has an average value.

$$\omega(k+1) = \lambda\omega(k) + (1-\lambda)\bar{\omega} + w(k) \tag{4.31}$$

where λ is the weight factor and $\bar{\omega}$ is the average value of the tremor frequency. It can be seen immediately that taking the expectation over both sides of the equation, the expected value of ω is $\bar{\omega}$. This is actually a generalization of the previous model for tremor frequency because of the λ. The weight factor λ can range from 0 to 1. By setting $\lambda = 1$, the model becomes random walk. The

smaller the λ, the larger the weight of the predetermined average value, thus the smaller the frequency fluctuation.

So, the final process equation is

$$\begin{bmatrix} r(k+1) \\ \omega(k+1) \\ \theta(k+1) \\ b(k+1) \end{bmatrix} = \begin{bmatrix} 1 & 0 & 0 & 0 \\ 0 & \lambda & 0 & 0 \\ 0 & 1 & 1 & 0 \\ 0 & 0 & 0 & 1 \end{bmatrix} \begin{bmatrix} r(k) \\ \omega(k) \\ \theta(k) \\ b(k) \end{bmatrix} + \begin{bmatrix} 0 \\ (1-\lambda)\bar{\omega} \\ 0 \\ 0 \end{bmatrix} + \mathbf{w}(k). \tag{4.32}$$

And the measurement model becomes

$$h(\mathbf{x}(k)) = \sum_{i=1}^{m} r_i(k) \sin\theta_i(k) + b(k) \tag{4.33}$$

$$z(k) = h(\mathbf{x}(k)) + v(k). \tag{4.34}$$

4.3.3 'Zero phase' characteristic of EKF

Before testing the algorithm, it is important to ensure that the EKF algorithm does not cause any phase lag to the tremor estimate. This characteristic is necessary for real-time attenuation of tremor. In the literature review section, it has been mentioned that although WFLC is a 'zero-phase' filter, the phase estimate is delayed due to the bandpass filter used. In this section, simulations are carried out to show that the EKF and its proposed modifications do not incur any phase delay.

To simulate tremor movement added with voluntary motion, the model in (4.7) [Timmer et al., 2000] is used. Similar initialization and parameters in Section 4.1.4 is used. Comparison with real tremor data from a PD patient is also given to show the similarity to the simulated signal (Fig. 4.15). The tremor SEMG signal (linear envelope) is obtained from a PD patient (wrist flexor, at rest). There are 'harmonics' in the tremor data due to the activity in between tremor bursts. This is probably because of crosstalk from the extensor. In general, the tremor is more regular compared to the simulated signal. The simulated signal has a few peaks, indicating that the frequency fluctuates more than tremor frequency.

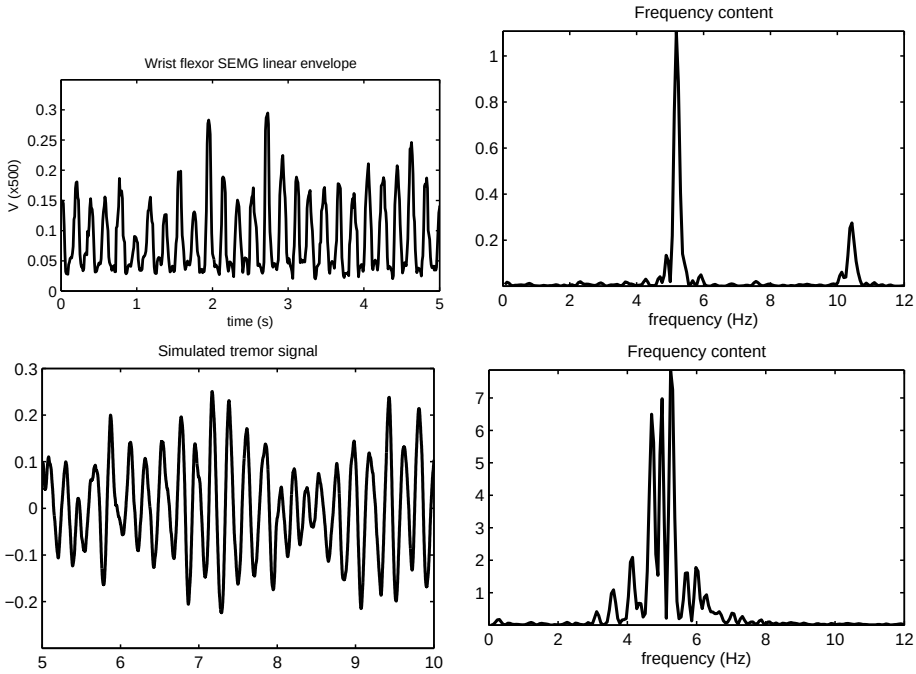

Figure 4.15: Comparison between real tremor signal from a PD patient (top) and simulated tremor signal using (4.7) (bottom). The respective power spectrum is given on the right side.

The EKF initialization parameters are

$$\begin{aligned}
\mathbf{x}(0|-1) &= \begin{bmatrix} 0 & 2\pi 5T & 0 & 0 \end{bmatrix}^T \\
\mathbf{P}(0|-1) &= \texttt{diag}\left\{ 10^{-4} \quad (2\pi 0.01T)^2 \quad 0.02 \quad 10^{-6} \right\} \\
\mathbf{Q} &= \texttt{diag}\left\{ 10^{-5} \quad 10^{-7} \quad 10^{-5} \quad 10^{-4} \right\} \\
\mathbf{R} &= [3 \times 10^{-4}] \\
\lambda &= 0.999
\end{aligned} \tag{4.35}$$

The sampling period is 0.001 s and the signal length is 10 s.

Monte Carlo simulation is done for 10000 trials and the delay between the simulated tremor signal and its estimate is calculated. Note that the delay calculation is only applied to the tremor component (after subtracting the total signal form the voluntary motion component). The delay is calculated by using cross correlation equation in (3.1).

The average delay for 10000 trials is 1.41±4.86 samples. The standard deviation is quite large because there are 6 trials which has large delay. Without these outliers, maximum delay is only 3 samples, which is very small. The outliers (ranging from 194 to 203 samples) are actually equivalent to one sinusoid period (5 Hz sinusoid with 1000 Hz sampling rate). Therefore in general the delay is indeed negligible.

4.4 Results and Discussion

In this part it will be shown, through simulation and real tremor data, that the proposed EKF algorithm can estimate the necessary parameters from the tremor signal recorded by SEMG. The SEMG signal is processed first (linear envelope) before the EKF algorithm is applied. The effect of the proposed modifications is also shown. Furthermore the complete EKF algorithm is tested with simulated tremor and real tremor data (both with and without voluntary tremor).

For simulation purpose, both tremor and voluntary motion are simulated using the model in (4.7) with the same parameters that have been used so far. The EKF is initialized with the parameters below. The simulation is carried out 1000 times. The RMSE of tremor estimate is 0.0799, while the standard deviation of the simulated tremor signal is 0.1586 (The error of the estimate is 50.4%). For the intended motion, the RMSE is 0.0794, out of 0.4087 (19.4% error). The plot for one trial is given in Fig. 4.16.

$$\begin{aligned}
\mathbf{x}(0|-1) &= \begin{bmatrix} 0 & 2\pi 5T & 0 & 0 \end{bmatrix}^T \\
\mathbf{P}(0|-1) &= \mathtt{diag}\left\{ 10^{-4} \quad (2\pi 0.01T)^2 \quad 0.02 \quad 10^{-6} \right\} \\
\mathbf{Q} &= \mathtt{diag}\left\{ 10^{-5} \quad 10^{-7} \quad 10^{-4} \quad 10^{-4} \right\} \\
\mathbf{R} &= [3 \times 10^{-4}] \\
\lambda &= 0.999
\end{aligned} \tag{4.36}$$

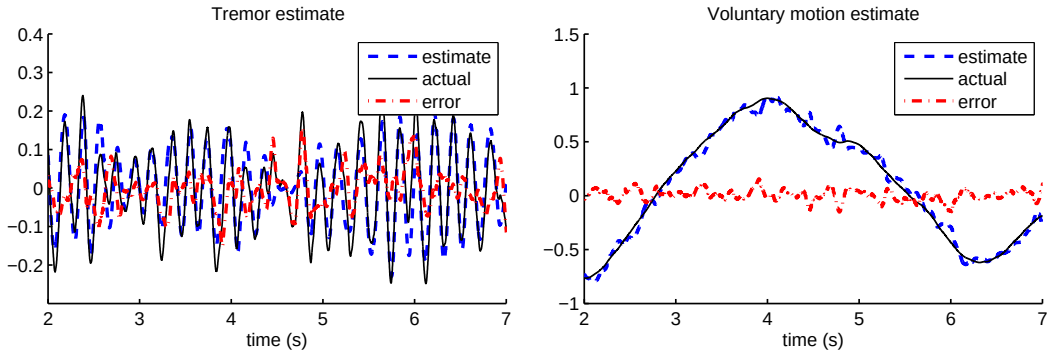

Figure 4.16: Tremor and voluntary motion estimate from EKF using simulated tremor signal.

The result of EKF in separating tremor and intended motion from real data is shown in Fig. 4.17. In that figure the data used is that from Fig. 4.12. The subject has Holmes' tremor which is characterized by existence of all types of tremor (rest, postural, and kinetic). Usually the tremor has low frequency (<4.5 Hz) [Deuschl et al., 2001]. The data is taken during finger-to-nose test and drawing of Archimedean spiral. In finger-to-nose test the patient is asked to touch repeatedly his nose and stretch to a target in front of him with his extended index finger. Thus since the patient has kinetic tremor, the recorded data contains both voluntary motion (finger-to-nose) and tremor. Data is acquired from SEMG system as described in Section 2.2.4. EKF is initialized as follow. There is no restricting term in this EKF, thus $\lambda = 1$. The initial tremor frequency can be obtained by previously collecting data from the patient.

$$\begin{aligned} \mathbf{x}(0|-1) &= \begin{bmatrix} 0 & 2\pi 3T & 0 & 0 \end{bmatrix}^T \\ \mathbf{P}(0|-1) &= \mathtt{diag}\left\{ 10^{-4} \quad (2\pi 0.01T)^2 \quad 0.02 \quad 10^{-6} \right\} \\ \mathbf{Q} &= \mathtt{diag}\left\{ 10^{-5} \quad 3\times 10^{-7} \quad 10^{-3} \quad 10^{-5} \right\} \\ \mathbf{R} &= [3\times 10^{-4}] \end{aligned} \tag{4.37}$$

The estimate of wrist flexor SEMG in the top two plots in Fig. 4.17 is obtained by adding the estimate of tremor and the intended motion from the bottom two

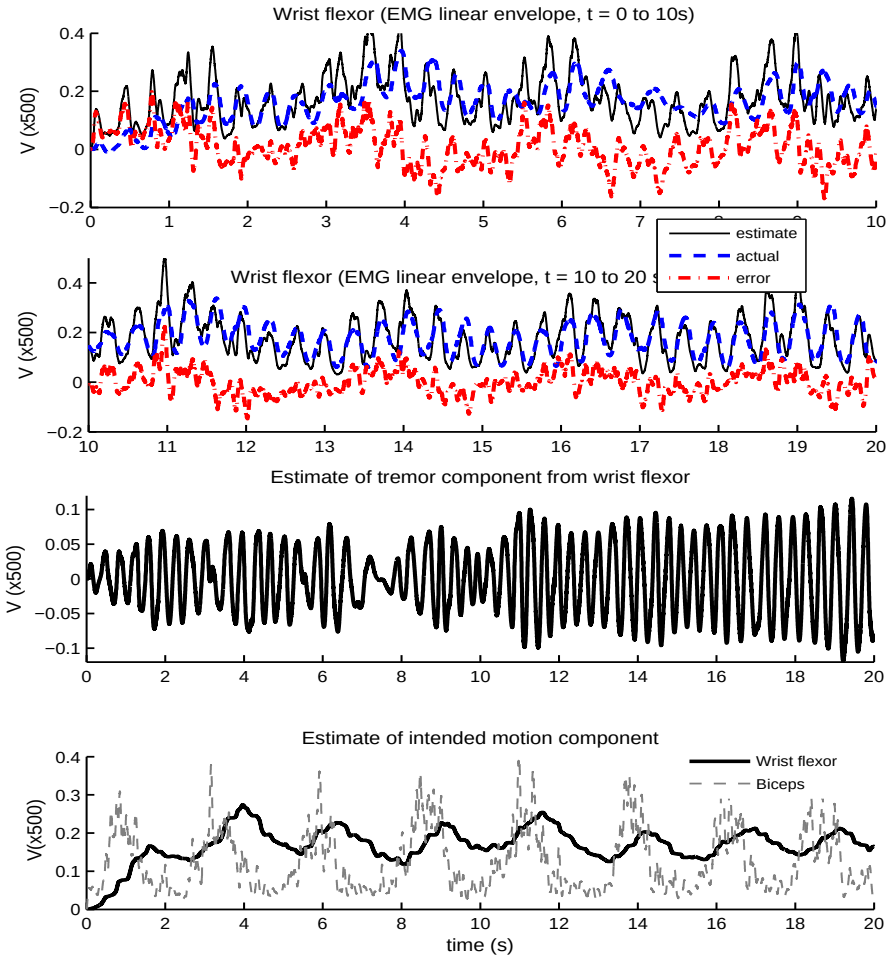

Figure 4.17: Result of EKF algorithm to separate tremor from intended motion (Holmes', finger to nose). The top two figures are the estimate and the measured linear envelope of the wrist flexor SEMG signal broken into two plots. The bottom two are the estimate of both tremor and intended motion component.

plots in the same figure.

In the bottom plot of Fig. 4.17, the estimate of the intended motion is given along the linear envelope of the biceps. There should be biceps contraction in the finger-to-nose experiment, as the lower arm is moving toward the nose. The wrist flexion follows after that as the finger touches the nose. Therefore the frequency of the biceps contraction and the estimate of the intended motion (from the wrist flexor) should be the same. This fact is confirmed in that bottom plot of Fig. 4.17.

As expected, the wrist flexion also occurs slightly after the biceps contraction. This means that in term of frequency the intended motion estimate is correct, although the correctness of its magnitude cannot be obtained as the recorded signal contains both tremor and the intended motion.

The frequency estimate of the tremor from EKF is given in Fig. 4.18. The estimate is compared with short term Fourier Transform (STFT) of the tremor data. The tremor data is passed to a 4^{th} order elliptic high pass filter to remove the intended motion, then the STFT operation is applied (1000 samples window, 800 samples overlap, and 8192 point FFT). The phase lead caused by the high pass filter is compensated by using zero-phase filtering routing from Matlab (`filtfilt`).

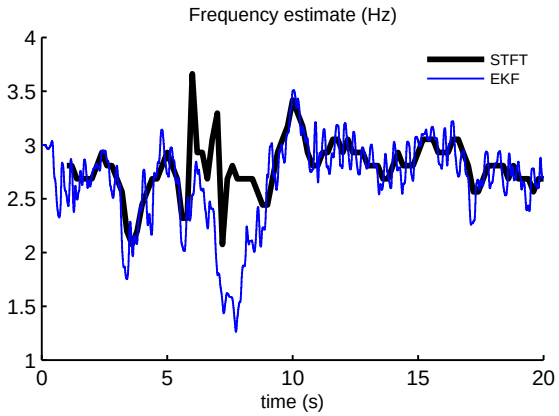

Figure 4.18: Tremor frequency estimate from EKF and STFT (Holmes', finger-to-nose).

The frequency estimate from EKF is almost consistent with the estimate from STFT except during the 7^{th} to 8^{th} second. Here what probably happens is that the EKF is tracking the intended motion instead of the tremor, but is able to subsequently retrace the tremor. Another possibility is that although there is still tremor, the SEMG signal is decreasing because of the cycle of the finger-to-nose movement. For example, from $t = 6$s to $t = 8$s in the left plot of Fig. 4.19, the SEMG level decreases because the intended motion decreases. Nevertheless

tremor still exists. The EKF may regard this as decrease in tremor amplitude instead, as shown in the right plot of Fig. 4.19.

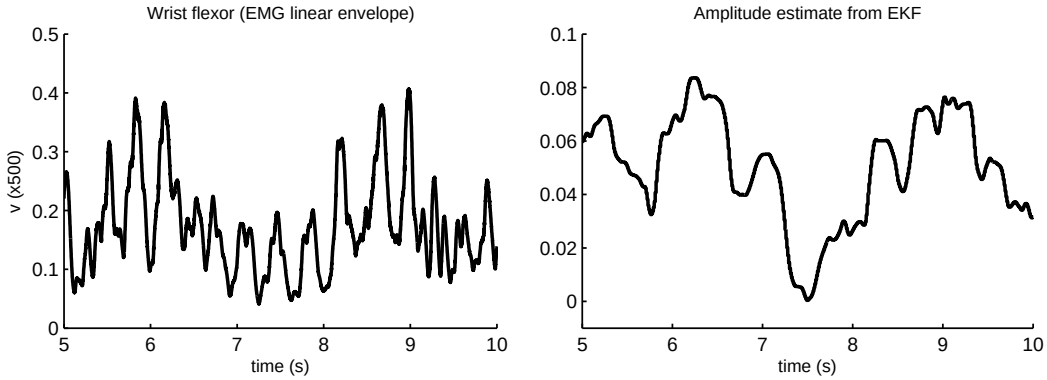

Figure 4.19: Tremor and voluntary motion estimate from EKF using simulated tremor signal (Holmes', finger-to-nose).

This problem can be overcome by reducing the rate of random walk of the frequency in the EKF. When $\lambda = 1$, it is a random walk model. But if λ is reduced, more weight is given to the predetermined average value $\bar{f}$, which will prevent the EKF to track other components (see (4.31)). The effect of modifying the EKF (using $\lambda = 0.999$) is shown in Fig. 4.20. With $\lambda = 0.999$, the frequency is now restricted to 3 Hz, thus the new estimate does not fluctuate as much as when $\lambda = 1$. Finally, the RMS error is not affected by changing λ. The RMS error is previously 0.0385 (44.6% of the standard deviation of the input signal) and after changing to $\lambda = 0.999$, it is 0.0397 (46% error).

Another set of tremor data is tested with the algorithm. In this dataset the same patient was asked to follow an Archimedean spiral on paper with a pen. The result in Fig. 4.21 also shows a good separation between intended motion and tremor. By changing the λ to 0.999, again the frequency does not fluctuate as large (Fig. 4.22 and 4.23). When $\lambda = 1$, RMSE = 0.0202 (43.5% from the standard deviation of the input signal), when $\lambda = 0.999$, RMSE = 0.0209 (45.0% error). These results together with those from the finger-to-nose experiment are tabulated in Table 4.2.

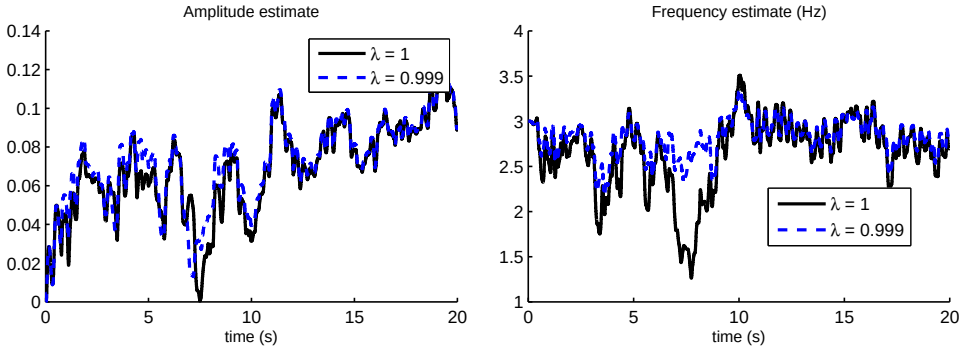

Figure 4.20: Tremor amplitude and frequency estimate from EKF with different λ (Holmes', finger-to-nose).

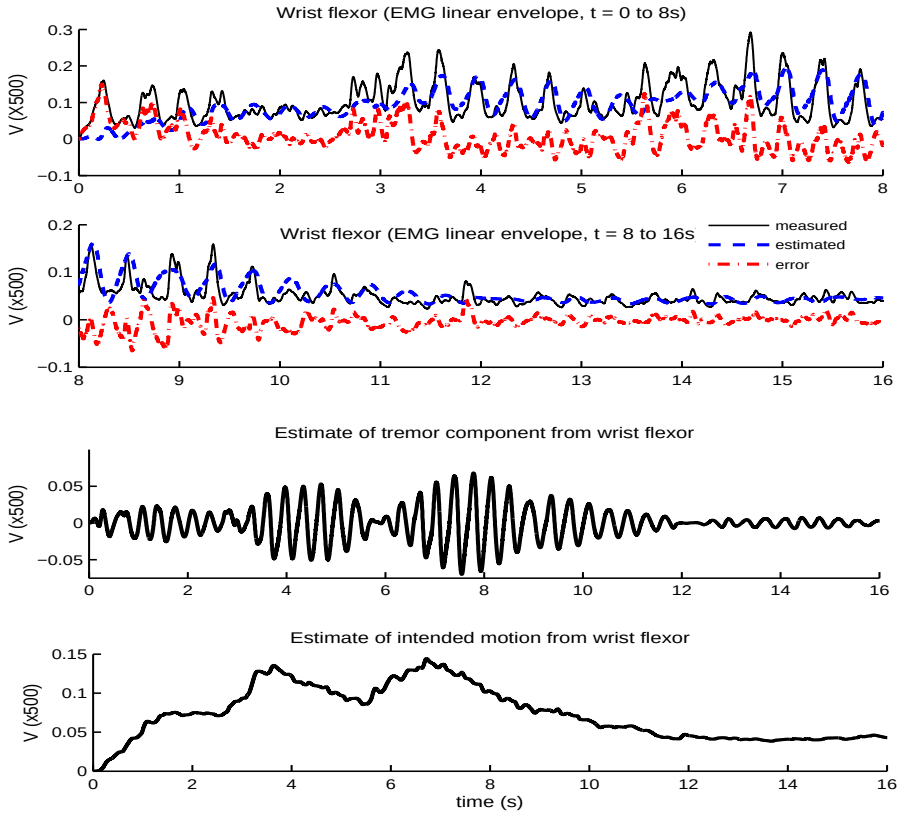

Figure 4.21: Result of EKF algorithm to separate tremor from intended motion (Holmes', Archimedean spiral). The top two figures are the estimate and the measured linear envelope of the wrist flexor SEMG signal broken into two plots. The bottom two are the estimate of both tremor and intended motion component.

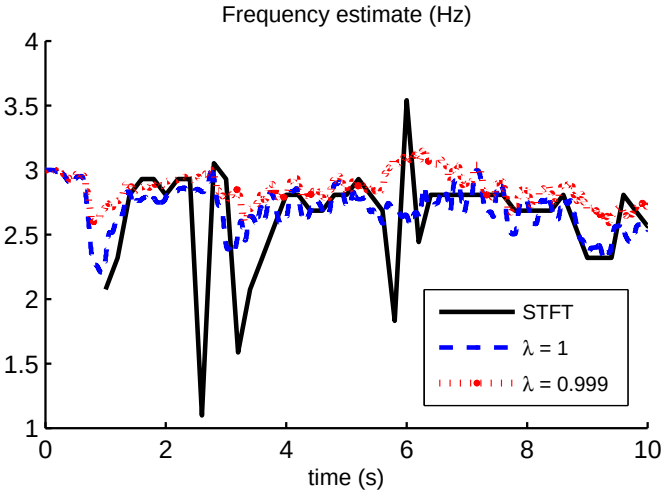

Figure 4.22: Tremor frequency estimate from EKF and STFT (Holmes', Archimedean spiral).

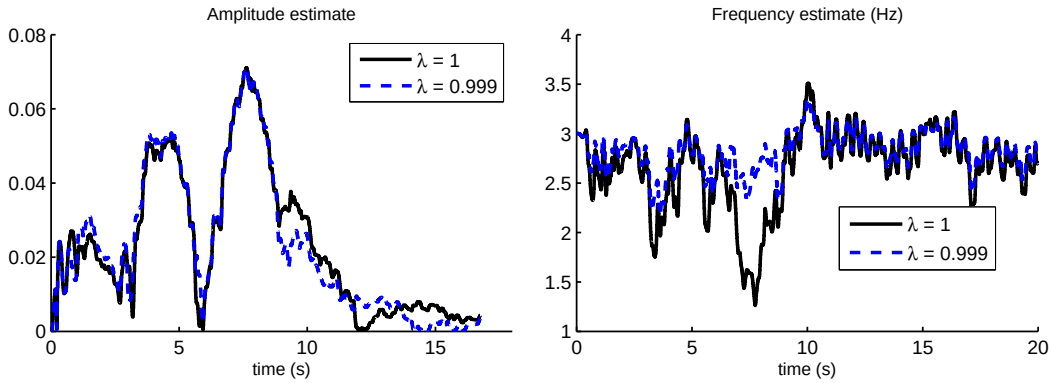

Figure 4.23: Tremor amplitude and frequency estimate from EKF with different λ (Holmes', Archimedian spiral).

To show that the algorithm works for general case of tremor (with and without voluntary motion), it is now tested with data which contains tremor only. In this case, the EKF does not track voluntary motion, but it will remove any offset, especially the offset caused by the linear envelope process. The tremor is modeled as sinusoid without any offset, hence it contains negative values. However due to the linear envelope process, that includes full rectification, all the values have positive sign. Thus it is the sinusoid offset caused by the rectification, which is

Table 4.2: Effect of the restricting term λ in one Holmes' tremor patient

RMSE in percentage	$\lambda = 1$	$\lambda = 0.999$
finger-to-nose	44.6	46
spiral	43.5	45

estimated by the EKF.

Figure 4.24 shows the tremor estimate from the same Holmes' tremor patient during rest position (sitting, arm on lap, natural pose). The figure also shows the 'voluntary motion' estimate which is actually an offset due to the linear envelope (in the figure, the 'voluntary motion' is labeled as 'offset'). This shows that the EKF can track general cases of tremor regardless of the existence of voluntary motion. The EKF initialization is the same as the last on (4.37), but with $\lambda = 0.999$.

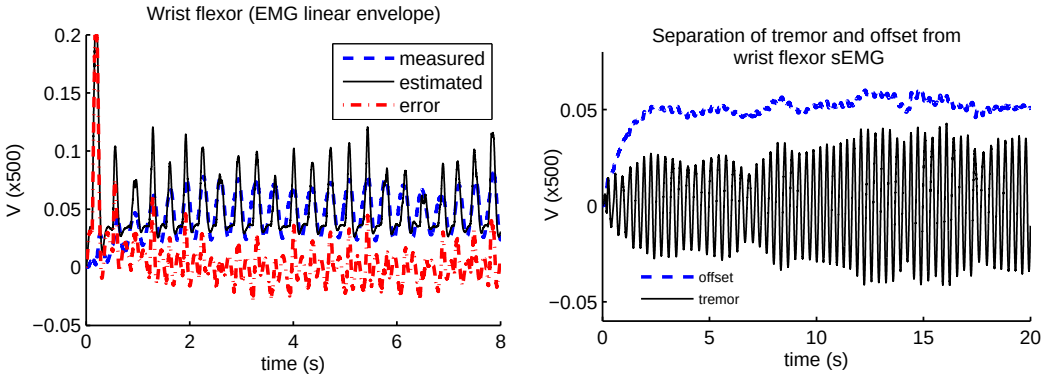

Figure 4.24: Tremor estimate and offset estimate from the EKF (Holmes', rest). The estimated signal on the left plot is the addition of the two components of the plot in the right.

Another result from a PD patient (PD1, at rest position) is given in Fig. 4.25. In both sets of data, the 'voluntary motion' estimate is quite constant as expected, indicating that there is no voluntary motion. The variation in the offset estimate is also caused by the rectification process. The rectification causes the minimum value of each tremor burst to be the same (roughly equivalent to the

noise level). Therefore the offset value cannot be constant since the amplitude is not constant.

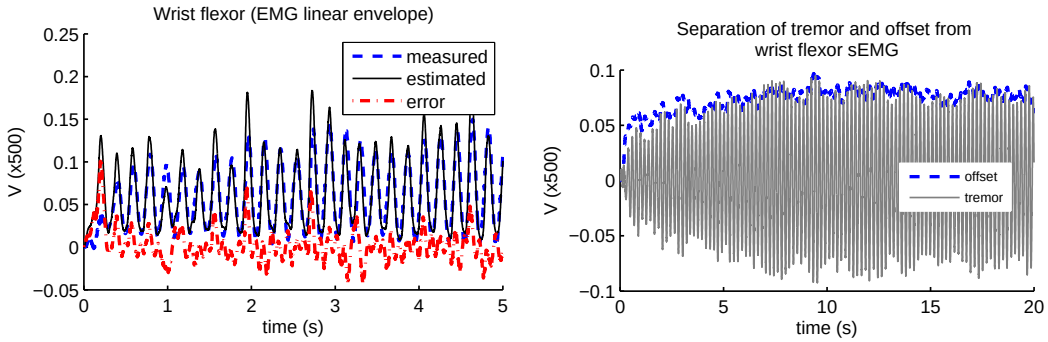

Figure 4.25: Tremor estimate and offset estimate from the EKF (PD1, rest). The estimated signal on the left plot is the addition of the two components of the plot in the right.

The initialization for EKF applied to the data in Fig. 4.25 is the same as before. The only exception is that the initial frequency is set to 5 Hz (not 3 Hz as previously set in (4.37)), which is about the tremor frequency of the patient. The initial frequency is important because the EKF models the tremor frequency as slowly varying (smaller covariance in process noise matrix $\mathbf{Q}$).

Furthermore, there is the restricting term in (4.31) which does not allow the frequency to deviate much from the expected tremor frequency. This effect of the restricting term is shown in Fig. 4.26. It can be seen that without the restricting term ($\lambda = 1$), the frequency estimate can adapt to the correct frequency within 2 to 3 seconds. On the contrary, when the restricting term exists ($\lambda = 0.999$), the frequency estimate locks into inaccurate tremor frequency.

Nevertheless, the restricting term is important when there are both the tremor and the intended motion. When there are both components in the measured signal, the EKF is expected to track only the tremor. If there is not any restricting term, the frequency estimate may lock into the frequency of voluntary motion. Therefore the initial frequency must be set properly. This can be easily done by a short data collection from the patient beforehand.

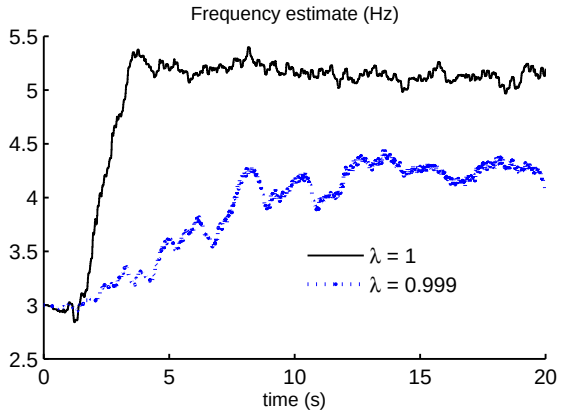

Figure 4.26: Tremor estimate from EKF with 3 Hz as its initial frequency (PD1, rest).

The algorithm is applied to data from another PD patient (PD2) with the same initialization (initial frequency is 5 Hz). In this case, the tremor signal is weaker than the previous one (PD1), thus the SNR is low. In the left plot of Fig. 4.27, the maximum value of the signal is about 0.03, while the minimum is about 0.01. This implies that the amplitude of tremor (about 0.02) is only two times larger than the noise level. As a consequence, the EKF may consider part of the tremor signal as noise and the tremor estimate is even smaller as shown in the right plot of Fig. 4.27. The tremor peak-to-peak value is around 0.01, which is half of the measured tremor. To alleviate this problem, the measurement noise covariance can be set to a smaller value.

This actually confirms the parameter design specification proposed in [Bittanti and Savaresi, 2000]. According to that paper, what matters in the design of EKF is the ratio between the measurement and process noise covariance. Therefore if the SNR of the signal is smaller, the ratio between those two values should be adjusted. In this case, we decrease the measurement covariance, R, from 3×10^{-3} to 10^{-4}, because this assumes that the recorded signal contains less noise.

The result is shown in Fig. 4.28 and Fig. 4.29. The tremor estimate with the new measurement covariance is now closer to the measured tremor (RMSE = 0.0023 – 40.4% of standard deviation of input signal, previously 0.0040 – 67.8%

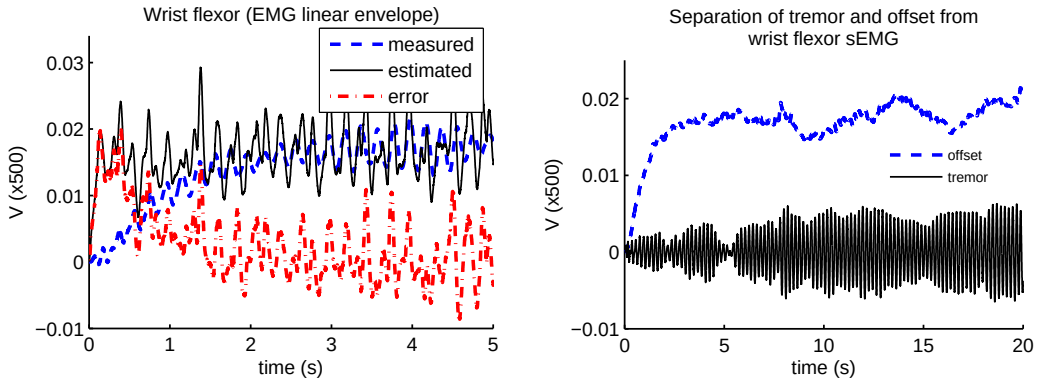

Figure 4.27: Tremor estimate and offset estimate from the EKF (PD2, rest). The estimated signal on the left plot is the addition of the two components of the plot in the right.

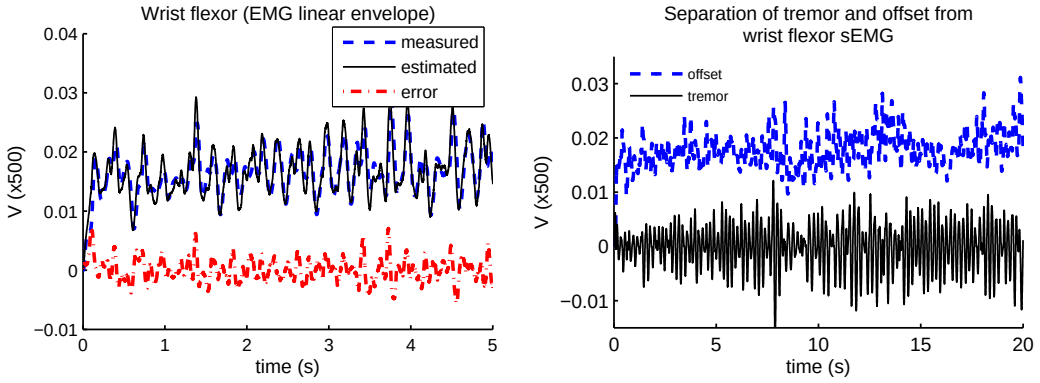

Figure 4.28: Tremor estimate and offset estimate from the EKF with different measurement covariance(PD2, rest). The estimated signal on the left plot is the addition of the two components of the plot in the right.

error, as shown in the error plots in Fig. 4.29). However, the smaller error is compromised by the larger offset estimation (both in magnitude and fluctuation). This can be seen in the right plot of Fig. 4.28. Indeed, the standard deviation of the offset estimate when $R = 10^{-4}$ is 0.0034 (69.4% of the standard deviation of the estimated signal). This is bigger than the offset estimate when $R = 3 \times 10^{-3}$ (0.0026, 59.1% from the estimated signal). Hence, the measurement covariance cannot be set too small, otherwise the EKF also tracks the noise component, which is not desirable.

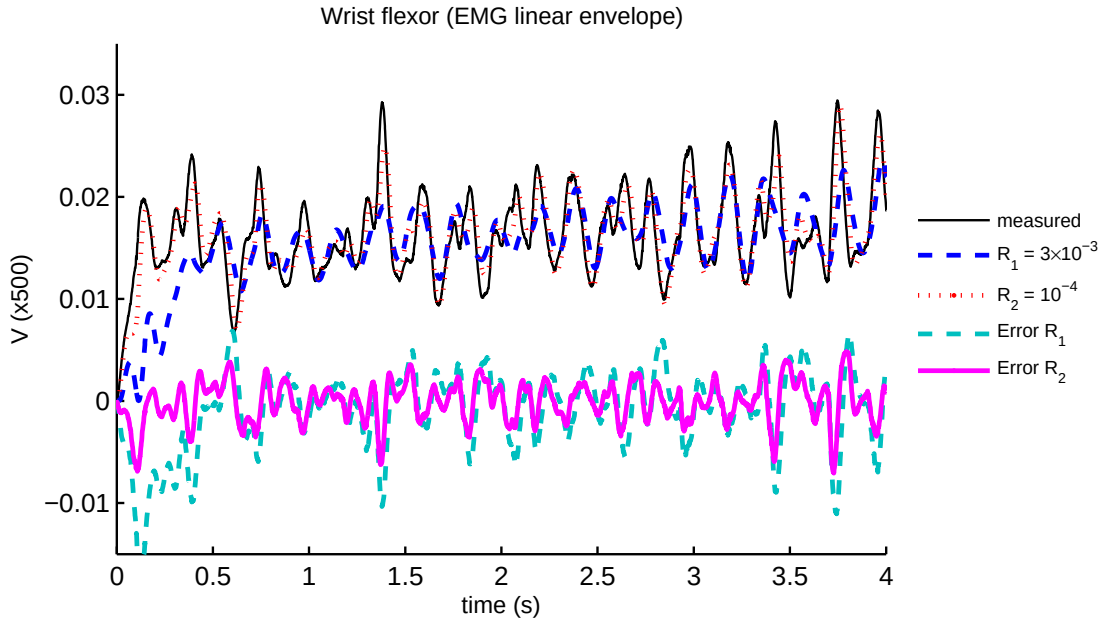

Figure 4.29: Tremor estimate from the EKF with different measurement covariance (PD2, rest). The errors are also shown.

The EKF algorithm proposed here also tracks the tremor phase. This information is useful for the actuation time of FES. In Fig. 4.30, the usefulness of the phase estimate is considered. In the figure, every time the phase estimate is zero, i.e. a start of one period of sinusoid, a vertical line is drawn to mark it. The markings are generally at the point where the SEMG starts to increase (beginning of contraction, or tremor onset). Thus the EKF can also be used to estimate SEMG onset. This fact saves the computational time to run another algorithm for onset estimation (e.g. one of the methods surveyed in [Staude et al., 2001]). Part of the next chapter will consider the phase information and how it is used to determine the starting and stopping of the stimulation.

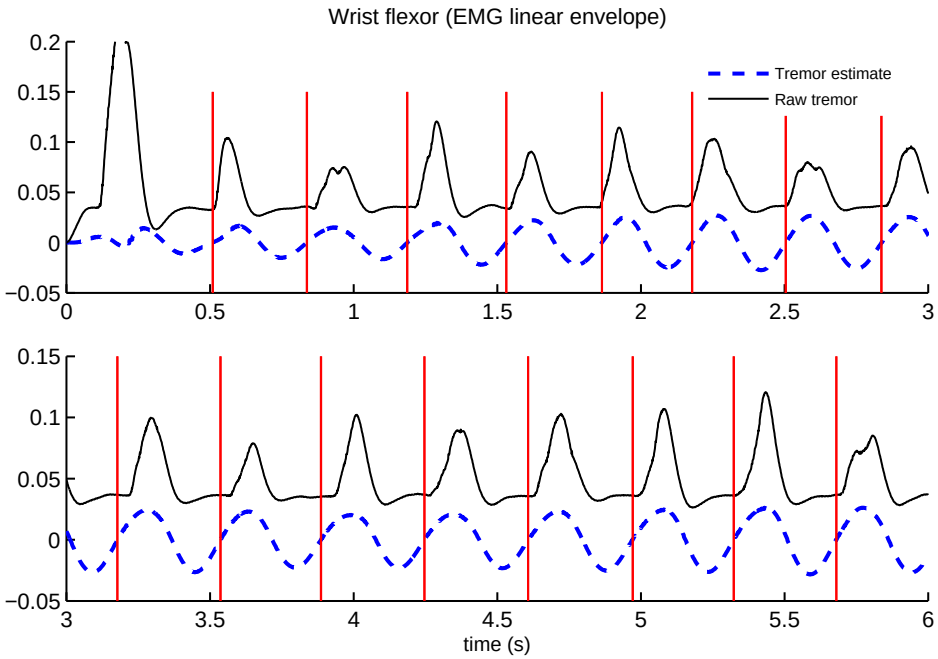

Figure 4.30: Tremor phase estimate is able to detect the beginning of tremor bursts in SEMG signal (Holmes', rest).

Chapter 5

Real-time Sensing for Tremor Attenuation

Having extracted the necessary information from the upper limb motion, we will now consider the actuation part. The extracted information is sent to the FES to actuate the muscle which in the end will compensate the tremor. Nevertheless, there are two major issues associated with the usage of FES. This chapter will tackle those two issues.

The first is the FES artifacts in the SEMG signal. Since FES is applied to the muscle, the SEMG will also capture the FES pulses and the resulting muscle activity. This unwanted signal has to be removed as much as possible so the estimation algorithm discussed in the previous chapter is not affected. The first section of this chapter deals with this problem. An algorithm to suppress the artifacts is proposed and it will be shown that the estimation algorithm is not affected with the FES by implementing the algorithm.

The second section of this chapter proposes a way to utilize the information from the tremor estimation algorithm to determine when to start/stop the FES stimulation to compensate tremor in anti phase. This is important because of the different EMD value between voluntary and electrically stimulated motion.

5.1 FES artifact suppression

In the literature, the problems of recording surface electromyography (SEMG) signal from electrically stimulated muscle are widely known. Functional Electrical Stimulation (FES) causes two types of artifacts in the SEMG reading. The first is the stimulation artifacts (SA). These are due to the electric field in the tissue and skin generated by the stimulation current [Sennels et al., 1997]. A typical SA takes a form of a spike and lasts for a few milliseconds [Langzam et al., 2006]. Its amplitude is much larger than the volitional SEMG reading and it can even saturate the SEMG amplifier [Frigo et al., 2000]. The sources of SA were first modeled in [McGill et al., 1982]. By considering the stimulator, electrode-skin interface, subcutaneous tissue of the limb, and the recording amplifier, four models to produce SA are proposed. Scott et al. also propose three coupling mechanisms for SA generation [Scott et al., 1997]. However they do not assume that common mode to differential mode conversion is insignificant.

The second artifact is the muscle responses (M-waves). These are due to the simultaneous activation of motor units caused by the stimulation [Sennels et al., 1997]. The M-waves spreads over most of the inter pulse interval [Langzam et al., 2006] and it can overlap the SA if the recording site is not sufficiently far away from the stimulus location [O'Keeffe et al., 2001]. The M-waves generated by the stimulation is a quasi-deterministic signal compared to the stochastic nature of the SEMG reading due to voluntary contraction [Merletti et al., 1992]. This is because the stimulation activates the neurons at around the same time, while during voluntary contractions the action potentials are almost asynchronous. Examples of the artifacts are shown in Fig. 5.1.

5.1.1 Literature review

In some cases where the effect of electrical stimulation to the muscle is of interest, only SA is removed. The M-waves is kept as much as possible to be analyzed further, e.g. [Erfanian et al., 1998]. However in our case, both SA and M-waves

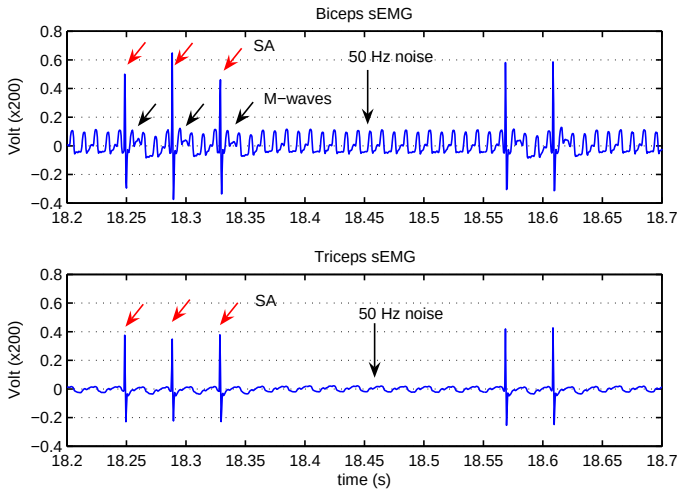

Figure 5.1: FES artifacts in biceps (SA and M-waves) and triceps (SA only since FES in only applied to biceps)

must be removed because we are interested only in the tremor signal. It is the tremor signal which, in the end, triggers the stimulation. If there is another signal which is detected, the stimulation may be turned on when it is not supposed to be. This section reviews various methods in removing SA and/or M-waves. In general, the methods can be categorized into two groups, hardware and software.

5.1.1.1 Hardware approach

Most of the solutions under this category employ blanking, i.e. not recording the signal during the stimulation. One of the earliest attempts to suppress the stimulus artifact using hardware solution was done by Freeman [Freeman, 1971]. The developed device consists of a gated sample-and-hold circuit. When the stimulus is applied, the output of the recording amplifier is held constant at the current value of the recorded signal for an adjustable period of time. After that, the circuit returns to the current value of the input signal from the recording amplifier. A similar work was also done by Roby and Lettich which was controlled by a timing pulse which may precede the stimulus by a desired period of time [Roby and Lettich, 1975]. This feature makes it possible to obtain a prestimulation baseline

when averaging evoked responses. This system consists of a control circuit and a switching circuit.

Another sample-and-hold amplifier system for stimulus artifact suppression–still in EEG–was also proposed by Babb et al. [Babb et al., 1978]. The system consists of an AC/DC differential preamplifier, designed to have a fast-recovery to baseline, and a sample and hold circuit, controlled by a synchronizing pulse provided by the stimulator. It is noted that the pulse must precede the stimulation (by 10-100μs) to allow the hold circuitry to operate prior to the stimulus artifact. All the circuits mentioned so far need a trigger signal to control them.

Minzly et al. [Minzly et al., 1993] also developed a sample-and-hold circuit to suppress stimulus artifact from FES during EMG recording. Their system consists of monostable multivibrator, CMOS switches, and sample-and-hold amplifier, which basically sense the FES pulse from the EMG reading then take the EMG reading only after a few milliseconds delay to blank the stimulus artifact. To enable this feature, the input to their system is not the amplified EMG signal, so that the real EMG signal will not be sensed as the stimulus artifact. Furthermore, this method may be preferable to prevent EMG amplifier saturation, which causes long recovery time from the artifact. This circuit is used to build a platform to evaluate the performance of SA suppression methods in tibialis anterior muscle [Langzam et al., 2006].

Other hardware solution involves switching between constant current and constant voltage stimulator [Knaflitz and Merletti, 1988]. The constant current stimulator is used during the FES pulse while the constant voltage is used in between pulses. This is because constant voltage stimulator behaves as a short circuit in between pulses, thus shortening the artifact transients. On the other hand, constant current stimulator provides reliable output current, independent of the load, during the stimulation phase. Further SA suppression is obtained by slew rate limiting before the raw signal enters the amplifier and signal blanking after the raw signal is amplified.

In the above systems, the recorded signal is not used as control signal for the stimulation side. For EMG-controlled FES systems, a solution is built based on a digital signal processor to control a switch to cut the connection at the beginning of stimulation [Sennels et al., 1997]. Another approach is to set the gain to unity during the stimulation under the control of the digital signal processor [Peasgood et al., 2000]. Other than those systems, an EMG amplifier is specially designed to minimize artifacts while maintaining the low cutoff frequency together and a fast recovery [Thorsen, 1999]. It is used in a prototype called MeCFES (Myoelectrically controlled FES) to recover significant hand functions with patients with CNS lesions [Thorsen et al., 2001]. An off-the-shelf EMG amplifier with SA removal is provided by Cambridge Electronic Design Limited, Cambridge, England. Based on a trigger signal, the input can be 'clamped' either to ground or to an averaged value of input during the last few milliseconds. This amplifier has been used in [Giuffrida and Crago, 2001] to restore elbow extension in C5-C6 SCI patients.

Apart from using the hardware circuits, efforts have been made also to understand factors affecting the SA. Thus by changing the recording parameters, it is expected that SA can be reduced. In the work by Erfanian et al., careful electrodes placement, size, and a pair of patch-ground electrodes have been found to remove the SA [Erfanian et al., 1998]. This route is taken because the blanking needs to be set beforehand, and for pulse width modulation, SA and M-waves may overlap in time thus M-waves may be removed. However this method is possible due to the usage of implanted FES (thus more selective stimulation) and small EMG electrode (5 mm diameter, again for higher selectivity).

Mandrile et al. have found that inter electrode distance of the recording system does not affect the amplitude of SA [Mandrile et al., 2003]. Using single or double differential does not affect the SA also. As expected, further distance of detecting electrodes from the stimulation electrodes decreases the SA amplitude. However in our work, the stimulation electrodes are placed at the same muscle group as the recording electrodes.

Another work highlighted that the input impedance of the EMG system does not affect the SA and that the major source of variation in SA is caused by the subject [Hamming and Lovely, 2007]. Hua et al. found that the tissues under the recording electrodes and the stimulation electrode-skin interface impedance both have a major influence on the SA appearance [Hua et al., 2006]. With regard to the tissue impedance (beneath the recording electrodes), it was found that the capacitance has a profound effect on artifact duration, while the resistance affects the amplitude. This work also found that the intervening tissue between the stimulation and recording site has little effect on the nature of the SA. These findings suggest that skin preparation is necessary before placing the stimulation electrodes.

5.1.1.2 Software approach

Hardware solutions offer a fast execution time, but software solutions offer more advanced techniques, especially for offline analysis. One example of offline SA suppression is given in [O'Keeffe et al., 2001] in which two-stage peak detection algorithm is able to remove SA with variable duration. However real-time implementation is of interest, thus only related methods are discussed.

Three signal processing (software) methods have been proposed to reduce SA in [McGill et al., 1982]: 1) Subthreshold, 2) Off-nerve, and 3) Double-stimulus method. These methods basically try to obtain an SA only signal and subtract it from SA-contaminated SEMG signal after scaling. The scaling assumes proportionality between the actual SA and its reference. This assumption is disputed in [Parsa et al., 1998]. In that work, the SA is modeled as truncated second order Volterra series and nonlinear adaptive filter is used to take care of the relation between the primary and reference SA.

Neural network is used to model the nonlinearity more completely, thus achieving better removal of SA [Grieve et al., 2000]. Only the SA portion (after being separated from the M-waves) is used for training. A new method is proposed

then that uses the neural network to model the relationship between the stimulus amplitude and the SA (done in subthreshold mode) [Boudreau et al., 2004]. To reduce the computational cost, neural network is substituted with a linear estimator, and result has shown that it performs better. Boudreau et al. also argues that using ensemble averaging method to get the SA reference (e.g. [Wichmann, 2000]) is not valid since SA is coherent with M-waves. Finally exponential approximation is used to estimate the SA thus avoiding the need of reference signal [Dotsinsky et al., 1999]. It is still possible for these techniques to be implemented in real time system.

5.1.1.3 M-wave suppression

Not only does the SA need to be removed, the M-waves must also be suppressed when SEMG signal from the nearby muscle is used to control the stimulation. For M-wave suppression, most of the methods cited previously are implemented in software. This is because the M-wave can spread over most of the inter pulse interval. Therefore hardware blanking approach is not acceptable since it takes out too much of the necessary SEMG signal.

A least square based adaptive filters has been used to predict current M-wave in [Sennels et al., 1997]. The M-wave estimate is then subtracted from the actual M-wave. However this technique is computationally demanding since it involves complex processes, such as QR decomposition and forward/backward substitution [Yeom et al., 2005]. In that case, Yeom et al. used Gram-Schmidt prediction error filter and implemented it in FPGA to obtain computational time of less than 1 ms for the filtering algorithm.

A summary of FES artifact suppression methods surveyed above is given in Table 5.1.

Table 5.1: Survey of FES artifact suppression methods

Stimulus Artifact (SA)
Hardware approach
No control signal from SEMG:
Blanking (sample and hold circuit)
Switching between constant current and constant voltage stimulator
With control signal from SEMG:
Blanking
Changing the SEMG amplifier gain
Special SEMG amplifier to reduce artifact
Understanding factors affecting SA (for implanted FES):
Careful electrode placement, size, skin preparation, etc.
Software approach
Subthreshold (stimulate before nerve excitation)
Off-nerve (use second pair of recording electrodes)
Double stimulus (during refractory period)
Neural network to model relationship between SA and stimulus amplitude.
SA approximation (thus no need of a reference signal)
Comments
Hardware approach is generally faster.
But it needs extra circuit.
Main idea of software approach: estimate SA then subtract.
But it needs more recording or stimulation electrodes.
M-waves
Least-squares method to predict M-wave
Gram-Schmidt prediction error filter (faster)
Comments
M-wave can span up to the inter pulse interval.
Therefore blanking cannot be used.
Usually software based.

5.1.2 Proposed method

In general, the hardware approach is basically a blanking method, in which the artifact is ignored by the system. This is suitable for the SA which extends only a few milliseconds. This blanking can also be implemented in software. However it should be noticed that the response time can only be as fast as one iteration time (e.g. 1 ms for 1000 Hz sampling rate). In hardware blanking the response time of ICs is usually very fast, can be in order of micro or nano seconds. However, by using software blanking, we can define lower threshold to start blanking. For

TTL operation, the minimum voltage for HIGH-input voltage level is 2V. This threshold can be set lower in software blanking to be around 0.5 V (but still higher than the maximum level of SEMG reading). The flexibility in selecting lower threshold and a fast sampling rate are the reasons software blanking algorithm is chosen over hardware blanking circuit.

Blanking method is also more preferable to a more complicated estimation method for SA suppression. The method in [Boudreau et al., 2004] based on neural network or linear estimator needs a training data. This training must be carried out quite often as muscle characteristics change over time. Neural network is computationally more expensive, but linear estimator requires more training data. Ensemble averaging method [Wichmann, 2000] is suitable for real-time application although it has been argued that it is not valid [Boudreau et al., 2004].

By further reflection, an accurate SA estimate from a more complicated algorithm is not necessary. Accurate SA estimate is needed only when we are interested in extracting the M-waves. However in this work, both SA and M-wave have to be suppressed as much as possible. Finally, as the control scheme used in this work is not complicated, software blanking is sufficient.

In this software blanking method, the SEMG signal is set to zero upon detection of the SA for a specific duration. The detection is based on a single threshold, because the SA amplitude is significantly larger than SEMG signal. The threshold value is set before hand based on the maximum SEMG produced by the subject.

The selection of blanking period is critical since it has to be long enough to remove SA while short enough not to remove the desired signal. Many algorithms, including blanking, are deemed by O'Keeffe et al. unable to adapt to the dynamic nature of the stimulation artifact, due to the nonlinearities of the stimulation procedure and hence suffer residual artifact [O'Keeffe et al., 2001]. Nevertheless the residual artifact will not be considered as long as a large portion of the stimulation artifact can be removed, as will be shown subsequently. Furthermore

the blanking duration considered here caters the removal of M-wave also [Frigo et al., 2000].

This method is also employed in [Giuffrida and Crago, 2001; Thorsen et al., 2001]. However, in their applications, the EMG amplifiers are also designed to suppress the SA besides the software blanking. The important thing to consider is that the amplifier must not be saturated due to the high amplitude of SA [Frigo et al., 2000]. Hence the gain of the amplifier is set to be low enough such that the SA amplitude is still within the input range of the amplifier.

To further reduce the noise due to the stimulation frequency and power line interference, comb filter has been proposed [Frigo et al., 2000; Thorsen et al., 2001]. Comb filter is ideal for real time signal processing as it consists of a simple difference equation [Peasgood et al., 2000].

$$y_k = \frac{x_k - x_{k-T_s}}{\sqrt{2}} \tag{5.1}$$

where x_k is the SEMG signal (already processed by the blanking window) at sampling time k and T_s is the inter stimulus interval expressed in number of samples. The term $\sqrt{2}$ is added as a scale factor required to keep the same power in the signal before and after filtering [Frigo et al., 2000]. This filter is basically attenuating the signal at the stimulating frequency and its harmonics.

5.1.3 Results and discussion

The flow of the SA suppression method implemented in this work is shown in Fig. 5.2. The sampling rate is 1000 Hz to accommodate the bandwidth of SEMG signal. Gain is set to 500 so that the SA does not saturate the amplifier and the bandpass filter set to have 10 and 500 Hz cutoff frequency.

The SEMG electrodes are placed on the wrist extensor (extensor carpi radialis) perpendicular to the muscle fibers. The FES electrodes are placed on the wrist flexor (flexor carpi radialis) and vice versa. This equipotential placement of SEMG electrode is first proposed in [Kornfield et al., 1985] to minimize SA.

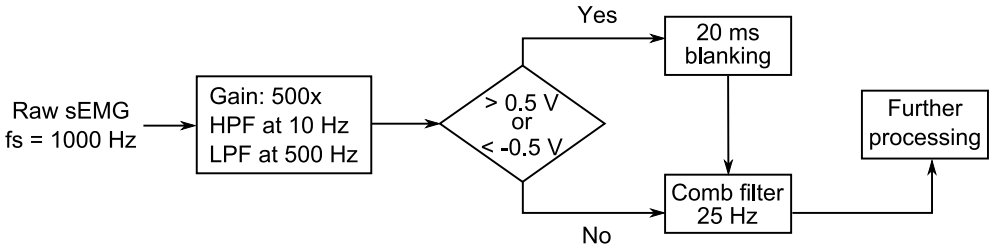

Figure 5.2: Flowchart of the FES artifact suppression method.

When the FES is applied to the muscle, there will be some artifacts in the SEMG recording. These artifacts are large in amplitude and will serve as an indicator to start the blanking window. For this experiment, a reading of raw SEMG smaller than -0.5 V or larger than 0.5 V is a sign that SA occurs. This occurrence will set the system to blank the signal for 20 ms.

In the literature, blanking time is set usually to a value around 20 ms [Frigo et al., 2000; Giuffrida and Crago, 2001; Langzam et al., 2006; Thorsen et al., 2001]. In this work, the pulse frequency of FES is set to 25 Hz, thus 20 ms of blanking will reduce half of the signal during stimulation. This is to ensure the removal of the M-wave which extends much longer than the SA. If the SEMG signal contains only SA, changing the blanking period drastically does not make much difference. This is shown in Fig. 5.3. However, if the blanking period is, for example, only 4 ms, while there is M-wave, the blanking may not cover the M-wave. The drawback of using a longer blanking period is that the stimulus frequency component may creep into the signal. Zeros in between stimulation pulses cause the envelope to decrease for a while before it increase again (after the blanking period finishes).

By using software blanking, there is still a portion of SA (at the beginning) which is retained in the processed SEMG signal. This is illustrated in Fig. 5.4(a). The figure shows one blanked artifact in SEMG signal recorded in an oscilloscope (5000 Hz sampling rate). So in 1000 Hz, there is 1 ms of retained SA. This situation is inevitable. Using the control signal to the stimulation as a trigger for the blanking window will result in the same problem because the control signal

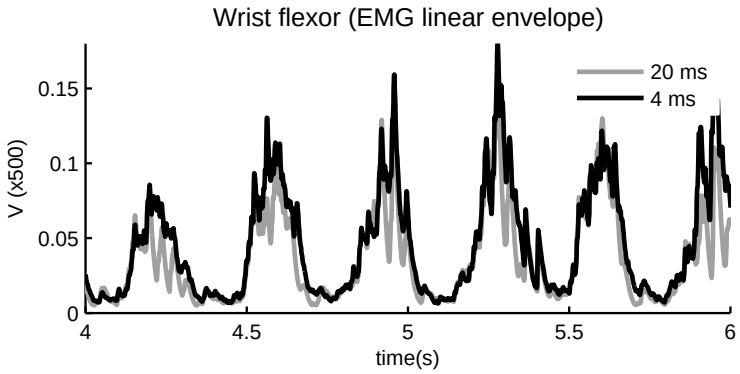

Figure 5.3: Comparison of using 4 ms and 20 ms blanking window in the linear envelope of SEMG contaminated with SA only.

will only be effective after one iteration. The effect of comb filtering is shown in Fig. 5.4(b). It can be seen that the filter can attenuate the 50 Hz noise because it is set to attenuate 25 Hz component (based on Eq. 5.1).

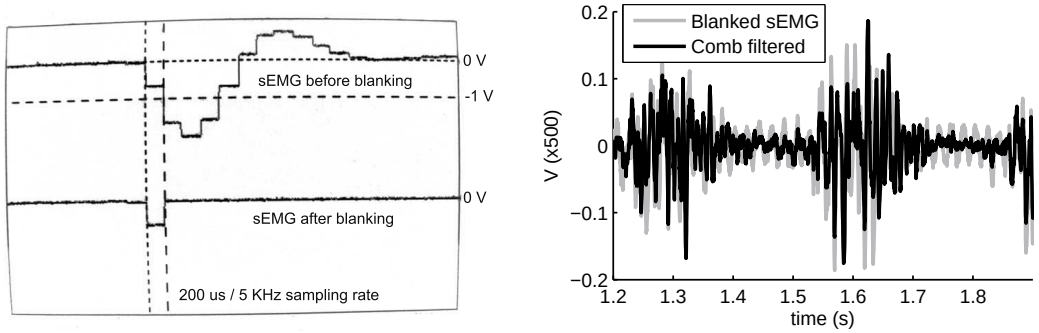

(a) (b)

Figure 5.4: Effect of blanking window in one FES pulse, shown by the oscilloscope (a) and effect of comb filtering (b).

So far we have considered the efficacy of the FES artifact suppression method separately (SA and M-wave suppression). An experiment is conducted whereby the subject is simulating a tremor-like wrist flexion-extension, while FES is applied to both wrist flexor and extensor. Results for the blanking and comb filter are shown in Fig. 5.5 and Fig. 5.6. Figure 5.7 shows that the artifact-suppressed SEMG is still very similar to the SEMG signal without artifact (no stimulation).

With this FES artifact suppression then, the tremor signal information can now be extracted.

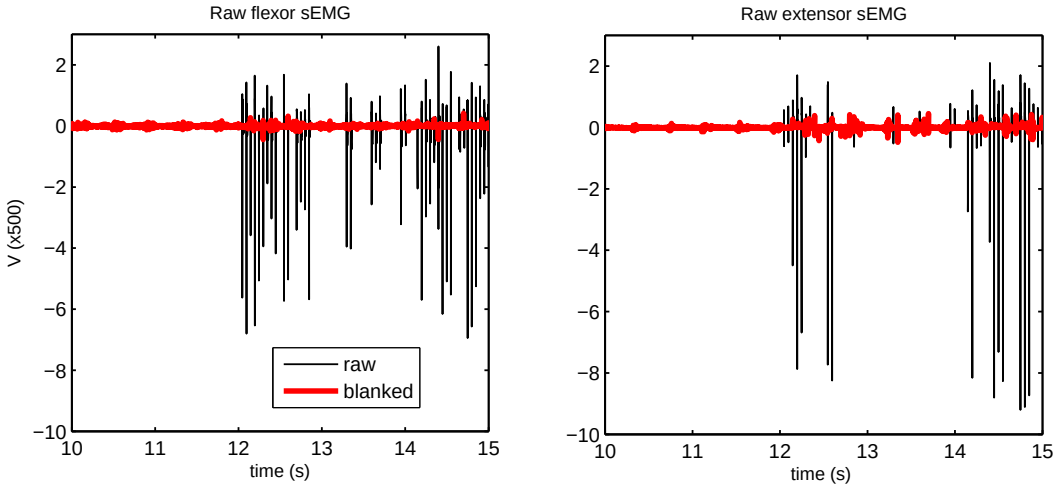

Figure 5.5: Effect of blanking.

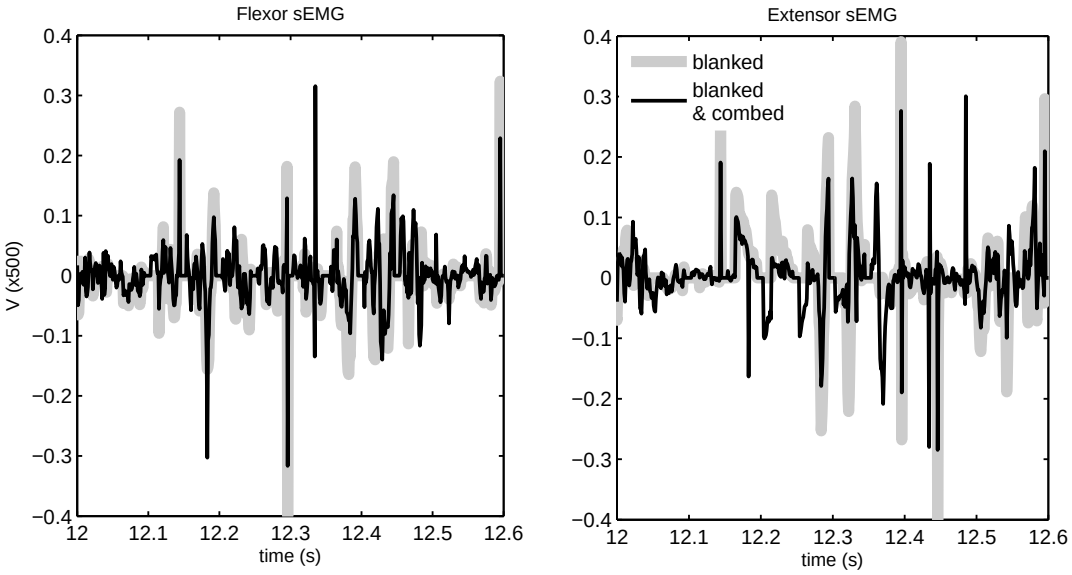

Figure 5.6: Effect of comb filtering.

As a final note, Fig. 5.8 shows that the proposed FES artifact suppression method does not significantly affect the performance of the proposed EKF from the last chapter. This is important because during tremor compensation, when

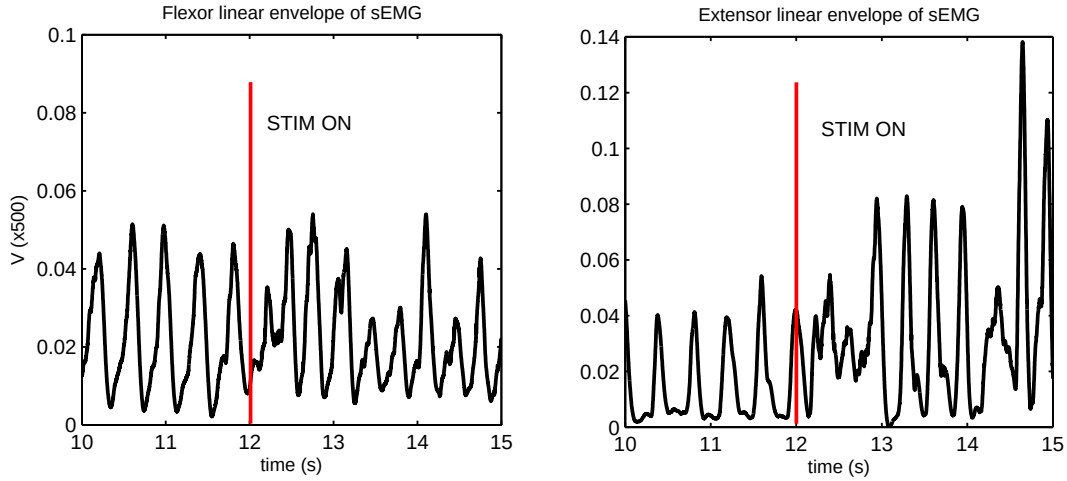

Figure 5.7: Linear envelope of artifact-suppressed SEMG.

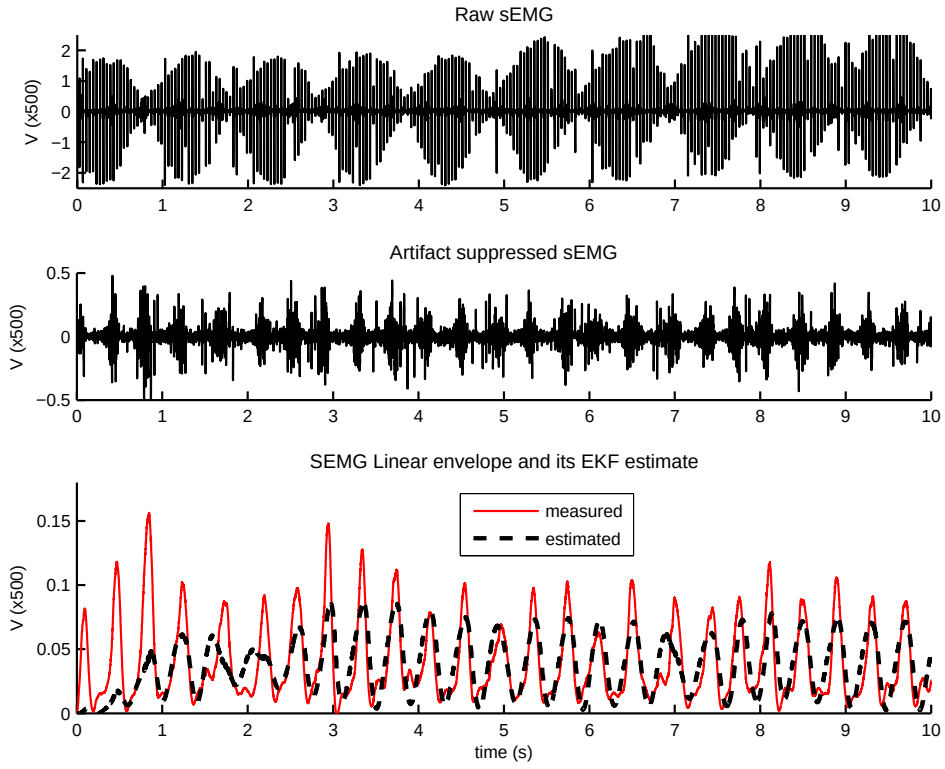

Figure 5.8: Raw sEMG with FES artifacts(top); its linear envelope and the EKF estimate (bottom). The FES artifact suppression algorithm does not affect the performance of the proposed EKF.

EKF estimates the tremor parameters and sends the signal to control the FES, FES itself will corrupt the sEMG signal upon which the EKF is based. Hence the importance of the artifact suppression algorithm. Although the suppression algorithm cannot completely eliminate the noise, the EKF is still able to extract the tremor parameters from the corrupted sEMG signal. The bottom panel of Fig. 5.8 shows that although the amplitude seems to be underestimated, the EKF still tracks the frequency and phase well.

5.2 Anti phase tremor compensation

The next issue to be addressed in the proposed real-time tremor compensation is the timing, i.e., when to start/stop the FES to compensate tremor in anti phase. Two issues are considered as part of the timing issue for FES control. One is the phase delay incurred due to the filters used in the linear envelope of the raw SEMG signal. The other is the electromechanical delay (EMD). These two parameters have to be estimated for precise FES control. Accelerometer (ACC) is used to estimate EMD together with SEMG.

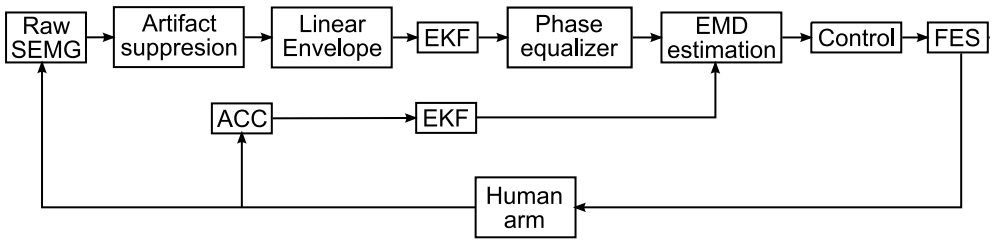

Figure 5.9: The algorithm sequences employed in the system

Extended Kalman Filter (EKF) is proposed to obtain the tremor parameters necessary to do the phase compensation and the EMD estimation. The EKF models the tremor as a sinusoidal signal and it tracks the varying signal parameters—amplitude, frequency, and phase. Furthermore the voluntary motion is filtered off with the EKF. This is necessary so that FES will only attenuate the tremulous component of the motion detected by SEMG and ACC. Since FES

will affect the SEMG reading, an artifact suppression algorithm is proposed to reduce the FES artifacts from SEMG reading.

The input of the EKF is the linear envelope of the raw SEMG signal. This is to limit the amount of information tracked by the EKF. The linear envelope operation consists of a full rectification and a 2^{nd} order low-pass elliptic filter. Due to the phase delay caused by the low-pass filter, the phase estimate by EKF is not the actual phase of the tremor. Thus the phase equalizer block is needed in Fig. 5.9.

The EMD caused both by the natural EMG signal and FES also affects the timing. When the tremor motion is detected by the SEMG, it is only some time later (20-100 ms) that the actual movement is seen. Similarly, when the muscle is stimulated by FES, it is only after some time after the stimulation does the upper limb move (e.g. about 40% of the voluntary EMD [Hopkins et al., 2007]). In fact, it is this delay that is utilized for all the processing necessary to compensate tremor in real-time. Therefore to exploit this delay, the effect of the filtering mentioned above must be estimated together with the EMD itself. To estimate the EMD, tremor parameters are also obtained from the accelerometer through the EKF.

In the real-time environment implemented in this dissertation, all the computation is done in one sampling period. The signal is acquired at 1000 Hz sampling rate. After one set of samples (SEMG and ACC) is acquired, the necessary computation is done within 1 ms and the corresponding actuation signal is sent to the FES. The algorithm proposed here requires the computer to store only the previous sample due to the nature of EKF.

The phase equalizer is discussed first in this section. Previous method in [Ang et al., 2006] is considered and based on the requirement for the tremor compensation system, a method is proposed. For the EMD estimation, special attention is given to the phase estimate since it is used to start/stop the actuation. This is because in sinusoidal signal, subtracting or adding the phase has the same effect as time delay/lead. Furthermore, changing the phase does not require a

long buffer to store the samples. Delaying the output by a certain amount of time requires the computer to store the corresponding amount of data. This may not be desirable in the implementation of a wearable orthosis.

5.2.1 Phase delay compensation

If a sinusoid is passed through a low-pass filter, the phase delay can be equalized by designing a high pass filter with an equal phase lead, according to the frequency response of the low pass filter. However if the sinusoid has time-varying parameters, such as in tremor, the high pass filter must be changed adaptively to match the phase delay by the low pass filter. The adaptation is based on the frequency estimate of the input signal since the phase response of the high pass filter varies with frequency. This is the main idea of the high-pass filter developed in [Ang et al., 2006].

It has been mentioned in the previous section that the raw SEMG passes through full rectification process followed by 2^{nd} order elliptic low-pass filter (0.5 dB passband ripple, 40 dB stopband attenuation, and 5 Hz cutoff frequency). This linear envelope of tremor SEMG is not a stationary signal but it is slowly varying in term of its frequency within a narrow band. With the assumption regarding the input signal, the problem boils down to designing an adaptive high pass filter which cancels the phase lag caused by the 2^{nd} order low-pass filter. The design of the high pass filter is done offline through brute force method summarized below [Ang et al., 2006]:

1. *Offline*: Assuming the input signal frequency is 2, 2.5, 3, 3.5, and 4 Hz, a 2^{nd} order elliptic high pass filter is found for each frequency such that the phase lead of the high pass filter is equal to the phase delay of the low-pass filter. This is done by checking the high pass filter of a slowly incremented cutoff frequency (thus the brute force method). The result is shown in Fig. 5.10.

2. *Offline*: It can be seen that the poles and zeros have linear relationships with the frequency (shown by a line as a visual aid in the figure). Thus by using linear regression, the relationship is obtained.

3. *Online*: Using the estimated frequency from the EKF and the relationship calculated from point 2, the high pass filter can be designed and applied to the signal.

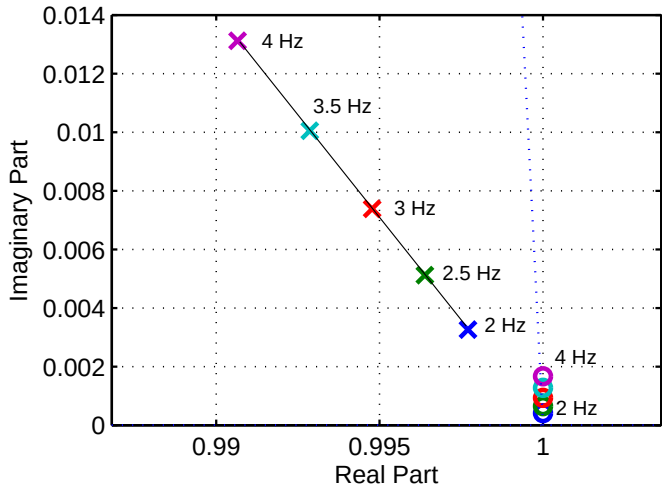

Figure 5.10: Zero-pole plot of the high pass filters derived with brute force method. There are actually two roots but each is complex conjugate of the other.

The problem with the approach in [Ang et al., 2006] is that the estimated tremor parameters will have to be recalculated after the tremor signal has passed through the high pass filter. This recalculation of tremor parameters takes more computation time and is not desirable for real-time computation, thus another simpler method is proposed here.

Using the estimates from EKF and the fact that the signal is almost sinusoidal, it is possible to estimate the phase delay of the tremor signal at a particular time. The phase estimate can be done by approximating the phase response within a certain frequency band with polynomials. For a 2^{nd} order elliptic filter (5 Hz cutoff frequency, 0.5 dB peak-to-peak ripple, and 40 dB minimum stop band

attenuation), the phase response between 2-5 Hz can be approximated with a quadratic polynomial. The approximation is shown in Fig. 5.11.

$$\phi_d(f_k) = -(0.9222 f_k^2 + 9.2673 f_k + 0.3489) \tag{5.2}$$

where $\phi_d(k)$ is the phase delay estimate (negative value) and f_k is the tremor frequency estimate obtained from the EKF.

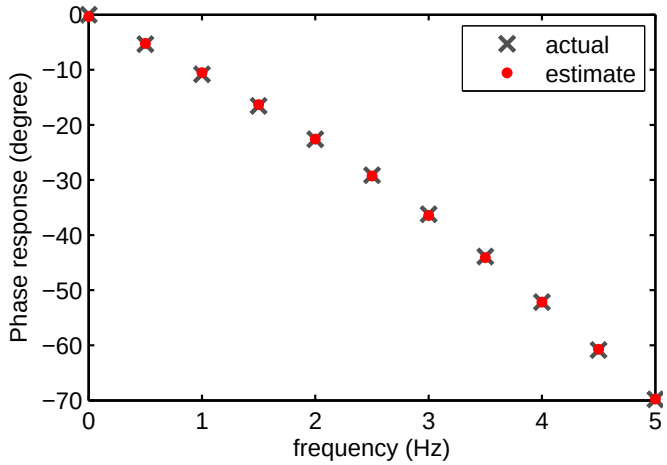

Figure 5.11: Approximating the phase response of a low pass filter with quadratic polynomial.

The result of the phase compensation using (5.2) is shown in Fig. 5.12. This algorithm is applied to the EKF estimate of the raw SEMG which has been passed through the 2$^{\text{nd}}$ low pass filter. So after the tremor parameters have been estimated by the EKF as in the previous chapter, the phase estimate is corrected according to (5.2). The tremor signal is then reconstructed from the parameters.

For the ground truth, the raw SEMG data is filtered with the zero phase filtering routine from Matlab (`filtfilt`). It performs zero-phase digital filtering by processing the input data in both the forward and reverse directions. After filtering in the forward direction, it reverses the filtered sequence and runs it back through the filter. It can be visually seen that the phase compensation algorithm can compensate the phase delay. Using (3.1), the delay between the zero-phase

filtered SEMG signal and the phase compensated signal is only 3 samples, while the delay with the standard low-pass filtered signal is 42 samples.

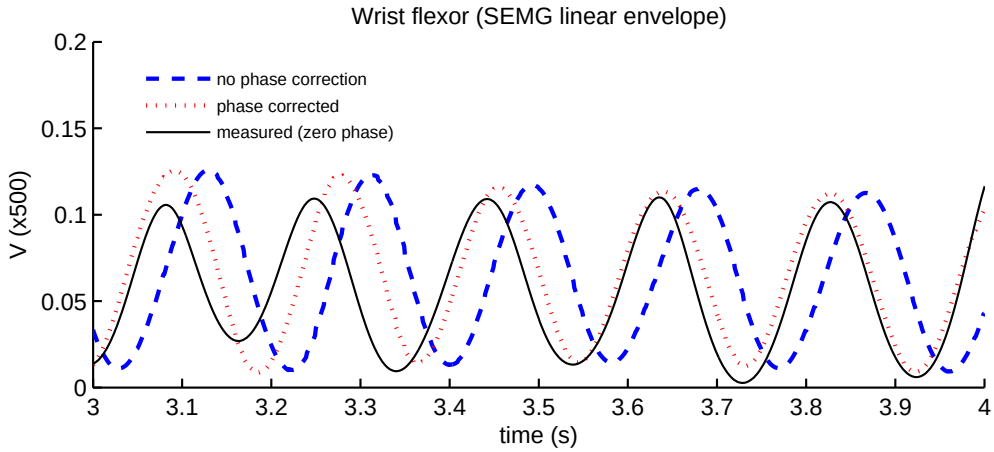

Figure 5.12: Tremor estimate from the EKF with phase compensation for the low-pass filter (PD2, rest).

In the FES artifact suppression algorithm, a comb filter is used. The delay due to the comb filter in (5.1) must also be considered. The filter in (5.1) is an FIR filter with the order of T_s (FES inter stimulus interval expressed in number of samples, not to be confused with sampling period T). Therefore, the group delay is given as $T_s/2$ samples [Lyons, 1997]. Here group delay is used instead of phase delay because we are interested in delay in the envelope of the signal. Converting the group delay in samples to phase delay in radian and together with the estimate of phase delay due to the low-pass filter, (4.19) becomes

$$\theta(k) = \sum_{\rho=1}^{k} \omega(\rho) T_s + \phi(k) - \phi_d(k) + \omega(k)\frac{T_s}{2}. \tag{5.3}$$

where ϕ_d is the phase delay calculated in (5.2). Hence this phase estimate is considered as the actual tremor phase at any particular time.

The result of phase compensation for the comb filter is given in Fig. 5.13. The delay between the zero-phase filtered raw SEMG (low-pass and comb filter) and the phase compensated reconstructed tremor signal is 4 samples. On the other

hand, the delay with the phase compensated signal (not including the comb filter delay) is 24 samples. This is according to the expectation that the group delay due to the comb filter is 20 samples.

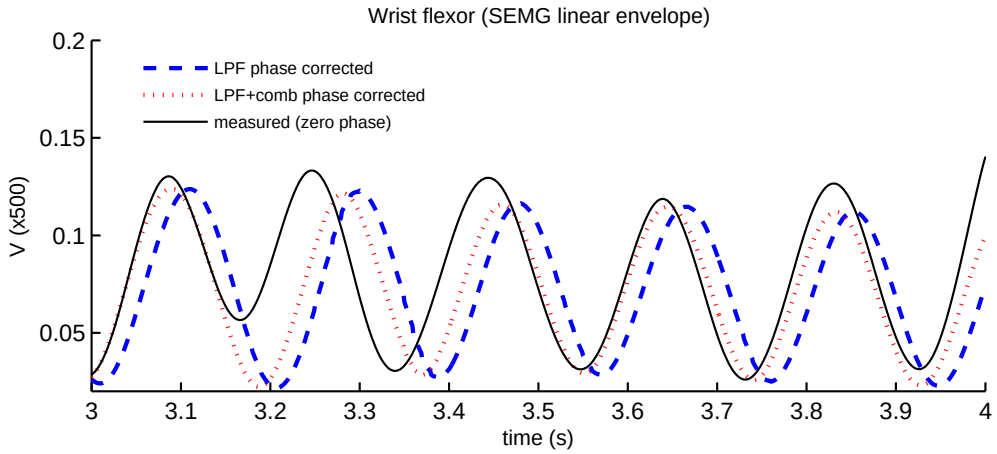

Figure 5.13: Tremor estimate from the EKF with phase compensation for the low-pass and comb filters(PD2, rest).

5.2.2 Electromechanical delay estimation

EMD caused by voluntary motion is longer than that caused by FES [Hopkins et al., 2007]. This is actually favorable for the real-time compensation since the difference between the two EMDs will be the time span to do the necessary processing. The difference between EMDs is illustrated in Fig. 5.14. This time difference is definitely longer than 1 ms (e.g. [Corcos et al., 1992; Hopkins et al., 2007] and since the sampling rate of the system is 1000 Hz, it is possible to do real-time tremor compensation. Of course it assumes that the delay caused by the filtering discussed previously has been taken care of.

The suggested reason for longer EMD in voluntary motion is the different muscle fiber recruited during voluntary and involuntary motion. The reason has been contradicted as discussed in Chapter 2.2.3. However what is of interest here is not the cause, but the actual fact that there is difference between EMD in voluntary and electrically stimulated motion.

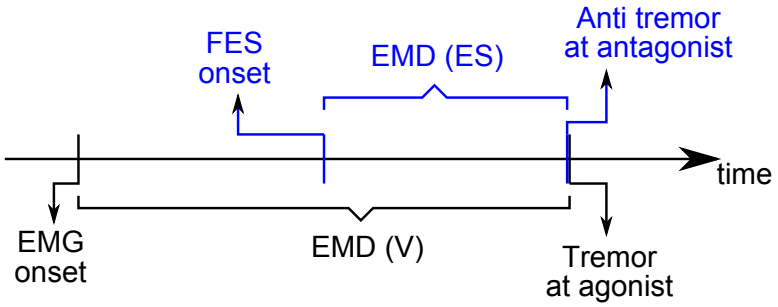

Figure 5.14: The possibility of real-time tremor compensation. EMD (V) = EMD caused by voluntary motion. EMD (ES) = EMD caused by electrical stimulation.

Experiments to confirm that fact are carried out in a healthy subject. FES is applied directly to the muscle (wrist flexor, in contrast to [Hopkins et al., 2007]). The actual motion is recorded by goniometer (Biometrics). The subject was asked to simulate 2.5 Hz tremulous motion at wrist flexion, with the aid of a sound cue. To determine the onset of flexion in goniometer, numerical differentiation is used because the motion data resembles sine wave. The peaks of the motion data are, therefore, the onset of the flexion/extension. Single threshold is used to determine the onset of SEMG data. For the test with FES, SEMG onset is the same as when FES starts. This can be located by looking at the FES artifacts. Offline zero phase low-pass filtering is applied when necessary to reduce noise. The EMD estimates (difference between onsets from goniometer and SEMG data) are shown in Table 5.2. In the table it can be observed that indeed the EMD by the voluntary motion is longer. In one data set it is even longer by more than twice the delay from the electrically stimulated movement.

Table 5.2: EMD estimates for wrist flexor for ±30-second datasets from one healthy subject.

EMD in ms	Set 1	Set 2	Set 3
Voluntary	62.55 ± 14.35	54.48 ± 15.69	73.89 ± 10.64
Involuntary	37.05 ± 4.42	42.52 ± 5.41	35.38 ± 4.49

5.2.2.1 EKF on accelerometer signal

The EMD in the previous section is measured by SEMG and goniometer to confirm that EMD caused by electrical stimulation is shorter than that caused by voluntary motion. In our proposed tremor compensation, instead of goniometer, we use accelerometer (ACC) together with SEMG to estimate the EMD. Furthermore, the above method to obtain the onset of motion from the goniometer cannot be used because of the numerical differentiation and zero-phase filtering involved. Numerical differentiation causes the noise to be amplified thus it is not feasible. Zero-phase filtering also cannot be implemented in real time. Thus the EKF as proposed in the previous chapter is employed to estimate the phase information from the ACC signal. The same rationale from the application of EKF to SEMG signal also applies in the ACC signal. Tremor motion is roughly sinusoidal and the differentiation of sinusoidal signal is also sinusoidal, although with different phase.

To show its estimation capability, the proposed EKF is applied to the ACC data obtained from a PD patient (PD1, rest). The ACC attached on the patient's wrist has 3 axis and for this application, the axis used is the one perpendicular to the hand. This is because that axis is not affected so much by the gravity when the hand and ACC are positioned such that the axis is parallel to the gravity [Elble, 2005]. To achieve this configuration, the patient is seated with hand rested on his thigh during the recording and the axis used is the z-axis of the ACC. Initialization for the EKF is the same as (4.37), except that the initial value for the offset is 1.6 as that is the value of zero acceleration in that particular ACC. However, since the sampling rate for the ACC is only 150 Hz, the measurement update is run at the same rate as the sampling frequency. The estimated tremor signal is given in Fig. 5.15. The RMS error is 0.2516 g, which is 22.85% of the standard deviation of the measured ACC signal at the z-axis. (The accelerometer has been calibrated according to the datasheet of the board manufacturer, i.e. zero offset = 1.66 V and sensitivity = 0.333 V/g).

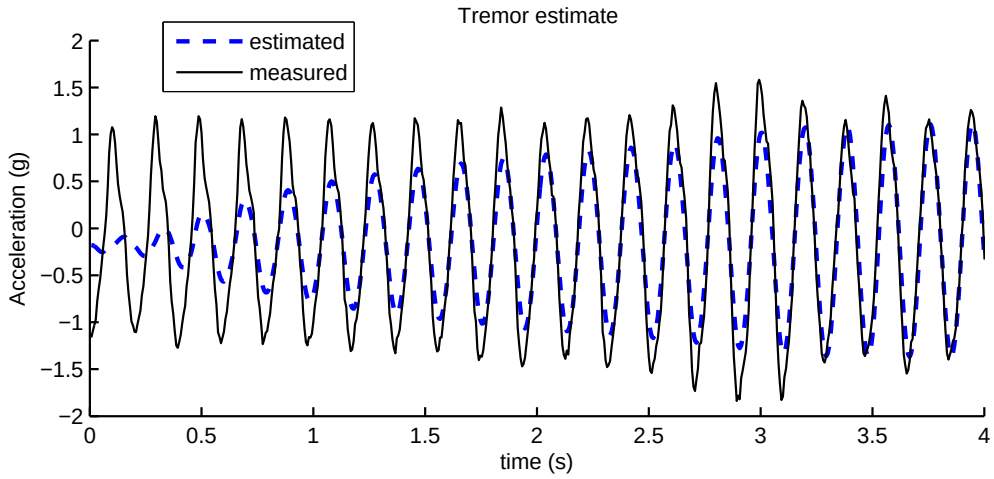

Figure 5.15: Tremor estimate from the ACC signal with the proposed EKF (PD1, rest).

5.2.2.2 The proposed method for EMD estimation

Once the phase information of the ACC signal is obtained with the EKF, the onset of the motion can be estimated. Since acceleration has a phase difference of 180°with the joint angle, the starting point of flexion/extension is located at the peaks of the sinusoid (measured signal). Thus when the phase of accelerometer signal is 90°or 270°, it can be considered as the start of the flexion or extension of the limb (see Fig. 4.1).

For the SEMG data the onset of flexion or extension is defined when the phase estimate equal to 0°as shown in Fig. 4.30. Hence the onsets of both neuromuscular and kinematics signal can also be obtained and their difference calculated.

$$\theta_{EMG}(k) = \sum_{\rho=1}^{k} \omega_{EMG}(\rho)T + \phi_{EMG}(k) - \phi_d(k) + \omega_{EMG}(k)\frac{T}{2} \tag{5.4}$$

$$\theta_{ACC}(k) = \sum_{\rho=1}^{k} \omega_{ACC}(\rho)T + \phi_{ACC}(k) \pm \frac{\pi}{2} \tag{5.5}$$

$$\theta_{EMD}(k) = \theta_{EMG}(k) - \theta_{ACC}(k) \tag{5.6}$$

where $\theta_{EMD}(k)$ is the EMD estimate.

To estimate the EMD caused by the FES is more challenging. The onset of the actual motion cannot be defined clearly. This is because the motion caused by the FES is basically a decrease in the tremor amplitude. This decrease in the amplitude cannot be easily located in time. One alternative is that the EMD is measured beforehand, thus providing an a priori value during the compensation. However this is not always possible if the patient has tremor when the EMD calculation is performed. Therefore what is done in this work is to assume a certain value for the delay due to FES (30°delay is chosen based on trial and error).

5.2.3 FES control

Control scheme using surface FES on upper limb is still a recent trend and there have been a few works on it (e.g. [Freeman et al., 2009]). As this study is to explore the feasibility of a new method in tremor suppression, the FES control is not considered at this stage. As such, constant FES parameters are employed. The timing of the FES is determined through both the estimated phase and amplitude of the SEMG. If the estimated amplitude exceeds a certain predefined threshold it will be considered as tremor. For the phase calculation, the FES will start after considering all the EMD estimates and the phase delay compensation due to the low-pass filter.

$$\theta_{FES}(k) = \theta_{EMG}(k) - \theta_{EMD}(k) + \theta_{EMD-FES} \tag{5.7}$$

where $\theta_{FES}(k)$ is the phase of control signal output to the FES and $\theta_{EMD-FES}$ is the EMD caused by FES. This equation applies both to flexor and extensor.

Hence, when $\theta_{FES}(k)$ is between 0°and 180°and the amplitude is bigger than the threshold, FES will be activated. However if the amplitude of the tremor at that point is too low, it will be considered only as noise.

5.3 Experiments with healthy subjects

To show the possibility of tremor compensation using accelerometer and surface electromyography, experiments are conducted with a healthy subject. This experiment is mainly to show the efficacy of the timing considerations that have been discussed in the previous section.

It has been reported that voluntarily simulated tremor has many similarities (in its frequency and regularity) with pathological tremor [Burkhard et al., 2002]. Hence we expect this preliminary experiment with healthy subject can show the efficacy of our proposed algorithm.

5.3.1 Experiment setup

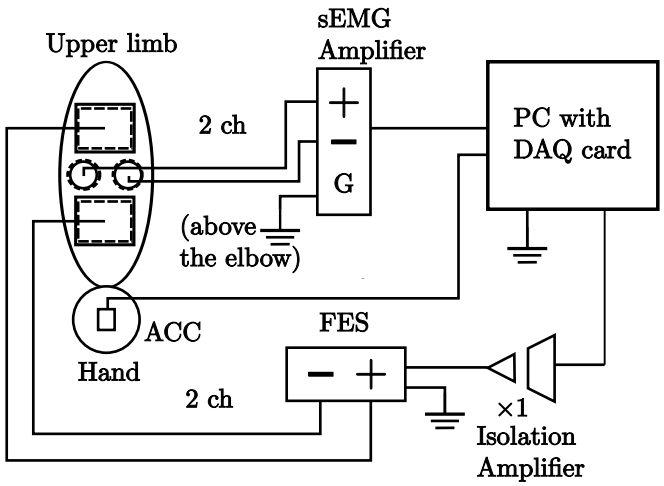

Figure 5.16: Hardware setup of real time tremor compensation.

The subject is attached to the system shown in Fig. 2.5 and asked to simulate periodic motion (wrist flexion-extension). The setup diagram is reproduced in Fig. 5.16. The SEMG from both wrist flexor and extensor and ACC signals are acquired by the DAQ attached to a desktop PC. The algorithms are all implemented using C language in QNX real-time operating system. The output of the algorithm is fed to the FES from the PC. The complete specification for

the system setup has been described in Chapter 2.2.4. A picture of the actual setup is given in Fig. 5.17.

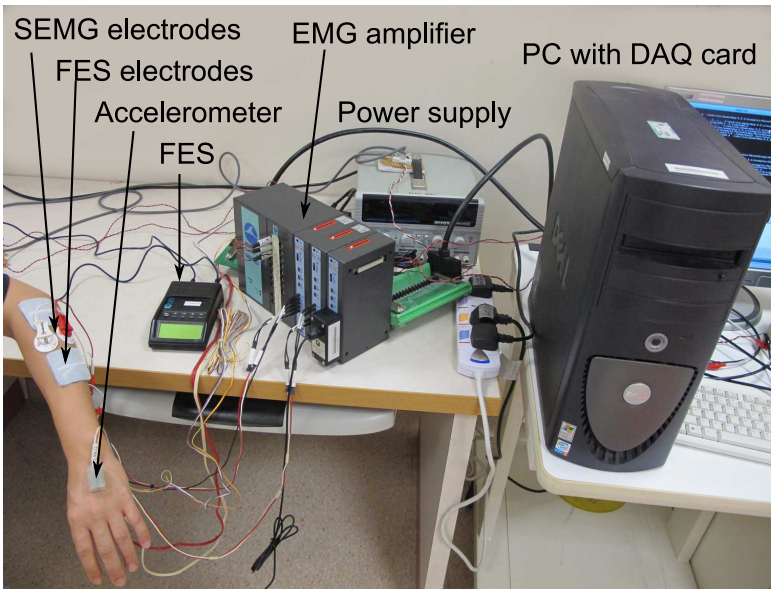

Figure 5.17: Hardware setup of real time tremor compensation.

To maintain a motion at certain frequency, the subject listens to a beeping sound at a defined frequency. Furthermore, during the experiment, the forearm and hand are supported on a structure which will allow the hand to move freely at 1 DoF (Fig. 5.18). The axis of the flexion-extension movement is parallel to gravity, so that both flexion and extension are not against gravity. As the ground truth, a goniometer (Biometrics Ltd) is also attached to the structure to record the joint angle.

In one trial, the subject simulates tremor for 50 seconds. The first and last 12 seconds are done without any compensation from the system. For the remaining period, the compensation algorithm is activated.

The main contribution of this work is to use both SEMG and ACC signal to determine a more precise timing for tremor compensation in real-time system. Therefore another set of experiment is conducted with the same subject. However in this set, there is no phase cancellation and EMD estimation. The linear

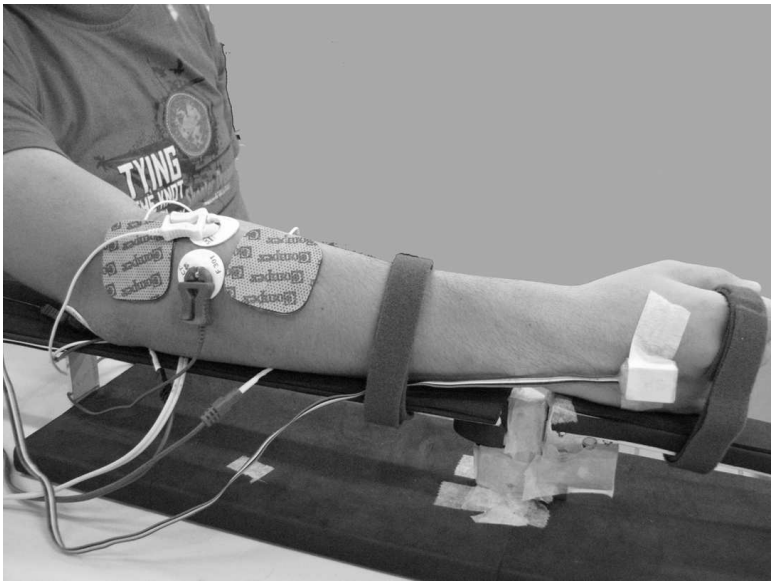

Figure 5.18: The structure to place the arm during the tremor experiment.

envelope of SEMG alone will determine when to start/stop the stimulation. This means that the FES control mentioned above is the same except that $\theta_{FES}(k)$ in (5.7) is set to be $\theta_{EMG}(k)$.

The following are the parameters for the algorithm described above:

- FES: biphasic pulse, 200 μs pulsewidth, 25 Hz pulse frequency, and 23 mA current

  The power line in which the experiments are conducted has 50 Hz frequency. Therefore the FES pulse frequency is set to 25 Hz so that the comb filter designed to attenuate 25 Hz noise is able to remove the 50 Hz power line interference (integer multiple of 25 Hz).

- Only one axis is needed to detect one DoF motion. The accelerometer axis recorded is parallel to the pronation–supination axis of the forearm.

- 20 ms blanking window (50% of the SEMG signal during stimulation since the inter stimulus interval is 40 ms). The blanking period should not be too short such that the slowly decaying FES artifact is not removed. On the

other hand, it should not be too long such that much of the useful SEMG signal is discarded.

- 2^{nd} order elliptic low pass filter with 0.5 dB passband ripple and 40 dB stopband attenuation. Cutoff frequency is set to 5 Hz.
- For the EKF $\lambda = 0.9993$ (see (4.31)).
- Amplitude threshold for FES activation is 0.005.
- EMD due to FES is fixed at 30°.
- The FES current amplitude is constant and is defined at the subject's comfortable level.

Tremor power, P_y is used to quantify the compensation effect. It is calculated based on the square root of the power spectrum of the most dominant frequency of the signal. This calculation is applied to the linear envelope of SEMG data (flexor-extensor) and goniometer data.

$$P_y = \max_f \sqrt{\frac{Y(f) \times Y(f)^*}{N}} \tag{5.8}$$

$Y(f)$ is the Fourier Transform of the signal y, f is frequency, and N is the number of data points. The mean of signal y is removed before applying the Fourier Transform. For the goniometer data, calibration is carried out by reading the voltage when the goniometer is positioned at 0°and 90°. It is assumed that the relationship between the voltage reading and the corresponding joint angle is linear.

5.3.2 Results and discussion

The power calculation of both goniometer and SEMG data in one healthy subject is given in Fig. 5.19, Table 5.3, and 5.4. Two trials are conducted for each set of experiment. The goniometer reading of one trial from each experiment is also

given in Fig. 5.20. From Fig. 5.19 (right), when the compensation is activated, there is a decrease in the tremor power as detected the goniometer (more than 50%). This is not the case in Fig. 5.19 (left) in which generally the tremor stays at the same level even when FES is active.

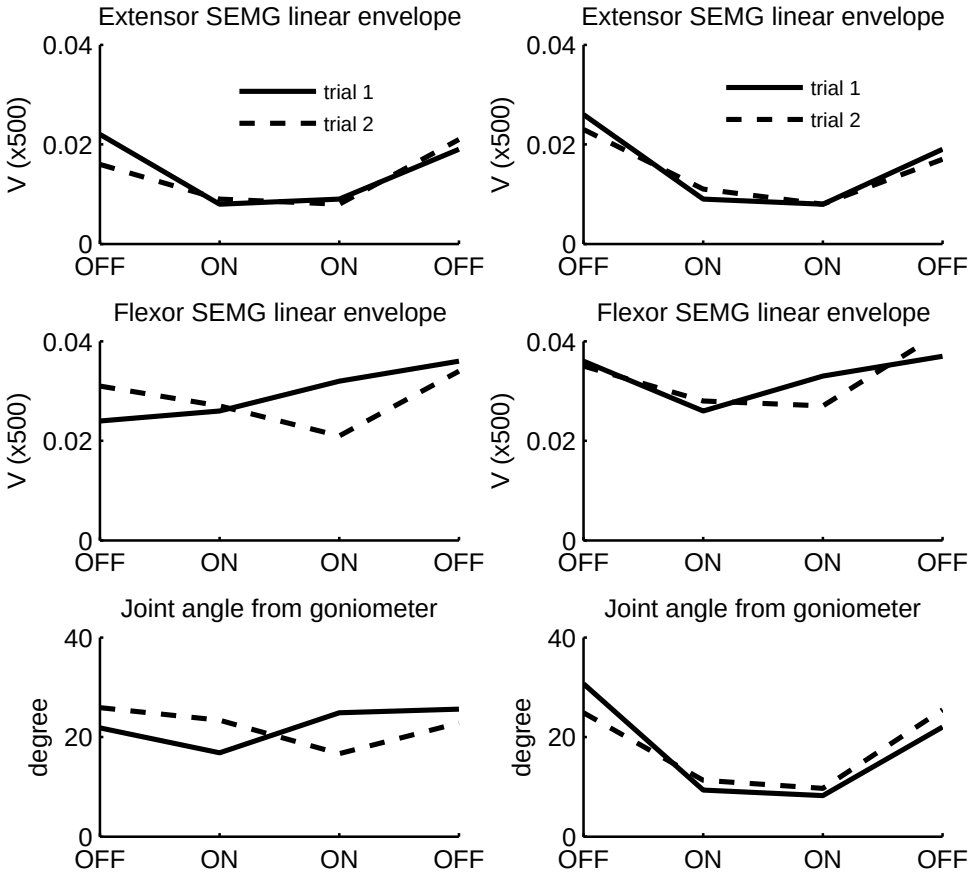

Figure 5.19: Tremor power during compensation of 4 Hz 'tremor' motion in a healthy subject. (left) without EMD estimation and phase compensation; (right) complete algorithm. ON = FES is activated; OFF = FES is not activated.

The major cause of this is that the phase compensation and the EMD estimation will affect when the FES starts to stimulate. If those steps are not implemented, FES will fire according to the amplitude and phase of the linear

Table 5.3: Tremor 'compensation' result of 4 Hz 'tremor' motion in a healthy subject without EMD estimation and phase compensation. The number in the bracket corresponds to the dominant frequency.

1st trial	Ext. (Vx500)	Flex. (Vx500)	ACC (g)	Goniometer (deg)
OFF	0.022 (4.01)	0.024 (4.01)	0.662 (4.00)	21.833 (4.00)
ON	0.008 (4.18)	0.026 (4.17)	0.925 (4.17)	16.823 (4.17)
ON	0.009 (4.24)	0.032 (4.26)	1.430 (4.26)	24.887 (4.26)
OFF	0.019 (4.04)	0.036 (4.04)	0.869 (4.04)	25.617 (4.04)
2nd trial	Ext. (Vx500)	Flex. (Vx500)	ACC (g)	Goniometer (deg)
OFF	0.016 (4.01)	0.031 (4.01)	0.807 (4.01)	25.883 (4.01)
ON	0.009 (4.27)	0.027 (4.29)	1.266 (4.29)	23.360 (4.29)
ON	0.008 (4.10)	0.021 (4.12)	0.853 (4.10)	16.678 (4.10)
OFF	0.021 (4.04)	0.034 (4.04)	0.725 (4.03)	22.811 (4.04)

Table 5.4: Tremor 'compensation' result of 4 Hz 'tremor' motion in a healthy subject with the complete algorithm. The number in the bracket corresponds to the dominant frequency.

1st trial	Ext. (Vx500)	Flex. (Vx500)	ACC (g)	Goniometer (deg)
OFF	0.026 (4.00)	0.036 (4.00)	0.947 (4.00)	30.683 (4.00)
ON	0.009 (4.67)	0.026 (4.67)	0.710 (4.65)	9.364 (4.67)
ON	0.008 (4.44)	0.033 (4.44)	0.568 (4.44)	8.231 (4.44)
OFF	0.019 (4.15)	0.037 (4.15)	0.712 (4.15)	22.002 (4.15)
2nd trial	Ext. (Vx500)	Flex. (Vx500)	ACC (g)	Goniometer (deg)
OFF	0.023 (4.04)	0.035 (4.03)	0.795 (4.03)	24.886 (4.03)
ON	0.011 (4.43)	0.028 (4.43)	0.733 (4.43)	11.314 (4.43)
ON	0.008 (4.29)	0.027 (4.29)	0.616 (4.29)	9.671 (4.29)
OFF	0.017 (4.00)	0.042 (4.00)	0.725 (4.00)	25.466 (4.00)

envelope of the SEMG. However FES should actually be started at a later time since the EMD caused by FES is shorter than that caused by voluntary motion. Starting the FES earlier than it should be may even cause the tremor to increase. This may be the case in the result in Fig. 5.19.

The SEMG level for extensor shown in Fig. 5.19 decreases every time the FES is activated. For the flexor, only in one trial does it increase during stimulation.

This fact may give a hint that actually the SEMG generated is actually lower when there is stimulation, while actually the motion generated is almost the same when there is no stimulation (Fig. 5.19 (left)).

However we should consider a few things in interpreting the SEMG level. Firstly, the blanking window employed during the FES artifact suppression. While there are still residuals from the FES artifact suppression routine, the blanking window removes (by setting to zero) half of the suppressed signal during the stimulation. So in the worst case when the blanking coincides with the firing of SEMG, half of its power is reduced.

Another thing in considering the SEMG data is the nonlinearity between SEMG and the corresponding movement. For example during the OFF period in the 2^{nd} trial (dashed line) of Fig. 5.20a, the weaker SEMG power (0.69 and 1.35 compared to 0.94 and 1.56) can produce a slightly larger motion (11.19 compared to 10.92)). It should be noted that the subject is simulating tremulous motion, thus at any moment of time, the motion is either caused by flexor or by extensor, not by both muscles. Therefore, the full range of motion is in fact caused by the total activities of both flexor and extensor, not by the difference of them. Finally, it is not easy to maintain the voluntary motion, both the amplitude and frequency level, when the subject is also stimulated by FES. Nevertheless, the timing issue is still important and it has been shown that the proposed algorithm can tackle it to a certain extent.

To show that the compensation strategy does not respond to the voluntary motion, the first subject is asked to perform a 1 Hz tremor motion. It is expected that the motion will not trigger the FES and the result in Fig. 5.21 confirms it. The raw SEMG signal does not contain FES artifacts, which means FES is not activated by the algorithm.

What happens is that the EKF is forced to track the 4 Hz frequency, while the actual movement is 1 Hz. This causes the EKF to estimate a very low amplitude in the 4 Hz sinusoid (Fig. 5.22). Then because the amplitude is still below the predefined threshold to turn on the FES, no stimulation occurs.

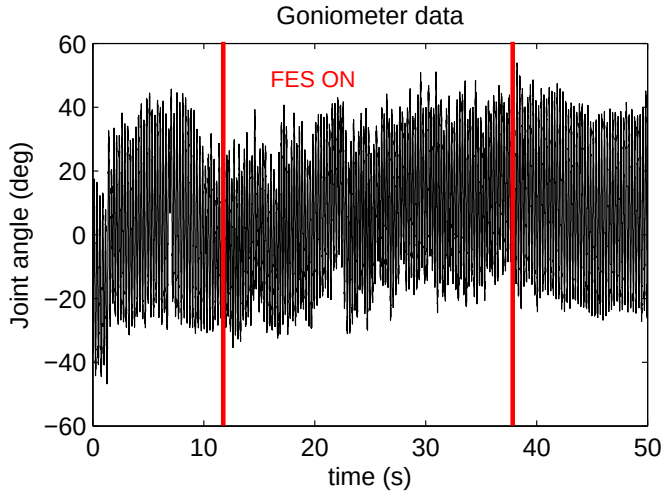

(a)

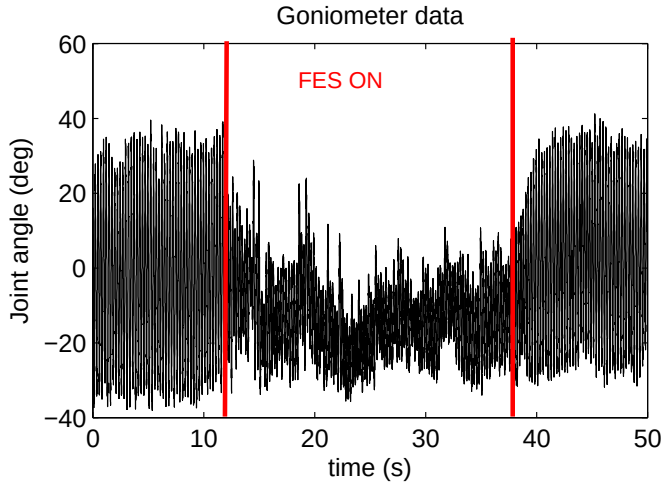

(b)

Figure 5.20: Goniometer reading during compensation of 4 Hz 'tremor' motion in a healthy subject: without emd estimation and phase compensation (a) and; with complete algorithm (b).

To extend the proposed algorithm to compensate multi DoF at one joint depends on how much from the SEMG signal can be acquired. Although surface electrodes are very convenient to use, they can only detect superficial muscles and cannot detect small muscles selectively [Luca, 2006]. More sophisticated algorithm to extract hand motion from SEMG can be explored in the future, e.g. [Momen et al., 2007]. It should be noted also that in the proposed algorithm, the

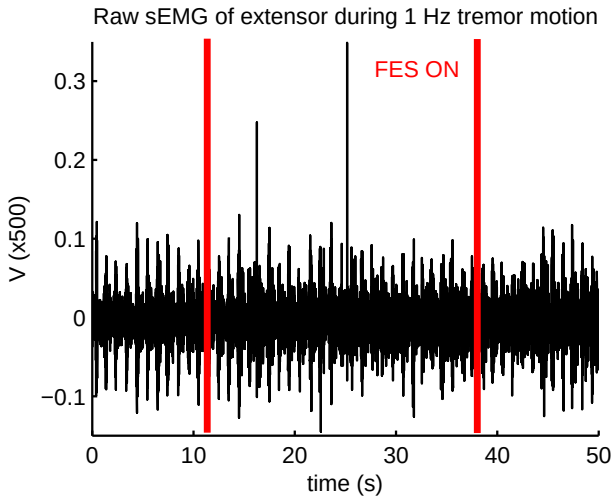

Figure 5.21: Compensation of voluntary 1 Hz 'tremulous' movement (ACC data).

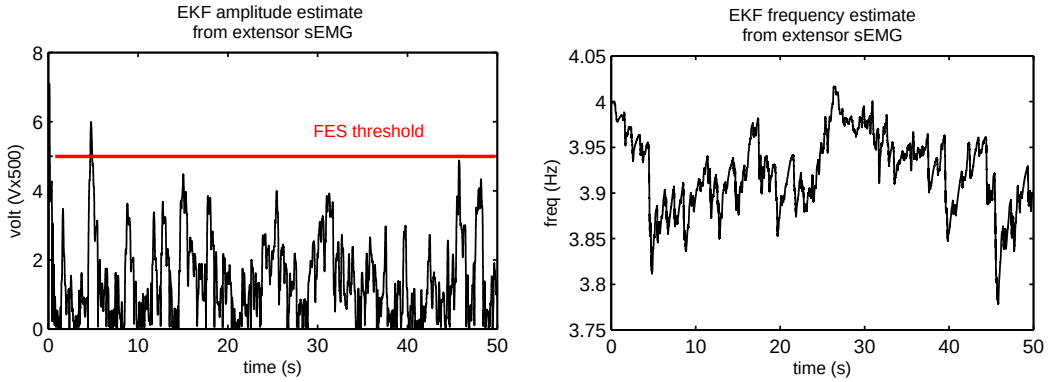

Figure 5.22: Amplitude (left) and frequency (right) estimate from extensor SEMG during the compensation of 1 Hz motion.

ACC must always capture periodic motion, otherwise the calculation of timing will be wrong. This is still feasible since the complete removal of tremor is unlikely to happen.

5.4 Experiments with tremor patients

In the last section, the complete algorithm has been tested with healthy subject simulating tremor movements. What can be shown from that experiment is

that the algorithm is able to stimulate the muscles at the correct moment, such that FES is stimulating the correct muscle to counteract the tremor. When the stimulation timing is correct, it is expected that with sufficient electrical energy, tremor will be compensated. Thus compensation experiments with tremor patients will definitely show the efficacy of our proposed system better. This section reports the experiment results from 1 essential tremor (ET) patient.

ET patients are chosen, rather than Parkinson's Disease (PD), because of a few factors. Firstly, ET is one of the most common neurological disorders [Louis, 2005]. Secondly, rest tremor at PD patients is usually in the form of finger tapping, hand clasping, and wrist pronation-supination [Connor et al., 2001]. The muscles related with finger movements and wrist pronation-supination are not superficial muscles, therefore not suitable for surface electrode-based approach such as ours. ET patients have higher chances to have wrist flexion-extension tremor and we are targeting for that movement.

Out of the 4 ET patients we managed to recruit, three of them actually do not have significant tremor. The tremor could hardly be seen by clinical inspection and its occurrences are very sporadic across time. Only one ET patient showed a significant tremor, especially at wrist flexion-extension, thus we tried out our proposed tremor compensation system on that patient. The hospital in which the experiment was conducted had given the ethics approval for the experiment and the patient had signed the consent form. The experiment was also supervised by the hospital's neurologist and was video-recorded.

The subject was asked to stretch his arm in front of him with the sensors and electrodes attached as shown in Fig. 5.23. The wrist flexion-extension is the observed degree of freedom and the main parameters are set according to those mentioned in Section 5.3.1. For the first 10 seconds, the algorithm did not send out the output signal to the stimulator (FES). After that, 10 seconds of stimulation followed. This is the period where compensation is expected. This 20 seconds of non-stimulation/stimulation period was immediately repeated, while

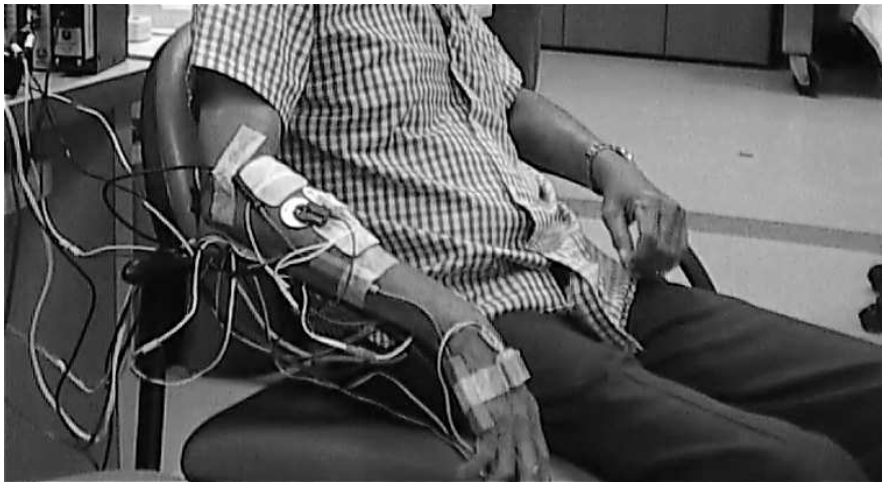

Figure 5.23: Snapshot of the video recording of tremor compensation experiment with one ET patient.

the subject was still stretching his arms. Hence, the whole sequence is: OFF (10 s) - ON (10 s) - OFF (10 s) - ON (10 s).

Part of the compensation result is shown in Fig. 5.24. The top two plots are the linear envelope of the wrist flexor and extensor SEMG. The accelerometer (ACC) reading is shown in the third plot, but here it has been filtered to remove the noise and drift to show the compensation in a clearer way. The filter is zero-phase third order elliptic filter with bandpass frequency between 1 and 20 Hz. For these three plots, only 7 seconds of data is shown for illustrating the compensation. The first two seconds are those in which no stimulation is applied to the muscles, while the stimulation is applied on the latter 5 seconds. The bottom plot shows the power of the signal at tremor frequency per 10 seconds block, thus there are 4 blocks, which represent either ON or OFF period.

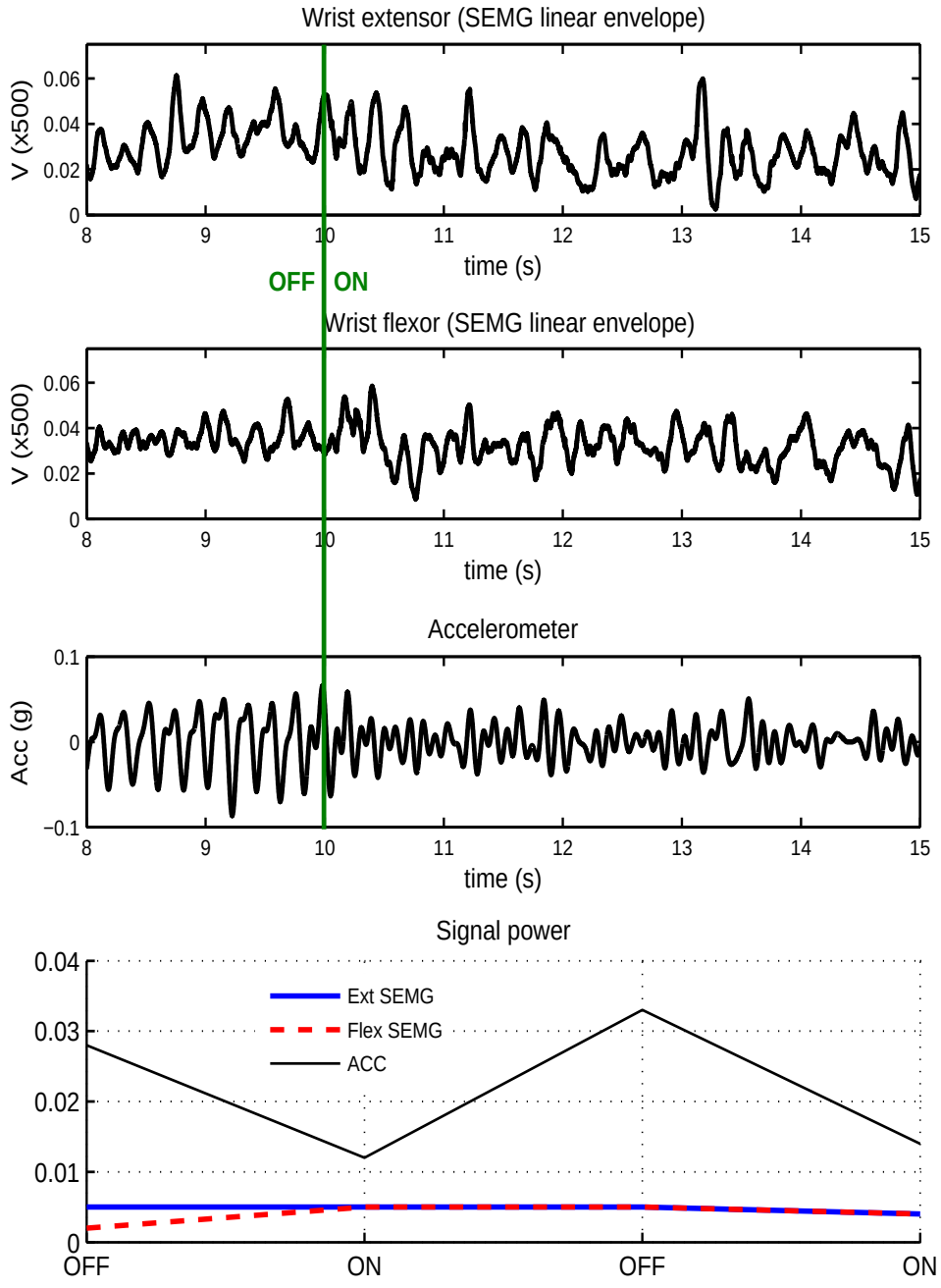

Figure 5.24: SEMG and accelerometer reading during tremor compensation from one of the ET patients (ET4). OFF = no stimulation is applied to the muscle. ON = stimulation is applied. Each data represented by ON and OFF is a 10 seconds recording.

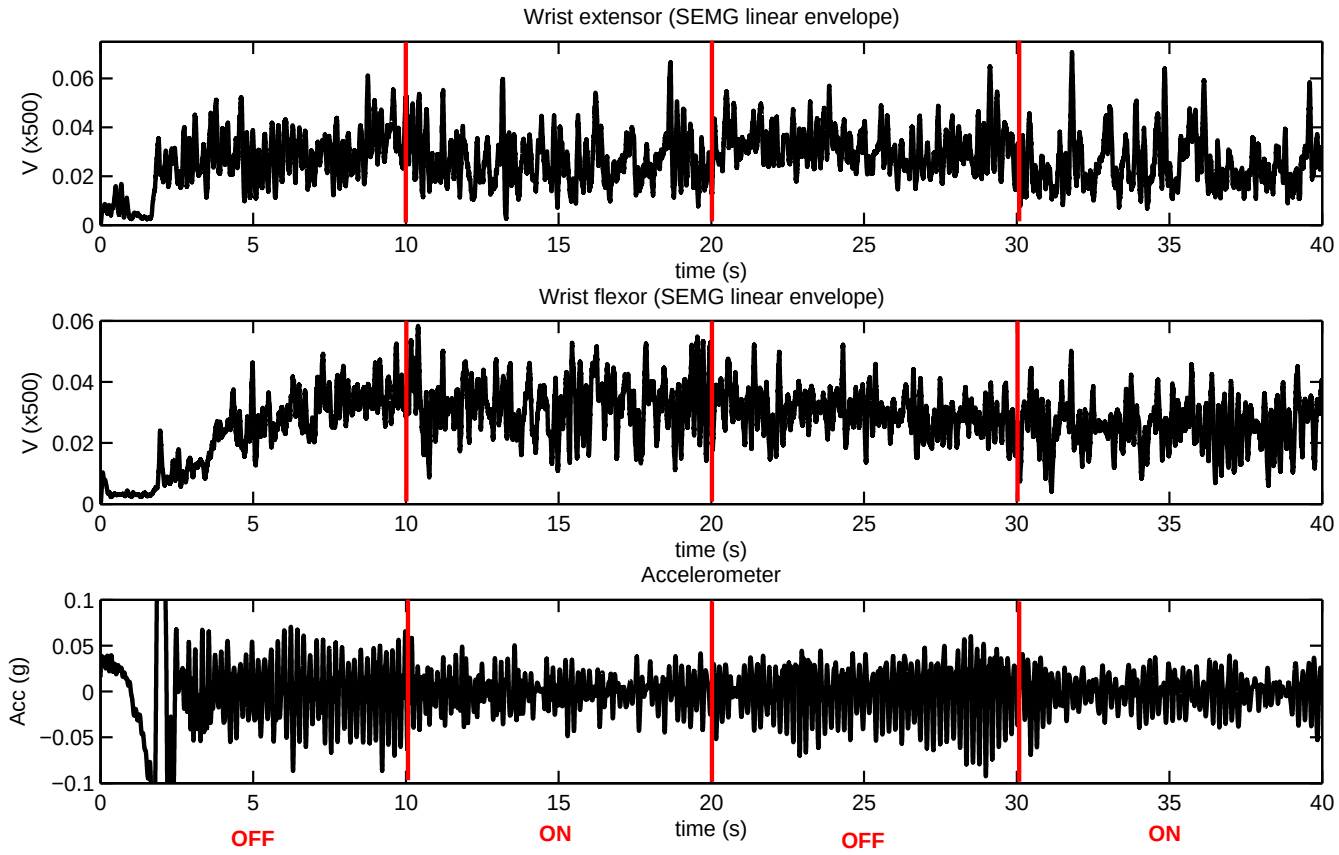

Figure 5.25: Complete SEMG and accelerometer reading during tremor compensation from one of the ET patients (ET4). OFF = no stimulation is applied to the muscle. ON = stimulation is applied. Each data represented by ON and OFF is a 10 seconds recording.

From the bottom plots, we can see that the SEMG level is almost constant throughout the experiment while the ACC level decreases during the ON period. If we consider as 100% the power of the ACC tremor frequency during the first OFF period, then in the first ON period, the compensation is 57%, while for the second ON period, it is 50%.

The complete recordings of the SEMG linear envelope and ACC signal are also shown for reference in Fig. 5.25. In the figure, the first 2-3 seconds was for the patient to stretch his arm from resting position. It can be clearly seen that the ACC signal decreases during ON period, while the SEMG stays about the same. This fact indicates that compensation occurs when the system provides the stimulation to the muscles.

To clarify the compensation more, Fourier Transform of the ACC signal for the first OFF and ON period is given in Fig. 5.26. In the figure, the tremor frequency component decreases after the algorithm is applied.

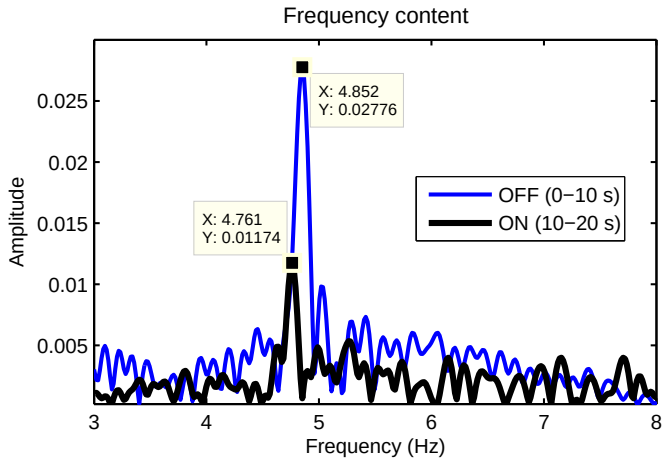

Figure 5.26: Fourier Transform of the ACC signal during tremor compensation from one of the ET patients (ET4). OFF = no stimulation is applied to the muscle. ON = stimulation is applied.

The indication that the tremor compensation is actually caused by FES is further confirmed in Fig. 5.27. In the figure, the raw SEMG data is plotted and the ON periods are clearly seen when the raw SEMG readings reach a few Volt

because of the FES artifact. This shows that the muscles are indeed stimulated throughout the ON period.

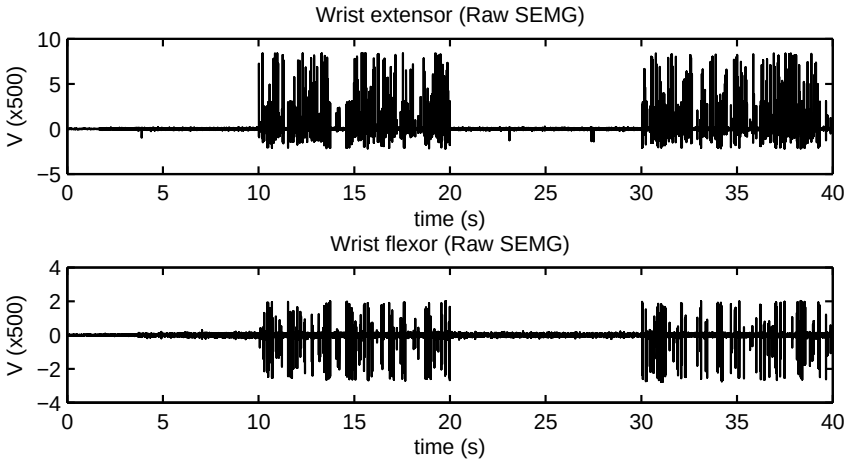

Figure 5.27: Raw SEMG signal from wrist flexor and extensor during tremor compensation from one ET patient (ET4).

The performance of the EKF in estimating the tremor parameters is considerably good. For the SEMG signal, the RMS error for the extensor is 23% of the standard deviation of the measured signal, while for the flexor RMSE is 22% of the signal. In overview, the estimated signals and the error plots for the SEMG are given in Fig. 5.28.

Our compensation result (57% tremor power reduction) is not as good as the result achieved in the exoskeleton by [Rocon et al., 2007], i.e. 81%. However, the advantage of the proposed algorithm is that the proposed system is less obtrusive than the method by [Rocon et al., 2007]. Furthermore, the exoskeleton weighs about 850 g, which is about 25% of the average human arm [Chandler et al., 1975], and the effect of the weight to the tremor is not discussed.

Nevertheless, there are a few probable explanations for the lower 57% compensation. Firstly, the compensation depends on the precision of the estimation algorithm, therefore when there is error in the estimation, tremor cannot be compensated correctly.

The second is that there is no adaptive algorithm to estimate how much stimulation to apply given any level of tremor magnitude. The issue of FES control is indeed very wide and it is not considered in this exploratory work. Furthermore, application of FES controller to upper limb has only been done recently. FES controller for upper limb is naturally more sophisticated than for lower limb since the movement of human upper limb is more complex, lower limb movements are more cyclic, whereas upper limb movements are more goal-directed. FES controller for upper limb has been proposed for the application of invasive stimulation, e.g. [Blana et al., 2009] and for surface stimulation, e.g. Freeman et al. [2009]. Out of the proposed FES controllers, not many deal with tremor application, e.g. [Bó et al., 2009].

What is proposed here is more towards the timing issue related with the FES stimulation. When the algorithm has decided when to start or stop the stimulation, constant FES amplitude is delivered to the muscles. The tremor amplitude itself is not constant. In the literature, [Gao, 2004] reports that tremor amplitude may vary within 30% of its mean amplitude. For this particular tremor data, the standard deviation of the amplitude estimate is about 50% of the mean (obtained from the accelerometer data). Therefore, it is expected that the algorithm did not compensate the tremor better than what is reported. Inspite of that, the overall algorithm has been shown to compensate tremor significantly.

Fatigue is definitely a concern whenever FES is used, especially when the target users of this application are generally older people. What is envisioned for this system is that the user will be able to use it only when it is really necessary, such as when they do not want their tremor to be seen in public, e.g. when signing a paper etc. In our experiment with one tremor patient, we applied FES for 10 seconds consecutively, but intermittently throughout 2 hours. In total, the subject experienced 5 minutes of stimulation on his arm. This is a relatively mild level of stimulation and the subject did not feel fatigue in his arm, but indeed further investigation with more patients is required.

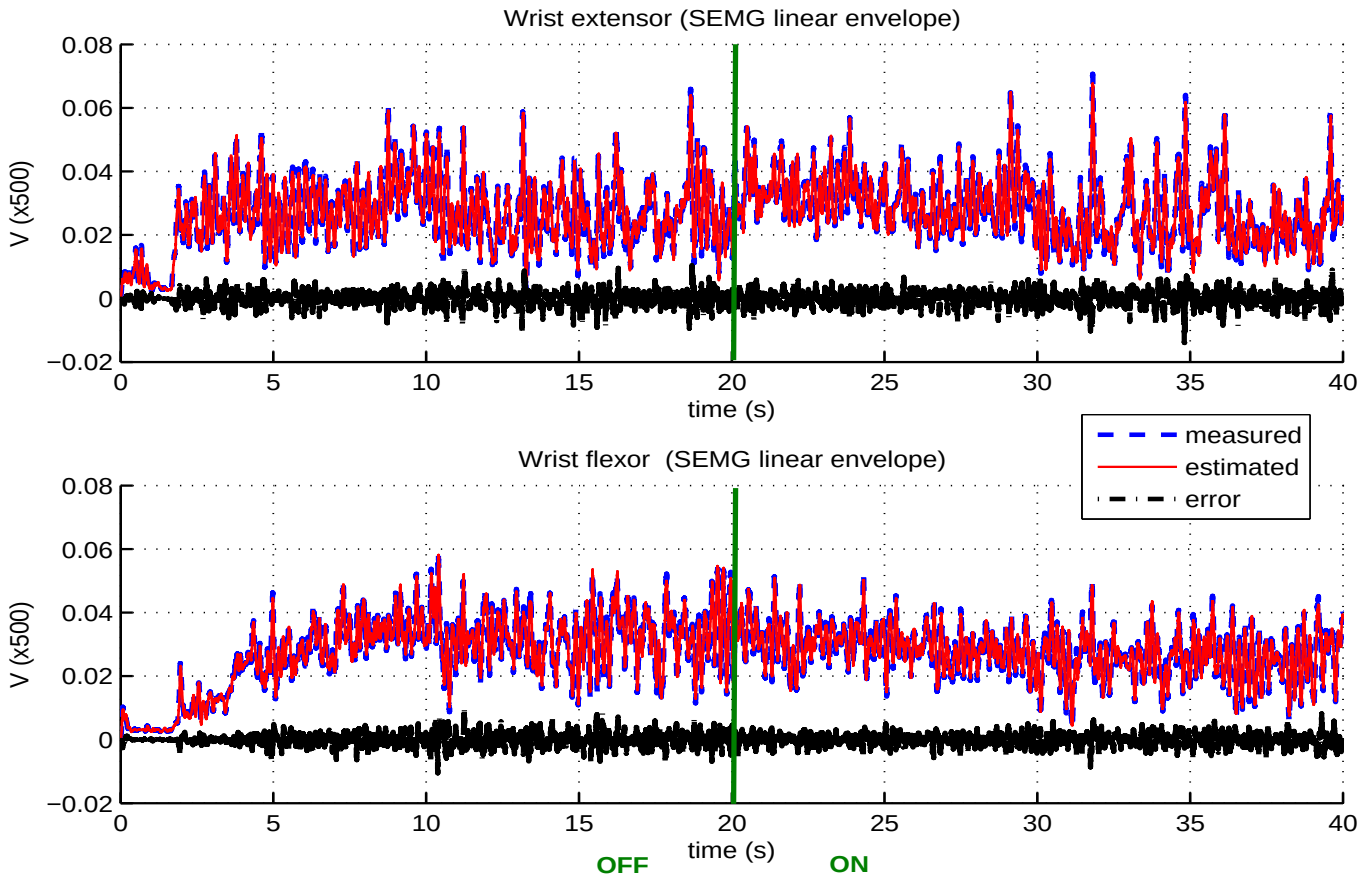

Figure 5.28: Estimated SEMG signals from EKF during tremor compensation from one of the ET patients (ET4). OFF = no stimulation is applied to the muscle. ON = stimulation is applied.

Chapter 6

Conclusion and Future Work

6.1 Conclusion

An alternative upper limb tremor compensation system in the line of assistive technology has been proposed in this thesis. The problem of pathological tremor is first formulated in Chapter 1. Tremor is the most common movement disorder and it causes various degrees of disability in performing activities of daily living. As the world is aging, prevalence of tremor will increase and not to mention the social and economical cost both to the person and his/her society.

Chapter 2 presents a review on the current sensor and actuators used in tremor literature. Current tremor compensation systems are also discussed. Subsequently, the sensor and actuator proposed in this work are explained. We use surface electromyography (SEMG) and accelerometer (ACC) to sense the upper limb movement. Functional Electrical Stimulation (FES) is adopted to counteract the tremulous part of the movement. Lastly, the whole system setup for real-time tremor compensation is presented in detail. The novelty of the proposed system here is the application of SEMG for tremor compensation.

Experiments were conducted to collect tremor data from 20 patients. Every subject performed standard therapeutic protocol, such as finger-to-nose movement, spiral drawing, etc. The data collected has been shown to be useful for tremor compensation as well as for diagnostic purposes. Preliminary results are

given in Chapter 3 alongside with other work based on our data for tremor classification. The classification is able to identify correctly at least 98% between tremor patients and healthy subjects and between Parkinson's Disease tremor and Essential tremor [Palmes et al., 2010]. The proposed classification method performs better than the other tested algorithm as shown in Fig. 3.10.

After demonstrating that the sensing system is capable to detect tremor, an Extended Kalman Filter (EKF) based algorithm is proposed to estimate tremor parameters from both the SEMG and ACC signal (Chapter 4). The important part of the proposed EKF algorithm is its ability to separate tremor and voluntary motion. By expanding the available EKF model, it can now track the tremor based on frequency. This is possible because the frequency of voluntary motion is smaller than that of tremor. Comparison of EKF and other notable methods in the literature is also provided in Table 4.1 and it has been found that the performance EKF is comparable if not better then the other tested methods. Thus is suitable for tremor parameter estimation. Simulation with real tremor data has shown that the proposed EKF can obtain up to 28% RMS error in estimating the SEMG signal.

When the necessary parameters are available, the compensation can be carried out. However, there are two issues related with the usage of FES to compensate tremor. Chapter 5 considers these two issues, i.e. FES artifacts and actuation time.

To be able to work with the SEMG signal, artifacts from the FES must first be reduced significantly. Review of current methods is provided and the commonly used method is employed in the proposed system, i.e. blanking and comb filter. All the algorithms are not implemented in hardware as usually done in the literature (for the blanking). Advantage of the employed algorithms is mainly simplicity, thus requiring little computational power which is more suitable for the envisioned wearable system.

The most crucial issue in tremor compensation is the actuation time. The stimulation by the FES must be applied at the correct moment so that the tremor

is attenuated in anti phase. To achieve this objective, two important facts are exploited. The first is that SEMG signal precedes the movement it gives command to. This is defined as electromechanical delay (EMD). Furthermore, it has been confirmed that the EMD caused by electrical stimulation is significantly shorter than that caused by voluntary motion. This difference provides us the necessary time window to process the information in advance and thus compensating the tremor in real-time.

To utilize this delay, the processing of data up to this point must not, ideally, cause phase delay. The proposed EKF has been shown to cause negligible time delay as compared to classical filter. Other part of the algorithm which has to be considered is the employed digital filter. In processing the raw SEMG signal, a low-pass filter is used. This filtering causes phase delay. Additionally, the comb filter as part of the FES artifact suppression algorithm also causes phase delay. Methods to minimize these delays are also presented in Chapter 5. Experiments with normal subjects have shown the efficacy of the complete proposed method in actuating the muscles in anti phase. FES control is not included in the thesis scope, thus only a simple control scheme is used.

Finally, experimental result from one tremor patient is reported, also in Chapter 5. The proposed algorithm could obtain 57% compensation, It shows that the proposed algorithm has significantly compensate the tremor in anti-phase manner although only a very simple control algorithm is implemented.

6.2 Contributions

In summary, the contributions of this thesis are as follow:

1. A novel approach in real-time tremor compensation.
   Utilizing unique feature of SEMG signal added with ACC data provides a novel approach in acquiring tremor data for compensation. Together with FES for actuating the muscles, a real-time system is developed to study the

feasibility of the novel tremor compensation algorithm. This system can further be developed into a wearable system in the future.

2. An EKF model for estimation of tremor parameters.
   The estimated tremor parameters are useful for tremor attenuation with FES. An important feature is also proposed, i.e. to separate tremor from voluntary motion.

3. Real-time sensing for tremor attenuation.
   A novel method to utilize both sensing information is also put forward to attenuate tremor at the correct moment. This is based on the different EMD caused by voluntary motion and electrically stimulated movement. By accommodating the difference, compensation can be carried out at the moment the tremor occurs (see Fig. 5.14).

6.3 Future Work

As this thesis is geared towards proposing new approach in tremor compensation and its feasibility, there are still many rooms for improvements. The proposed system is useful from engineering and clinical point of view and the future works may be directed towards these two areas.

From engineering point of view, many improvements can be done to improve the compensation ability of the system. One main area is FES control, which in itself is a very large area. The proposed system currently does not employ either sophisticated adaptive control or elaborated musculoskeletal inverse model (see Fig. 1.1). This is one of the probable reasons why the algorithm could not achieve a better compensation than the current 57%. Tremor characteristics, including amplitude, fluctuate over time, thus implementing a simple on-off controller does not capture the tremor dynamics. If a good musculoskeletal model is worked out,

the FES stimulation can be controlled such that the current produced to compensate tremor is equal to the tremor itself. This model may require additional sensors, apart from SEMG and accelerometer that are currently employed.

Fatigue is definitely a concern whenever FES is used, especially when the target users of this application are generally older people. What is envisioned for this system is that the user will be able to use it only when it is really necessary, such as when they do not want their tremor to be seen in public, e.g. when signing a paper, etc. In our experiment with one tremor patient, we applied FES for 10 seconds consecutively, but intermittently throughout 2 hours. In total, the subject experienced 5 minutes of stimulation on his arm. This is a relatively mild level of stimulation and the subject did not feel fatigue in his arm, but indeed further investigation with more patients is required.

With respect to the tremor patients, there are a few challenges ahead besides fatigue. Based on our experience with tremor patients, many of them exhibit tremor at multiple degree of freedom (DoF) in one joint, e.g. wrist flexion-extension and pronation-supination. While the proposed system here can be easily extended to accommodate multi-DoF compensation, doing it in one joint is difficult. The problem lies with the nature of surface electrodes. Some muscles are not located near the skin, therefore with surface electrodes, it is not trivial to obtain their SEMG signal. One possible solution is to have more electrodes attached systematically and then develop more complex classification and estimation algorithm to obtain information about a particular DoF at one joint.

Better compensation result can definitely be attained with a better estimation algorithm. In this work, EKF based algorithm has been proposed to estimate tremor parameters and to separate tremor from voluntary motion. This algorithm is based mainly on tremor phenomenon, such as its rhythmical patter and higher frequency than normal voluntary motion. Therefore in the future, with increasing knowledge on the pathophysiology of tremor, better model can be proposed which includes not only phenomenological aspects of tremor.

In this thesis, the onset estimation of the movement is based on amplitude thresholding and the phase estimate from the EKF. Thus more complex method may be proposed for the tremor parameters estimation, with the focus on the timing. The more precise the stimulation timing, the better the compensation is. Algorithms for the FES artifact suppression may also be improved with modeling of the artifacts. More complex algorithms can of course be proposed, but the balance with the computational cost must be kept in mind as the time window for tremor compensation is in the order of tens of milliseconds at most.

Finally, to commercialize the system and make it more widely accessible to the society, the whole system must be made into a wearable orthosis. We envision having a sleeve-like orthosis with the electrodes inside which can be worn under a shirt. The data is then transmitted (through wireless protocol) to a microcontroller system which can also be carried by the person using it. All these leave us with many engineering challenges.

For the clinical aspect, until now there is not any standard protocol to diagnose tremor. The tools developed are mainly questionnaire which is very subjective. Even the same clinician can give different ratings at different occasion for the same case. Thus it is expected that by having a quantitative measurement of the tremor, a more accurate and objective diagnosis can be done by the doctors. This will then improve the way tremor patients are treated.

Initial attempts to classify tremor have been carried out. A generic way of optimizing the Support Vector Machine model for tremor diagnosis using SEMG data has been proposed. The results from 14 healthy subjects and 13 tremor patients are encouraging. Nevertheless in the future, the algorithm has to be tested on more subjects for further validation. Practicality of the algorithm has to be checked in real-world scenario. And finally improvement on the algorithm must be explored, e.g. by obtaining features from wavelet transform and other sensing modalities.

References

Anderson, B. D. O. and J. B. Moore (1979). *Optimal filtering*. Englewood Cliffs, N.J.: Prentice-Hall. 81

Ang, W. T., M. Krichane, and T. Sim (2006). Zero phase filtering for active compensation of periodic physiological motion. In *IEEE/RAS-EMBS International Conference on Biomedical Robotics and Biomechatronics*, Volume 2006, pp. 182–187. 118, 119, 120

Arnold, A. S., M. J. Rosen, and M. L. Aisen (1993). Evaluation of a controlled-energy-dissipation orthosis for tremor suppression. *Journal of Electromyography and Kinesiology 3*(3), 131–148. 22

Au, A. T. C. and R. F. Kirsch (2000). EMG-based prediciton of shoulder and elbow kinematics in able-bodied and spinal cord injured individuals. *IEEE Transactions on Rehabilitation Engineering 8*(4), 471–480. 73

Babb, T. L., E. Mariani, and G. M. Strain (1978). A sample and hold amplifier system for stimulus artifact suppression. *Electroencephalography and Clinical Neurophysiology 44*(4), 528–531. 106

Bishop, B. (2006). Tremors. *The Journal for Nurse Practitioners 2*(4), 273–275. 3

Bittanti, S. and S. M. Savaresi (2000). On the parameterization and design of an extended kalman filter frequency tracker. *IEEE Transactions on Automatic Control 45*(9), 1718–1724. 98

Blana, D., R. F. Kirsch, and E. K. Chadwick (2009). Combined feedforward and feedback control of a redundant, nonlinear, dynamic musculoskeletal system. *Medical and Biological Engineering and Computing 47*(5 SPEC. ISS.), 533–542. 143

Bó, A. P. L., P. Poignet, D. Zhang, and W. T. Ang (2009). FES-controlled co-contraction strategies for pathological tremor compensation. In *IEEE/RSJ International Conference on Intelligent Robots and Systems*, St. Louis, MO, pp. 1633–1638. 143

Bonato, P. (2003). Wearable sensors/systems and their impact on biomedical engineering. *IEEE Engineering in Medicine and Biology Magazine 22*(3), 18–20. 5

Bonato, P., D. M. Sherrill, D. G. Standaert, S. S. Salles, and M. Akay (2004). "data mining techniques to detect motor fluctuations in Parkinson's disease". In *International Conference of the IEEE EMBS*, Volume 2, San Francisco, USA, pp. 4766–4769 Vol.7. 20

Boudreau, B. H., K. B. Englehart, A. D. C. Chan, and P. A. Parker (2004). Reduction of stimulus artifact in somatosensory evoked potentials: Segmented versus subthreshold training. *IEEE Transactions on Biomedical Engineering 51*(7), 1187–1195. 109, 111

Bureau, U. C. (2004). Global population profile: 2002. Technical report. 3

Burkhard, P. R., J. W. Langston, and J. W. Tetrud (2002). Voluntarily simulated tremor in normal subjects. *Neurophysiologie Clinique/Clinical Neurophysiology 32*(2), 119–126. 128

Burne, J. A., M. W. Hayes, V. S. C. Fung, C. Yiannikas, and D. Boljevac (2002). The contribution of tremor studies to diagnosis of parkinsonian and essential tremor: a statistical evaluation. *Journal of Clinical Neuroscience 9*(3), 237–242. 20

Cappello, A., A. Leardini, M. G. Benedetti, R. Liguori, and A. Bertani (1997). Application of stereophotogrammetry to total body three-dimensional analysis of human tremor. *IEEE Transactions on Rehabilitation Engineering 5*(4), 388–393. 16

Chandler, R. F., C. E. Clauser, J. T. McConville, H. M. Reynolds, and J. W. Young (1975). Investigation of inertial properties of the human body. Technical report AMRL-TR-74-137, Aerospace Medical Research Laboratory, Wright-Patterson. 142

Chou, K. L. (2008). Adverse Events from the Treatment of Parkinson's Disease. *Neurologic clinics 26*(3 SUPPL.), 65–83. 5

Clancy, E. A., O. Bida, and D. Rancourt (2006). Influence of advanced electromyogram (emg) amplitude processors on emg-to-torque estimation during constant-posture, force-varying contractions. *Journal of Biomechanics 39*(14), 2690–2698. 73

Clancy, E. A. and N. Hogan (1999). Probability density of the surface electromyogram and its relation to amplitude detectors. *IEEE Transactions on Biomedical Engineering 46*(6), 730–739. 27

Clancy, E. A., E. L. Morin, and R. Merletti (2002). Sampling, noise-reduction and amplitude estimation issues in surface electromyography. *Journal of Electromyography and Kinesiology 12*(1), 1–16. 27

Connor, G. S., W. G. Ondo, M. A. Stacy, and J. Jankovic (2001). Essential Tremor: A practical guide to evaluation diagnosis and treatment. *Clinician 19*(2), 1–15. 51, 137

Cooper, R. A. (1998). Harmonization of assistive technology standards. In *Proceedings of the 20th Annual International Conference of the IEEE Engineering in Medicine and Biology Society*, Volume 6, pp. 3367–3369. 5

Corcos, D. M., G. L. Gottlieb, M. L. Latash, G. L. Almeida, and G. C. Agarwal (1992). Electromechanical delay: An experimental artifact. *Journal of Electromyography and Kinesiology 2*(2), 59–68. 7, 23, 28, 123

Deuschl, G., J. Raethjen, M. Lindemann, and P. Krack (2001). The pathophysiology of tremor. *Muscle and Nerve 24*(6), 716–735. 3, 53, 90

Dipietro, L., A. M. Sabatini, and P. Dario (2003). Artificial neural network model of the mapping between electromyographic activation and trajectory patterns in free-arm movements. *Medical and Biological Engineering and Computing V41*(2), 124–132. 73

Dotsinsky, I., A. Dos Santos, and I. Tashev (1999). Artefact cancellation in motor-sensory evoked potentials: Two approaches using adaptive filtration and exponential approximation. *Medical and Biological Engineering and Computing 37*(1). 109

Edwards, R. and A. Beuter (1999). Indexes for identification of abnormal tremor using computer tremor evaluation systems. *IEEE Transactions on Biomedical Engineering 46*(7), 895–898. 16

Elble, R. J. (2005). Gravitational artifact in accelerometric measurements of tremor. *Clinical Neurophysiology 116*(7), 1638–1643. 125

Elble, R. J. and W. C. Koller (1990). *Tremor*. Baltimore: Johns Hopkins University Press. 1, 59, 71

Engin, M. (2007). A recording and analysis system for human tremor. *Measurement 40*(3), 288–293. 17, 21

Erfanian, A., H. J. Chizeck, and R. M. Hashemi (1998). Using evoked emg as a synthetic force sensor of isometric electrically stimulated muscle. *IEEE Transactions on Biomedical Engineering 45*(2), 188–202. 104, 107

Farina, D., C. Cescon, and R. Merletti (2002). Influence of anatomical, physical, and detection-system parameters on surface emg. *Biological Cybernetics 86*(6), 445–456. 28

Findley, L. J. (2007). The economic impact of parkinson's disease. *Parkinsonism and Related Disorders 13*(SUPPL. SEPT.), S8–S12. 3

Freeman, C. T., A. . Hughes, J. H. Burridge, P. H. Chappell, P. L. Lewin, and E. Rogers (2009). Iterative learning control of FES applied to the upper extremity for rehabilitation. *Control Engineering Practice 17*(3), 368–381. 127, 143

Freeman, J. A. (1971). An electronic stimulus artifact suppressor. *Electroencephalography and Clinical Neurophysiology 31*(2), 170–172. 105

Frigo, C., M. Ferrarin, W. Frasson, E. Pavan, and R. Thorsen (2000). EMG signals detection and processing for on-line control of Functional Electrical Stimulation. *Journal of Electromyography and Kinesiology 10*(5), 351–360. 32, 34, 104, 112, 113

Gao, J. (2004). Analysis of amplitude and frequency variations of essential and parkinsonian tremors. *Medical and Biological Engineering and Computing 42*(3), 345–349. 78, 143

Giansanti, D., G. Maccioni, and V. Macellari (2005). The development and test of a device for the reconstruction of 3-d position and orientation by means of a kinematic sensor assembly with rate gyroscopes and accelerometers. *IEEE Transactions on Biomedical Engineering 52*(7), 1271–1277. 19

Giansanti, D., V. Macellari, G. Maccioni, and A. Cappozzo (2003). Is it feasible to reconstruct body segment 3-d position and orientation using accelerometric data? *IEEE Transactions on Biomedical Engineering 50*(4), 476–483. 18, 21

Gillard, D. M., T. Cameron, A. Prochazka, and M. J. A. Gauthier (1999). Tremor suppression using Functional Electrical Stimulation: a comparison between digital and analog controllers. *IEEE Transactions on Rehabilitation Engineering [see also IEEE Trans. on Neural Systems and Rehabilitation] 7*(3), 385–388. 6, 22

Giuffrida, J. P. and P. E. Crago (2001). Reciprocal EMG control of elbow extension by FES. *IEEE Transactions on Neural Systems and Rehabilitation Engineering 9*(4), 338–345. 107, 112, 113

Godfrey, A., R. Conway, D. Meagher, and G. Laighin (2008). Direct measurement of human movement by accelerometry. *Medical Engineering and Physics 30*(10), 1364–1386. 8, 23

Gonzalez, J. G., E. A. Heredia, T. Rahman, K. E. Barner, and G. R. Arce (2000). Optimal digital filtering for tremor suppression. *IEEE Transactions on Biomedical Engineering 47*(5), 664–673. 6, 21

Gregory, C. M. and C. S. Bickel (2005). Recruitment patterns in human skeletal muscle during electrical stimulation. *Physical Therapy 85*(4), 358–364. 33

Grieve, R., P. A. Parker, B. Hudgins, and K. Englehart (2000). Nonlinear adaptive filtering of stimulus artifact. *IEEE Transactions on Biomedical Engineering 47*(3), 389–395. 108

Hamming, N. and D. F. Lovely (2007). Influence of recording instrumentation on the stimulus artifact tail in the surface acquisition of somatosensory evoked potentials. *Medical Engineering and Physics 29*(1), 148–153. 108

Hariz, M. (2009). Deep brain stimulation versus best medical therapy for advanced Parkinson's disease. *The Lancet Neurology 8*(3), 223–224. 5

Hashemi, S. M., M. F. Golnaraghi, and A. E. Patla (2004). Tuned vibration absorber for suppression of rest tremor in parkinson's disease. *Medical and Biological Engineering and Computing 42*(1), 61–70. 22

Hayashibe, M., D. Guiraud, and P. Poignet (2009). EMG-to-force estimation with full-scale physiology based muscle model. In *IEEE/RSJ International Conference on Intelligent Robots and Systems*, St. Louis, USA. 73

Hermens, H. J., B. Freriks, C. Disselhorst-Klug, and G. Rau (2000). Development of recommendations for semg sensors and sensor placement procedures. *Journal of Electromyography and Kinesiology 10*(5), 361–374. 39, 41, 42

Héroux, M. E., G. Pari, and K. E. Norman (2009). The effect of inertial loading on wrist postural tremor in essential tremor. *Clinical Neurophysiology 120*(5), 1020–1029. 6, 22

Hopkins, J. T., J. B. Feland, and I. Hunter (2007). A comparison of voluntary and involuntary measures of electromechanical delay. *International Journal of Neuroscience 117*(5), 597–604. 8, 23, 28, 118, 123, 124

Hou, M. (2005). Amplitude and frequency estimator of a sinusoid. *IEEE Transactions on Automatic Control 50*(6), 855–858. 61, 62, 63, 64

Hsu, L., R. Ortega, and G. Damm (1999). A globally convergent frequency estimator. *IEEE Transactions on Automatic Control 44*(4), 698–713. 61, 62, 63

Hua, Y., D. F. Lovely, and R. Doraiswami (2006). Factors affecting the stimulus artifact tail in surface-recorded somatosensory-evoked potentials. *Medical and Biological Engineering and Computing 44*(3), 226–241. 108

Hyde, R. A., L. P. Ketteringham, S. A. Neild, and R. J. S. Jones (2008). Estimation of upper-limb orientation based on accelerometer and gyroscope measurements. *IEEE Transactions on Biomedical Engineering 55*(2), 746–754. 18, 19, 21

Jakubowski, J., K. Kwiatos, A. Chwaleba, and S. Osowski (2002). Higher order statistics and neural network for tremor recognition. *IEEE Transactions on Biomedical Engineering 49*(2), 152–159. 3, 17, 21

Kay, S. M. and S. L. Marple Jr. (1981). Spectrum Analysis – A Modern Perspective. *Proceedings of the IEEE 69*(11), 1380–1419. 60

Keller, T. (2001). *Surface Functional Electrical Stimulation (FES) Neuroprosthesis for Grasping*. Ph. D. thesis, ETH Zurich. 31

Kim, S. and J. McNames (2006). Tracking tremor frequency in spike trains using the extended kalman smoother. *IEEE Transactions on Biomedical Engineering 53*(8), 1569–1577. 65

Knaflitz, M. and R. Merletti (1988). Suppression of simulation artifacts from myoelectric-evoked potential recordings. *IEEE Transactions on Biomedical Engineering 35*(9), 758–763. 106

Kornfield, M. J., J. Cerra, and D. G. Simons (1985). Stimulus artifact reduction in nerve conduction. *Archives of Physical Medicine and Rehabilitation 66*(4), 232–235. 112

La Scala, B. F., R. R. Bitmead, and B. G. Quinn (1996). An extended kalman filter frequency tracker for high-noise environments. *IEEE Transactions on Signal Processing 44*(2), 431–434. 64

Langzam, E., E. Isakov, and J. Mizrahi (2006). Evaluation of methods for extraction of the volitional EMG in dynamic hybrid muscle activation. *Journal of NeuroEngineering and Rehabilitation 3*. 104, 106, 113

Lauk, M., B. Koster, J. Timmer, B. Guschlbauer, G. Deuschl, and C. H. Lucking (1999). Side-to-side correlation of muscle activity in physiological and pathological human tremors. *Clinical Neurophysiology 110*(10), 1774–1783. 20, 21

Louis, E. D. (2005). Essential tremor. *The Lancet Neurology 4*(2), 100–110. 3, 4, 137

Louis, E. D. and E. Rios (2009). Embarrassment in essential tremor: Prevalence, clinical correlates and therapeutic implications. *Parkinsonism and Related Disorders 15*(7), 535–538. 2

Luca, C. J. D. (1997). The use of surface electromyography in biomechanics. *Journal of Applied Biomechanics 13*, 135–163. 28

Luca, C. J. D. (2006). Electromyography. In J. G. Webster (Ed.), *Encyclopedia of Medical Devices and Instrumentation*, pp. 98–109. Wiley-Interscience. ix, 26, 135

Luinge, H. J., P. H. Veltink, and C. T. M. Baten (2007). Ambulatory measurement of arm orientation. *Journal of Biomechanics 40*(1), 78–85. 18

Lundervold, D. A., R. Pahwa, P. A. Ament, and D. Corbin (2003). Validity of clinical and patient ratings of tremor disability among older adults. *Parkinsonism & Related Disorders 10*(1), 15–18. 5

Lynch, C. L. and M. R. Popovic (2008). Functional electrical stimulation. *IEEE Control Systems Magazine 28*(2), 40–50. 32, 33

Lyons, R. G. (1997). *Understanding digital signal processing*. Reading, MA: Addison Wesley. 122

Mandrile, F., D. Farina, M. Pozzo, and R. Merletti (2003). Stimulation artifact in surface emg signal: Effect of the stimulation waveform, detection system, and current amplitude using hybrid stimulation technique. *IEEE Transactions on Neural Systems and Rehabilitation Engineering 11*(4), 407–415. 107

Mann, K. A., F. W. Werner, and A. K. Palmer (1989). Frequency spectrum analysis of wrist motion for activities of daily living. *Journal of Orthopaedic Research 7*(2), 304–306. 6, 60, 84

Manto, M., M. Topping, M. Soede, J. Sanchez-Lacuesta, W. Harwin, J. Pons, J. Williams, S. Skaarup, and L. Normie (2003). Dynamically responsive intervention for tremor suppression. *IEEE Engineering in Medicine and Biology Magazine 22*(3), 120–132. 3, 6

Marino, R. and P. Tomei (2002). Global estimation of n unknown frequencies. *IEEE Transactions on Automatic Control 47*(8), 1324–1328. 61

Maybeck, P. S. (1979). *Stochastic models, estimation and control*. Mathematics in science and engineering, v. 141. New York: Academic Press. 70

McGill, K. C., K. L. Cummins, L. J. Dorfman, B. B. Berlizot, K. Luetkemeyer, D. G. Nishimura, and B. Widrow (1982). On the nature and elimination of stimulus artifact in nerve signals evoked and recorded using surface electrodes. *IEEE Transactions on Biomedical Engineering 29*(2), 129–137. 104, 108

Merletti, R. (1999). Standards for reporting EMG data. *Journal of Electromyography and Kinesiology 9*(1), III–IV. 39, 165

Merletti, R., M. Knaflitz, and C. J. DeLuca (1992). Electrically evoked myoelectric signals. *Critical Reviews in Biomedical Engineering 19*(4), 293–340. 104

Merletti, R. and P. Parker (2004). *Electromyography : physiology, engineering, and noninvasive applications*. Hoboken, N.J.: IEEE Press ;Wiley-Interscience. ix, 24, 25, 27, 41, 42, 73

Merletti, R., A. Rainolde, and D. Farina (2001). Surface electromyography for noninvasive characterization of muscle. *Exercise and Sport Sciences Reviews 29*(1), 20–25. 27, 28

Milanov, I. (2000). Clinical and electromyographic examinations of parkinsonian tremor. *Parkinsonism & Related Disorders 6*(4), 229–235. 19, 51

Milanov, I. (2001). Electromyographic differentiation of tremors. *Clinical Neurophysiology 112*(9), 1626–1632. 3, 19, 21

Milanov, I. (2002). Clinical and electromyographic assessment of essential tremor treatment. *Parkinsonism & Related Disorders 8*(5), 343–348. 19

Milanov, I., D. Georgiev, and T. Todorov (2000). Clinical and electromyographic characteristics of tremor in patients with depression. *Parkinsonism & Related Disorders 6*(2), 101–105. 20

Miller, J. L. (2002). Parkinson's disease primer. *Geriatric Nursing 23*(2), 69–75. 4

Miltenburger, C. and G. Kobelt (2002). Quality of life and cost of multiple sclerosis. *Clinical Neurology and Neurosurgery 104*(3), 272–275. 3

Minzly, J., J. Mizrahi, N. Hakim, and A. Liberson (1993). Stimulus artefact suppressor for EMG recording during FES by a constant-current stimulator. *Medical and Biological Engineering and Computing 31*(1), 72–75. 106

Mobasser, F., J. M. Eklund, and K. Hashtrudi-Zaad (2007). Estimation of elbow-induced wrist force with emg signals using fast orthogonal search. *IEEE Transactions on Biomedical Engineering 54*(4), 683–693. 73

Mojiri, M. and A. R. Bakhshai (2004). An adaptive notch filter for frequency estimation of a periodic signal. *IEEE Transactions on Automatic Control 49*(2), 314–318. 61

Mojiri, M. and A. R. Bakhshai (2007). Estimation of n frequencies using adaptive notch filter. *IEEE Transactions on Circuits and Systems II: Express Briefs 54*(4), 338–342. 61

Momen, K., S. Krishnan, and T. Chau (2007). Real-time classification of forearm electromyographic signals corresponding to user-selected intentional movements for multifunction prosthesis control. *IEEE Transactions on Neural Systems and Rehabilitation Engineering 15*(4), 535–542. 135

Morris, J. R. W. (1973). Accelerometry–a technique for the measurement of human body movements. *Journal of Biomechanics 6*(6), 729–732. 18

Nawab, S. H., S. H. Roy, and C. J. De Luca (2004). Functional activity monitoring from wearable sensor data. In *International Conference of the IEEE EMBS*, Volume 1, San Francisco, USA, pp. 979–982 Vol.2. 20

Nishiyama, K. (1997). A nonlinear filter for estimating a sinusoidal signal and its parameters in white noise: On the case of a single sinusoid. *IEEE Transactions on Signal Processing 45*(4), 970–981. 65

Norman, K. E., R. Edwards, and A. Beuter (1999). The measurement of tremor using a velocity transducer: comparison to simultaneous recordings using transducers of displacement, acceleration and muscle activity. *Journal of Neuroscience Methods 92*(1-2), 41–54. 15, 21

O'Keeffe, D. T., G. M. Lyons, A. E. Donnelly, and C. A. Byrne (2001). Stimulus artifact removal using a software-based two-stage peak detection algorithm. *Journal of Neuroscience Methods 109*(2), 137–145. 104, 108, 111

Padgaonkar, A. J., K. W. Krieger, and A. I. King (1975). Measurement of angular acceleraion of a rigid body using linear accelerometers. *Journal of Applied Mechanics, Transactions ASME 42 Ser E*(3), 552–556. 18

Pahwa, R. and K. E. Lyons (2003). Essential tremor: differential diagnosis and current therapy. *The American Journal of Medicine 115*(2), 134–142. 5

Palmes, P., F. Widjaja, L. Tan, W. T. Ang, and W. L. Au (2010). Pattern mining of multi-channel sEMG for tremor classification. *IEEE Transactions on Biomedical Engineering*. 55, 56, 146

Parker, P. J. and B. D. O. Anderson (1990). Frequency tracking of nonsinusoidal periodic signals in noise. *Signal Processing 20*(2), 127–152. 64, 65, 70, 78, 79, 82

Parsa, V., P. Parker, and R. Scott (1998). Convergence characteristics of two algorithms in non-linear stimulus artefact cancellation for electrically evoked potential enhancement. *Medical and Biological Engineering and Computing 36*(2), 202–214. 108

Peasgood, W., T. Whitlock, A. Bateman, M. E. Fry, R. S. Jones, and A. Davis-Smith (2000). EMG-controlled closed loop electrical stimulation using a digital signal processor. *Electronics Letters 36*(22), 1832–1833. 107, 112

Peckham, P. H. and J. S. Knutson (2005). *Functional electrical stimulation for neuromuscular applications*, Volume 7. 31

Pellegrini, B., L. Faes, G. Nollo, and F. Schena (2004). Quantifying the contribution of arm postural tremor to the outcome of goal-directed pointing task by displacement measures. *Journal of Neuroscience Methods 139*(2), 185–193. 16, 21

Pledgie, S., K. E. Barner, S. K. Agrawal, and T. Rahman (2000). Tremor suppression through impedance control. *IEEE Transactions on Rehabilitation Engineering [see also IEEE Trans. on Neural Systems and Rehabilitation] 8*(1), 53–59. 6, 21

Popović, D., A. Stojanović, A. Pjanović, S. Radosavljević, M. Popović, S. Jović, and D. Vulović (1999). Clinical evaluation of the Bionic Glove. *Archives of Physical Medicine and Rehabilitation 80*(3), 299–304. 6

Popovic, M. R., T. Keller, I. P. I. Pappas, V. Dietz, and M. Morari (2001). Surface-stimulation technology for grasping and walking neuroprostheses: Improving quality of life in stroke/spinal cord injury subjects with rapid prototyping and portable fes systems. *IEEE Engineering in Medicine and Biology Magazine 20*(1), 82–93. 31

Powell Jr., H. C., M. A. Hanson, and J. Lach (2009). On-body inertial sensing and signal processing for clinical assessment of tremor. *IEEE Transactions on Biomedical Circuits and Systems 3*(2). 17

Pradalier, A., E. Apartis, D. Vincent, and C. Campinos (2002). Primary orthostatic tremor. *Rev Med Interne 23*(2), 193–197. 3, 4

Prochazka, A., J. Elek, and M. Javidan (1992). Attenuation of pathological tremors by functional electrical stimulation i: Method. *Annals of Biomedical Engineering V20*(2), 205–224. 6, 7, 22, 23

Pugliatti, M., S. Sotgiu, and G. Rosati (2002). The worldwide prevalence of multiple sclerosis. *Clinical Neurology and Neurosurgery 104*(3), 182–191. 4

Raethjen, J., M. Lauk, B. Koster, U. Fietzek, L. Friege, J. Timmer, C. H. Lucking, and G. Deuschl (2004). Tremor analysis in two normal cohorts. *Clinical Neurophysiology 115*(9), 2151–2156. 20, 21

Rainoldi, A., G. Galardi, L. Maderna, G. Comi, L. Lo Conte, and R. Merletti (1999). Repeatability of surface EMG variables during voluntary isometric contractions of the biceps brachii muscle. 28

Rajaraman, V., D. Jack, S. V. Adamovich, W. Hening, J. Sage, and H. Poizner (2000). A novel quantitative method for 3d measurement of parkinsonian tremor. *Clinical Neurophysiology 111*(2), 338–343. 16

Rank, M., O. Stursberg, and W. Ang (2008). A rate-dependent linear modelling approach for pathological tremor applications. In *IASTED Int. Conf. on Biomedical Engineering*, Innsbruck, Austria, pp. 246–251. 10

Rau, G., E. Schulte, and C. Disselhorst-Klug (2004). From cell to movement: to what answers does emg really contribute? *Journal of Electromyography and Kinesiology 14*(5), 611–617. 27

Regalia, P. A. (1991). An improved lattice-based adaptive iir notch filter. *IEEE Transactions on Signal Processing 39*(9), 2124–2128. 61

Reich, S. G. (1995). Common disorders of movement: Tremor and Parkinson's disease. In L. Barker, J. Burton, and P. Zieve (Eds.), *Principles of Ambulatory Medicine (Fourth ed.)*, pp. 1217–1229. Baltimore: Williams and Wilkens. 5

Riley, P. O. and M. J. Rosen (1987). Evaluating manual control devices for those with tremor disability. *Journal of Rehabilitation Research & Development 24*(2), 99–110. 6, 21

Rissanen, S. M., M. Kankaanp, A. Meigal, M. P. Tarvainen, J. Nuutinen, I. M. Tarkka, O. Airaksinen, and P. A. Karjalainen (2008). Surface emg and acceleration signals in parkinson's disease: Feature extraction and cluster analysis. *Medical and Biological Engineering and Computing 46*(9), 849–858. 20

Riviere, C. and N. V. Thakor (1995). Assistive computer interface for pen input by persons with tremor. In *Proceedings of the RESNA Annual Conference*, pp. 440–442. 6, 21

Riviere, C. N., R. S. Rader, and N. V. Thakor (1998). Adaptive cancelling of physiological tremor for improved precision in microsurgery. *IEEE Transactions on Biomedical Engineering 45*(7), 839–846. 8, 66, 67, 70

Roby, R. J. and E. Lettich (1975). A simplified circuit for stimulus artifact suppression. *Electroencephalography and Clinical Neurophysiology 39*(1), 85–87. 105

Rocon, E., J. M. Belda-Lois, A. F. Ruiz, M. Manto, J. C. Moreno, and J. L. Pons (2007). Design and validation of a rehabilitation robotic exoskeleton for tremor assessment and suppression. *IEEE Transactions on Neural Systems and Rehabilitation Engineering 15*(3), 367–378. 6, 7, 22, 23, 142

Routray, A., A. K. Pradhan, and K. P. Rao (2002). A novel kalman filter for frequency estimation of distorted signals in power systems. *IEEE Transactions on Instrumentation and Measurement 51*(3), 469–479. 65

Rushton, D. N. (1997). Functional electrical stimulation. *Physiological Measurement 18*(4), 241–275. 31, 32

Salarian, A., H. Russmann, C. Wider, P. R. Burkhard, F. J. G. Vingerhoets, and K. Aminian (2007). Quantification of tremor and bradykinesia in parkinson's disease using a novel ambulatory monitoring system. *IEEE Transactions on Biomedical Engineering 54*(2), 313–321. 18, 21

Samii, A., J. G. Nutt, and B. R. Ransom (2004). Parkinson's disease. *The Lancet 363*(9423), 1783–1793. 5, 51

Scott, R. N., L. McLean, and P. A. Parker (1997). Stimulus artefact in somatosensory evoked potential measurement. *Medical and Biological Engineering and Computing 35*(3), 211–215. 104

Sennels, S., F. Biering-Sorensen, O. T. Andersen, and S. D. A. H. S. D. Hansen (1997). Functional neuromuscular stimulation controlled by surface electromyographic signals produced by volitional activation of the same muscle: adaptive removal of the muscle response from the recorded EMG-signal. *IEEE Transactions on Rehabilitation Engineering [see also IEEE Trans. on Neural Systems and Rehabilitation] 5*(2), 195–206. 104, 107, 109

Sinclair, P. J., R. M. Smith, and G. M. Davis (2004). The effect of joint angle on the timing of muscle contractions elicited by neuromuscular electrical stimulation. *IEEE Transactions on Neural Systems and Rehabilitation Engineering 12*(2), 303–306. 29

Smaga, S. (2003). Tremor. *American Family Physician 68*(8), 1545–1552. xv, 1, 2, 60

Sobocki, P., M. Pugliatti, K. Lauer, and G. Kobelt (2007). Estimation of the cost of ms in europe: Extrapolations from a multinational cost study. *Multiple Sclerosis 13*(8), 1054–1064. 2

Spieker, S., C. Jentgens, A. Boose, and J. Dichgans (1995). Reliability, specificity and sensitivity of long-term tremor recordings. *Electroencephalography and Clinical Neurophysiology - Electromyography and Motor Control 97*(6), 326–331. 19

Spyers-Ashby, J. M., M. J. Stokes, P. G. Bain, and S. J. Roberts (1999). Classification of normal and pathological tremors using a multidimensional electromagnetic system. *Medical Engineering & Physics 21*(10), 713–723. 16

Staude, G., C. Flachenecker, M. Daumer, and W. Wolf (2001). Onset detection in surface electromyographic signals: A systematic comparison of methods. *Eurasip Journal on Applied Signal Processing 2001*(2), 67–81. 100

Stoica, P. (1993). List of references on spectral line analysis. *Signal Processing 31*(3), 329–340. 60

Strambi, S., B. Rossi, G. De Michele, and S. Sello (2004). Effect of medication in Parkinson's disease: A wavelet analysis of EMG signals. *Medical Engineering and Physics 26*(4), 279–290. 7, 23

Tan, C.-W. and S. Park (2005). Design of accelerometer-based inertial navigation systems. *IEEE Transactions on Instrumentation and Measurement 54*(6), 2520–2530. 18, 21

Thorsen, R. (1999). An artefact suppressing fast-recovery myoelectric amplifier. *IEEE Transactions on Biomedical Engineering 46*(6), 764–766. 107

Thorsen, R., R. Spadone, and M. Ferrarin (2001). A pilot study of myoelectrically controlled FES of upper extremity. *IEEE Transactions on Neural Systems and Rehabilitation Engineering 9*(2), 161–168. 107, 112, 113

Timmer, J., M. Lauk, S. Haussler, and V. Radt (2000). Cross-spectral analysis of tremor time series. *International Journal of Bifurcation and Chaos 10*(11), 2595–2610. 68, 87

Trapero, J. R., H. Sira-Ramirez, and V. F. Batlle (2007). An algebraic frequency estimator for a biased and noisy sinusoidal signal. *Signal Processing 87*(6), 1188–1201. 8, 61, 63, 65, 70

Vaillancourt, D. E. and K. M. Newell (2000). The dynamics of resting and postural tremor in parkinson's disease. *Clinical Neurophysiology 111*(11), 2046–2056. 20, 21

Van Someren, E. J. W., B. F. M. Vonk, W. A. Thijssen, J. D. Speelman, P. R. Schuurman, M. Mirmiran, and D. F. Swaab (1998). A new actigraph for long-term registration of the duration and intensity of tremor and movement. *IEEE Transactions on Biomedical Engineering 45*(3), 386–395. 17

von Campenhausen, S., B. Bornschein, R. Wick, K. Botzel, C. Sampaio, W. Poewe, W. Oertel, U. Siebert, K. Berger, and R. Dodel (2005). Prevalence and incidence of parkinson's disease in europe. *European Neuropsychopharmacology 15*(4), 473–490. 3, 4

Weaver, F. M., K. Follett, M. Stern, K. Hur, C. Harris, W. J. Marks Jr., J. Rothlind, O. Sagher, D. Reda, C. S. Moy, R. Pahwa, K. Burchiel, P. Hogarth, E. C. Lai, J. E. Duda, K. Holloway, A. Samii, S. Horn, J. Bronstein, G. Stoner, J. Heemskerk, and G. D. Huang (2009). Bilateral deep brain stimulation vs best medical therapy for patients with advanced parkinson disease: A randomized controlled trial. *JAMA - Journal of the American Medical Association 301*(1), 63–73. 5

Weiner, W. J. and A. E. Lang (1989). Tremor. In *Movement Disorders: A comprehensive survey*, pp. 221–256. New York: Futura Publishing. 5

Wharrad, H. J. and D. Jefferson (2000). Distinguishing between physiological and essential tremor using discriminant and cluster analyses of parameters derived from the frequency spectrum. *Human Movement Science 19*(3), 319–339. 17, 21

Whitmarsh, T. E. (2003). Homeopathy in multiple sclerosis. *Complementary Therapies in Nursing and Midwifery 9*(1), 5–9. 4

Wichmann, T. (2000). A digital averaging method for removal of stimulus artifacts in neurophysiologic experiments. *Journal of neuroscience methods 98*(1), 57–62. 109, 111

Yang, M.-H., Y.-H. Sheu, Y.-H. Shih, and M. S. Young (2003). Portable tremor monitor system for real-time full-wave monitoring and analysis. *Review of Scientific Instruments 74*(3), 1303–1309. 17, 21

Yeom, H., Y. Park, and H. Yoon (2005). Gram-schmidt M-wave canceller for the EMG controlled FES. *IEICE Transactions on Information and Systems E88-D*(9), 2213–2217. 109

Yu, S., C. R. Allen, D. Geng, D. Burn, U. Brechany, G. D. Bell, and R. Rowland (2003). 3-D motion system (data-gloves): application for Parkinson's disease. *IEEE Transactions on Instrumentation and Measurement 52*(3), 662–674. 16, 21

Yun, X. and E. R. Bachmann (2006). Design, implementation, and experimental results of a quaternion-based kalman filter for human body motion tracking. *IEEE Transactions on Robotics 22*(6), 1216–1227. x, 19, 21, 84, 85

Zhu, R. and Z. Zhou (2004). A real-time articulated human motion tracking using tri-axis inertial/magnetic sensors package. *IEEE Transactions on Neural Systems and Rehabilitation Engineering 12*(2), 295–302. 19

Ziarani, A. K. and A. Konrad (2004). A method of extraction of nonstationary sinusoids. *Signal Processing 84*(8), 1323–1346. 8, 62, 63, 64, 65, 70

Zipp, P. (1982). Recommendations for the standardization of lead positions in surface electromyography. *European Journal of Applied Physiology 50*(1), 41–54. ix, 42, 43

Appendix A

Standards for Reporting EMG Data

This section reproduces parts of [Merletti, 1999] which are relevant to the thesis.

The "Standards for Reporting EMG Data" have been written by Dr. Roberto Merletti and are endorsed by the International Society of Electrophysiology and Kinesiology (ISEK). The standards are also published in the Journal of Electromyography and Kinesiology (JEK).

Surface Electrode Reports on surface recording of EMG should include:

- electrode material (e.g., Ag/AgCl, etc.)
- electrode shape (discs, bars, rectangular, etc.)
- size (e.g., diameter, radius, width x length)
- use of gel or paste, alcohol applied to cleanse skin, skin abrasion, shaving of hair, etc.
- inter electrode distance
- electrode location, orientation over muscle with respect to tendons, motor point and fiber direction

EMG Detection Detection mode and amplification should be described by the following:

- monopolar , differential, double differential, etc.
- input impedance
- Common Mode Rejection Ratio (CMRR)
- signal-to-noise ratio (SNR)
- actual gain range used

Filtering of the raw EMG should be specified by:

- filter types (e.g., Butterworth, Chebyshev, etc.)
- low and/or high pass cut-off frequencies
- slopes of the cut-offs (dB/octave or dB/decade)

The power density function of the surface EMG signals has negligible contributions outside the range 5-10 Hz to 400-450 Hz. The bandwidth of the amplifier-filter should be within this range e.g. high pass 5 Hz, low pass 500 Hz)

Intramuscular and needle recordings should be made with the low-pass cut-off set at least at 1500 Hz.

Rectification If analog signal rectification is carried out full or half-wave rectification should be specified.

Sampling EMG into the computer In computer processing of the EMG it is important to consider these important factors:

1. It is advisable that the raw EMG (after amplification and bandpass filtering) is stored in the computer for digital processing. The minimal acceptable sampling is at least twice the highest frequency cut-off of the bandpass filter, e.g., if a bandpass filter of 10-400 Hz was used, the minimal sampling

rate employed to store the signal in the computer should be at least 800 Hz (400 x 2), as specified by Nyquist theorem, and preferably higher to improve accuracy and resolution. Sampling rates below twice the highest frequency cut- off are incorrect unless evidence is provided that there is no noise in the frequency band between the highest signal frequency and the cut-off frequency of the lowpass filter.

2. If rectification and smoothing with a low-pass filter is performed with hardware prior to sampling and storing data in the computer, the sampling rate could be drastically reduced because of the reduced bandwidth of the linear envelope. Rates of 50-100 Hz are sufficient to introduce the EMG envelope into the computer.

3. Number of bits, model, and manufacturer of A/D card used to sample data into the computer should be given.

Appendix B

Publication list

Journal

- **F. Widjaja**, C. Y. Shee, W. L. Au, P. Poignet, and W. T. Ang, "Sensing of Pathological Tremor Using Surface Electromyography and Accelerometer for Real-time Attenuation," *Journal of Mechanics in Medicine and Biology*, 2011. (revision)
- D. Zhang, P. Poignet, **F. Widjaja**, and W. T. Ang, "Neural Oscillator based Control for Pathological Tremor Suppression via Functional Electrical Stimulation," *Control Engineering Practice*, vol. 19, no. 1, pp. 74-88, 2011.
- P. Palmes, **F. Widjaja**, L. Tan, W. T. Ang, and W. L. Au, "Pattern Mining of Multi-Channel sEMG for Tremor Classification", *IEEE Transactions on Biomedical Engineering*, vol. 57, no. 12, pp. 2795-2805, 2010.
- **F. Widjaja**, C. Y. Shee, D. Zhang, W. T. Ang, P. Poignet, A. Bo, and D. Guiraud, "Current progress on pathological tremor modeling and active compensation using functional electrical stimulation," *Gerontechnology*, vol. 7, no. 2, p. 240, 2008.

Conference Proceedings

- **F. Widjaja**, C. Y. Shee, W. L. Au, P. Poignet, and W. T. Ang, "Anti phase tremor attenuation system using Surface Electromyography and Accelerometer," *IEEE International Conference on Robotics and Automation*, Shanghai, China, 2011. (accepted)
- **F. Widjaja**, C. Y. Shee, P. Poignet, and W. T. Ang, "Filtering of intended motion for real-time tremor compensation in human upper limb using surface

electromyography," *Annual International Conference of the IEEE Engineering and Medicine Society*, Minneapolis, USA, September 2009, pp. 2996-2999.

- **F. Widjaja**, C. Y. Shee, P. Poignet, and W. T. Ang, "FES artifact suppression for real-time tremor compensation," *IEEE International Conference on Rehabilitation Robotics*, Kyoto, Japan, June 2009, pp. 53-58.
- **F. Widjaja**, C. Y. Shee, W. L. Au, P. Poignet, and W. T. Ang, "An Extended Kalman Filtering of Accelerometer and Electromyography Data for Attenuation of Pathological Tremor," *IEEE RAS / EMBS International Conference on Biomedical Robotics and Biomechatronics*, Scottsdale, USA, October 2008, pp. 193-198.
- A. P. L. Bo, P. Poignet, **F. Widjaja** and W. T. Ang, "Online pathological tremor characterization using extended Kalman filtering," *Annual International Conference of the IEEE Engineering and Medicine Society*, Vancouver, Canada, August 2008, pp. 1753-1756.
- **F. Widjaja**, C. Y. Shee, W. T. Latt, W. L. Au, P. Poignet, and W. T. Ang, "Kalman Filtering of Accelerometer and Electromyography (EMG) data in Pathological Tremor Sensing System," *IEEE International Conference on Robotics and Automation*, Pasadena, USA, May 2008, pp. 3250-3255.
- **F. Widjaja**, C. Y. Shee, W. L. Au, P. Poignet, and W. T. Ang, "Towards A Sensing System for Quantification of Pathological Tremor," *International Conference on Intelligent and Advanced System*, Kuala Lumpur, Malaysia, November 2007, pp. 986-991.
- D. G. Zhang, W. T. Ang, **F. Widjaja**, C. Y. Shee, "Neural oscillator based control for wrist tremor attenuation," *IEEE International Conference on Computational Cybernetics*, Gammarth, Tunisia, October, 2007, pp.197-202.

Others

- U.-X. Tan, W. T. Latt, **F. Widjaja**, C. Y. Shee, C. N. Riviere, and W. T. Ang, "Tracking control of hysteretic piezoelectric actuator using adaptive rate-dependent controller," *Sensors and Actuators A: Physical*, vol. 150, no. 1, pp. 116-123, 2009.
- W. T. Latt, U. X. Tan, **F. Widjaja**, C. Y. Shee, and W. T. Ang, "A study of a hand-held instruments angular motion due to physiological tremor in micromanipulation tasks", *Annual International Conference of the IEEE Engineering and Medicine Society*, Vancouver, Canada, Aug. 2008, pp. 1952-1955.